

# Physical-chemical properties of complex natural fluids

Vorgelegt von  
Diplom-Geochemiker Diplom-Mathematiker  
Sergey Churakov  
aus Moskau

an der Fakultät VI  
- Bauingenieurwesen und Angewandte Geowissenschaften -  
der Technischen Universität Berlin

zur Erlangung des akademischen Grades  
Doktor der Naturwissenschaften  
- Dr. rer. nat. -

genehmigte Dissertation

Berichter: Prof. Dr. G. Franz  
Berichter: Prof. Dr. T. M. Seward  
Berichter: PD. Dr. M. Gottschalk

Tag der wissenschaftlichen Aussprache: 27. August 2001

Berlin 2001

D83

## Abstract

The dissertation is focused on the processes of transport and precipitation of metals in high temperature fumarole gases (a); thermodynamic properties of metamorphic fluids at high pressures (b); and the extent of hydrogen-bonding in supercritical water over wide range of densities and temperatures (c).

(a) At about 10 Mpa, degassing of magmas is accompanied by formation of nearly 'dry' salt melts as a second fluid phase, very strong fractionation of hydrolysis products between vapour and melts, as well as subvalence state of metals during transport processes. Based on chemical analyses of gases and condensates from high-temperature fumaroles of the Kudryavy volcano (i Iturup, Kuril Arc, Russia), a thermodynamic simulation of transport and deposition of ore- and rock-forming elements in high-temperature volcanic gases within the temperature range of 373-1373 K at 1 bar pressure have been performed. The results of the numerical simulations are consistent with field observations. Alkali and alkali earth metals, Ga, In, Tl, Fe, Co, Ni, Cu, and Zn are mainly transported as chlorides in the gas phase. Sulfide and chloride forms are characteristic of Ge, Sn, Pb, and Bi at intermediate and low temperatures. Be, Al, and Si migrate as fluorides and oxides, while As and Sb as sulfides and oxides. More complex, oxyfluoride and oxychloride species are typical for Ti, Zr, V, Mo, W, and Re. Cd (at high temperatures) and Hg (within the whole temperature range) are transported in the native form. The calculations revealed some general regularities in the variation of element species in the gas phase at a low (1 bar) pressure and high temperatures.

(b) Based on the thermodynamic perturbation theory, the equation of state (EOS) for the H-O-C-N-S-F-Cl-Br-I-B-Si-He-Ne-Ar-Kr fluid system has been developed. The EOS currently involves 98 different components and possess the following attractive features: 1) It is based on four substance specific parameters with clear physical meaning (dipole moment, polarizability and two parameters of the Lennard-Jones potential). 2) The EOS can be safely extrapolated to higher temperatures and pressures beyond the range of available P-V-T measurements. 3) The properties of fluid mixtures are determined from that of the pure fluid components. No additional parameters are involved. 4) New components can be easily added. The approach can be used as a basis for more general fluid systems involving strong electrolytes.

(c) A series of *Monte-Carlo* and *Molecular Dynamics* simulations have been performed to study the extent of hydrogen-bonding in supercritical water over a wide range of temperatures and pressures. Depending on the *P-T* conditions, three different structural states of supercritical water were identified: 1) liquid-like structure dominated by the existence of the infinite percolating H-bonded network; 2) vapor-like structure dominated by separate low-molecular (<10-20 molecules) clusters; and 3) intermediate type, where clusters of any size can be found in the bulk fluid. The stability field of the third structural type approximately corresponds to the density interval of 0.55-0.7 g/cm<sup>3</sup>. Even at densities below 0.02 g/cm<sup>3</sup> noticeable amounts of H-bonded clusters can be found in supercritical water. No significant density and temperature dependence of the relative abundance for topologically different water clusters of the small size was observed. The chain-like clusters were found to predominate under supercritical conditions over other possible cluster geometry.

## Zusammenfassung

Die vorgelegte Dissertation beschäftigt sich mit (a) dem Transport und der Kristallisation von verschiedenen chemischen Komponenten in hochtemperierten Fumarolen; (b) den thermodynamischen Eigenschaften von georelevanten Fluiden bei hohen Drucken und Temperaturen; und (c) der Bildung von Wasserstoffbrückenbindungen im überkritischen Wasser über einen großen Dichtebereich.

(a) Am Kudryavy Vulkan (Iturup, Kurilen Bogen, Rußland) werden hochtemperierte Exhalationen beobachtet. Dort steht ein andesitisches Magma bei 10 MPa mit zwei weiteren fluiden Phasen im Gleichgewicht. Dabei handelt es sich um eine sehr salzhaltige kochende flüssige Phase und einen wässrigen Dampf. Zwischen Dampf und Flüssigkeit sind die Hydrolyseprodukte stark fraktioniert. Generell sind die thermodynamischen Eigenschaften aller drei fluiden Phasen stark unterschiedlich, was sich auf die Wertigkeit, die Speziation, die Fraktionierung, die Transporteigenschaften von Elementen und deren Ausfällung in Form von Mineralen auswirkt. Basierend auf chemischen Analysen der Gase und deren Kondensate wurde ein physikalisch-chemisches Modell des Transportes und der Abscheidung von Erzen beziehungsweise gesteinsbildender Komponenten angefertigt. Die Ergebnisse der numerischen Simulationen sind mit den Feldbeobachtungen konsistent. Alkali- und Erdalkalimetalle sowie Ga, In, Tl, Fe, Co, Ni, Cu und Zn werden in der Gasphase hauptsächlich in chloridischer Form transportiert. Für Ge, Sn, Pb und Bi sind bei tiefen und mittleren Temperaturen sulfidische und chloridische Komplexe charakteristisch. Be, Al und Si werden in der Form von fluoridischen und oxidischen Komplexen und As und Sb als sulfidische und oxidische Komplexe transportiert. Höher komplexe Oxysulfid- und Oxychloridverbindungen sind für die Elemente Ti, Zr, V, Mo, W und Re typisch. Cd wird bei höheren Temperaturen und Hg über den gesamten Temperaturbereich in elementarer Form transportiert. Mit Hilfe der thermodynamischen Berechnungen konnten einige Gesetzmäßigkeiten des Transport und der Ausfällung von Elementen in hochtemperierten Fumarolen erarbeitet werden.

(b) Unter Verwendung der thermodynamischen „Störungstheorie“ wurde eine Zustandfunktion für Fluide im System H-O-C-N-S-F-Cl-Br-I-B-Si-He-Ne-Ar-Kr entwickelt. Die Zustandfunktion berücksichtigt 98 verschiedene Spezies und besitzt die folgenden Merkmale: 1. die Zustandfunktion basiert lediglich auf vier substanzspezifischen Parameter mit jeweils eindeutiger physikalischer Bedeutung (Dipolmoment, Polarisierbarkeit und die beiden Parametern des Lennard-Jones Potentials); 2. die Zustandfunktion kann zu hohen Drucken und Temperaturen extrapoliert werden; 3. die Eigenschaften der einzelnen Spezies in Mischungen kann aus den Eigenschaften des jeweils reinen Fluids abgeleitet werden, und werden keine zusätzliche Parameter benötigt; 4. weitere Spezies können relativ einfach hinzugefügt werden.

(c) Um die Bedeutung von Wasserstoffbrückenbindungen im überkritischen Wasser über einen weiten Temperatur- und Druckbereich zu untersuchen, wurde eine Serie von Monte-Carlo und Molekulardynamischen Simulationen angefertigt. In Abhängig von Dichte und Temperatur konnte im überkritischen Wasser zwischen drei verschiedenen „Stukturzuständen“ unterschieden werden: 1. die „flüssige“ Struktur ist durch eine völlige Vernetzung von H<sub>2</sub>O-Molekülen über Wasserstoffbrückenbindungen charakterisiert; 2. in der „gasförmigen“ Struktur dominieren einzelne Cluster aus wenigen (<10-20) Molekülen; und 3. in der „intermediären“ Struktur scheinen Cluster jeder Größe vorzukommen. Das Stabilitätsfeld der „intermediären“ Struktur findet man im wesentlichen in einem Dichtebereich von 0.55 bis 0.70 g/cm<sup>3</sup>. Jedoch selbst bei Dichten unter 0.02 g/cm<sup>3</sup> konnten noch deutliche Konzentrationen von Clustern festgestellt werden. Am häufigsten scheinen kettenähnliche Cluster vorzukommen. Die Konzentration von H<sub>2</sub>O-Clustern unterschiedlicher Strukturen scheinen jedoch weder eine Funktion der Dichte noch der Temperatur zu sein.

## Анотация

В диссертации охарактеризованы: а) процессы транспорта и отложения рудных элементов из высокотемпературных вулканических газов; б) термодинамические свойства многокомпонентных флюидов при высоких давлениях и температурах; в) структура и распространенность водородных связей в сверхкритической воде в широком интервале температур и давлений.

(а) При 10 МПа дегазация силикатных расплавов сопровождается отделением солевого расплава как второй флюидной фазы; интенсивными процессами фракционирования продуктов гидролиза между флюидом и расплавом; субвалентным состоянием металлов в газовой фазе и высокой чувствительностью состава флюидной фазы к процессам отложений минеральных сублиматов. С использованием данных химических анализов fumarольных газов и сублиматов вулкана Кудрявый (о. Итуруп, Курильская о-ва) проведено термодинамическое моделирование процессов транспорта/отложения рудных и породообразующих элементов в интервале температур 1373-373К при давлении 1 бар. Было показано, что результаты численного моделирования находятся в хорошем соответствии с полевыми наблюдениями. Так, щелочные и щелочноземелиные металлы, а также, Ga, In, Tl, Fe, Co, Ni, Cu и Zn переносятся в газовой фазе главным образом в виде хлоридных соединений. Сульфидные и хлоридные формы характерны для Ge, Sn, Pb и Bi при низких и средних температурах. Be, Al и Si мигрируют в виде хлоридов и оксидов, в то время как As и Sb- в виде сульфидов и оксидов. Ti, Zr, V, Mo, W и Re переносятся в виде сложных оксихлоридных и оксифторидных молекул. Cd (при высоких температурах) и Hg (во всем температурном интервале) транспортируются в самородном состоянии. При анализе результатов моделирования выявлены и сформулированы основные закономерности транспорта различных химических элементов в газовой фазе в зависимости от температуры при давлении 1 бар.

(б) С использованием термодинамической теории возмущений было сформулировано уравнение состояния (УС) для флюидов в системе H-O-C-N-S-F-Cl-Br-I-V-Si-He-Ne-Ar-Kr. В настоящее время УС включает 98 различных соединений и обладает следующими важными характеристиками. (1) УС включает всего лишь 4 параметра для каждой молекулы, имеющих ясный физический смысл (дипольный момент молекулы, ее поляризуемость и два параметра потенциала Леннарда-Джонса). (2) УС может быть экстраполировано на высокие температуры и давления за пределами имеющихся экспериментальных данных. (3) Свойства многокомпонентных флюидов полностью определяются данными для чистых компонентов. (4) Новые соединения могут быть с легкостью включены в систему. Предложенное УС может быть взято за основу при описании более сложных флюидных систем включая растворы сильных электролитов.

(в) Методами молекулярной динамики и Монте-Карло исследованы топология и распространенность водородных связей в сверхкритической воде в широком интервале температур. В зависимости от P-T условий выявлены 3 различные структурные состояния сверхкритической воды: 1) жидкоподобное, характеризующееся наличием бесконечного кластера водородно-связанных молекул; 2) пароподобное состояние, где присутствуют лишь кластеры небольшого размера, до 10-20 молекул; 3) промежуточное состояние, в котором вода содержит кластеры произвольного размера. Третий структурный тип характерен для интервала плотностей 0.55-0.7 г/см<sup>3</sup>. Было обнаружено, что даже при плотностях менее 0.02 г/см<sup>3</sup> молекулы сверхкритической воды образуют ощутимое количество водородно-связанных кластеров. Детальный анализ структуры кластеров малого размера показал отсутствие корреляции между топологией кластеров и термодинамическими условиями. Показано, что кластеры линейной формы преобладают над остальными конфигурациями.

# Table of Contents

<b>INTRODUCTION</b>	1
<b>CHAPTER I. <u>Geochemistry and Thermodynamics of High Temperature Volcanic Gases</u></b>	
<b>I.1 Natural fluid phases at high temperatures and low pressures</b>	10
• Abstract	11
• Introduction	12
• L–V equilibrium	12
• Hydrolysis of the salt melt	15
• Sublimate minerals formation	17
• Native elements	18
• Vapour phase species	19
• Mass transport by gases	24
• Conclusions	25
• Acknowledgements	25
• References	25
<b>I.2 Evolution of composition of high-temperature fumarolic gases from Kudrjavy Volcano, Iturup, Kuril Islands: The thermodynamic modelling</b>	28
• Abstract	29
• Thermodynamic model	30
• Calculation techniques and thermodynamic data	34
• Thermodynamic analyses of gas and condensates composition	36
• Comparison of the calculated results and the data from natural objects	39
• Forms of element transport	43
• General regularities of gas transport	55
• Conclusions	58
• Acknowledgement	58
• References	59
<b>CHAPTER II. <u>An Equation of State for Complex Mixtures of Non-Electrolytes</u></b>	
<b>II.1 Perturbation theory based equation of state for polar molecular fluids:</b>	
<b>I. Pure fluids</b>	62
• Abstract	63
• Introduction	64
• Thermodynamic model	68
• Limitations of the proposed EOS	71
• Derivation methods of the potential parameters for pure fluids	72
• Results and discussion	74

• Conclusions	86
• Acknowledgement	87
• References	87
• Appendix II.1	92
<b>II.2 Perturbation theory based equation of state for polar molecular fluids:</b>	
<b>II. Fluid mixtures</b>	97
• Abstract	98
• Introduction	99
• Thermodynamic model	100
• Calculated properties in the systems H <sub>2</sub> O-CO <sub>2</sub> , H <sub>2</sub> O-N <sub>2</sub> and H <sub>2</sub> O-CO <sub>2</sub> -CH <sub>4</sub>	102
• Phase separation at high pressures	108
• Conclusions	111
• Acknowledgement	111
• References	112
• Appendix II.2	116
<b>CHAPTER III.      <u>Thermodynamics and Structure of Supercritical Water</u></b>	
<b>III.1 Size and topology of molecular clusters in supercritical water:</b>	
<b>a molecular dynamics simulation</b>	119
• Abstract	120
• Introduction	121
• Molecular dynamics simulations	121
• Results and discussion	123
• Conclusions	129
• Acknowledgement	129
• References	129
<b>III.2 Size, structure, and abundance of molecular clusters in supercritical water</b>	
<b>over wide range of densities: Monte Carlo simulations</b>	131
• Abstract	132
• Introduction	133
• Method of modeling	133
• Results and discussion	134
• References	141
<b>LIST OF PUBLICATIONS</b>	143
<b>ACKNOWLEDGEMENT</b>	144
<b>CURRICULUM VITA</b>	145

Fluid phases are involved in various geological and geochemical processes taking place in the Earth's crust and upper mantle. For example fluids partly control the rheology of rocks. They are present on grain boundaries and components like  $\text{H}_2\text{O}$ ,  $\text{OH}^-$  and  $\text{H}^+$  can be incorporated in minerals altering their physical and chemical properties significantly. In deeper crust, fluids act as solvents dissolving solids and are able to transport and to concentrate dissolved components. Properties of a fluid phase like its density, compressibility or viscosity as well as its speciation vary significant with temperature and pressure. Therefore to explain or to predict a particular geological process the fluid properties must be known in detail.

In fluids where the concentration of one component is substantially higher than the concentrations of any other, the main component is called the solvent and the minor components are the solutes. The nature of the solvent determines the principal properties of the fluid and governs those of the solutes. In most cases water is the main component of natural fluids. By studying the properties of even pure water it is therefore possible to predict the behaviour of natural fluids at various  $P$ - $T$  conditions.

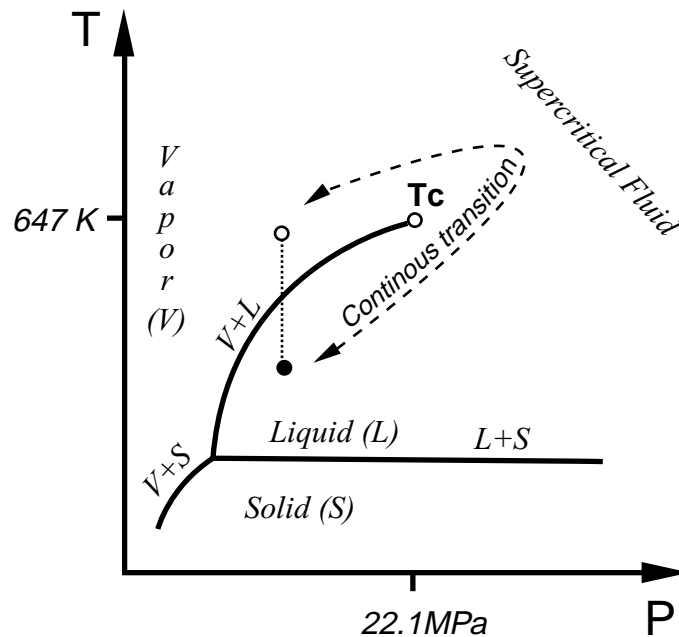


Fig 1. Schematic phase diagram of water.

The schematic phase diagram of water is shown in Fig 1. The lines labelled as  $V+S$ ,  $V+L$  and  $L+S$  separate the stability fields of the solid ( $S$ ), liquid ( $L$ ) and vapour ( $V$ ) phases. The line describing the vapour-liquid equilibrium ( $V+L$ ) terminates at the *critical point* which is located at 647 K and 22.1 MPa. At these conditions the properties of vapour and liquid become indistinguishable. At conditions above either the critical temperature or pressure the fluid phase is referred to as *supercritical*.

If a liquid phase (solid circle in Fig. 1) below the critical pressure is isobarically heated (dotted line) the system will eventually pass the phase transition and the liquid boils to become a vapour (empty circle). Due to the existence of the critical point it is possible, however, to transform a vapour into a liquid and vice versa without passing such a phase transition (dashed line). In this case, no phase transition will be observed, but the properties of the fluid will change continuously. In a closed thermodynamic system, the state of a fluid (e.g. energy, volume, structure) is independent of the way how it was reached. In contrast, geochemical processes often behave as open thermodynamic systems and the  $P$ - $T$  paths of thermodynamic transformation are of principal importance.

Liquid-like water has a strong dielectric constant that is responsible for the high solubility of ionic salts. At ambient conditions, dissolved components are fully dissociated (strong electrolytes, like halogenides of alkali metals), or partially dissociated (weak electrolytes, like carbonates and sulfates of transition metals for example). In contrast the solubility of gases in water is very low at ambient conditions. At high temperatures and pressures relevant to the Earth's crust the dielectric constant of water is substantially lower than its value at ambient conditions. As a consequence, ionic components do not dissociate and preferentially form neutral ionic pairs. The solubility of ionic components in supercritical water decreases with temperature resulting in high temperature fluid immiscibilities. In contrast, non-polar gases usually have non limited solubility in high temperature supercritical water. Pressure also has a strong influence on the phase equilibria in the water-rich fluids. Its effect on the solubility of the non-polar and ionic compounds is the contrary. High pressures may cause the formation of two-phase equilibria in water-non-polar gas mixtures but generally reduce immiscibility in water-salt systems.

An accurate thermodynamic description of natural fluids is rather difficult. For geological purposes there are no unified thermodynamic descriptions of complex multicomponent fluid mixtures. Often, the  $P$ - $T$  range of interest is divided into subspaces and different approaches are applied for liquids, vapours and/or supercritical fluids. However, the existence of a continuous path to transform a vapour into a liquid constrains the form of an

universal *equation of state* (EOS) providing the properties of a fluid. The successful *EOS* must describe both vapour and liquid simultaneous, as well as the vapour-liquid phase equilibrium and the critical point. The general approach should take into account all kinds of interactions between different molecules in the fluid. Some of these types of interaction are specific to particular chemical components. H<sub>2</sub>O molecules, for example, are able to form strong hydrogen bonds, which are to a large degree responsible for its unique chemical and physical properties.

In this thesis the thermodynamic properties of natural fluids at various temperatures and pressures are discussed. It contains three chapters that consist of two articles each. These articles are published together with other scientists. The first chapter covers the geochemistry and the thermodynamics of high temperature hydrothermal systems associated with recent magmatic activities. In the second chapter a general equation of state for multicomponent mixtures of non-electrolytes has been developed. In the third chapter recent investigations concerning hydrogen bonding in supercritical H<sub>2</sub>O are compiled. In the following, a general introduction to these special topics is given.

## **I. Geochemistry and thermodynamics of high temperature volcanic gases**

Gases of complex chemical composition were documented in high temperature hydrothermal systems associated with active volcanism. It is well established that the main components of these high temperature fumaroles are H<sub>2</sub>O, CO<sub>2</sub>, SO<sub>2</sub>, H<sub>2</sub>S, HCl and HF. The surface temperatures of volcanic gases vary significantly and range from 373K to 1213K. The gases are produced by boiling of shallow level magmas which are cooled by mixing with cold meteoric water. This simple model is supported by stable isotope studies (O<sup>18</sup>/O<sup>16</sup>, D/H) which show a strong correlation between the temperature of the gas jets and its fraction of meteoric water.

Because of low density volcanic gases, it is possible to apply a very simplified but still accurate thermodynamic description of such systems. Based on these thermodynamic models one can explain and predict basic peculiarities of the chemical transport and the precipitation of chemical elements in high temperature hydrothermal systems.

Volcanic gases with the highest temperatures bear direct information of the composition of the magmas from which they are released, especially in respect to the volatile and trace element contents leading to ore mineralisation. The contents of ore- and rock-forming elements in the fumaroles vary between 1 ppb to 100 ppm. This seems to be a very

small number but taking the bulk emission of volcanic gases into account, which is estimated to be as much as 200 metric tons per day (CONSPEC measurements on Kudriavy volcano, see the main text for details), the total mass of the ore-forming elements released in few years of degassing is quite large.

Due to the specific chemistry of the volcanic gas jets their associated mineral sublimates are in many aspects different from typical hydrothermal mineralisations. The sublimates form monomineralic clusters of fine grained tiny crystals, mainly chlorides and sulphides, of ore metals with compositions corresponding to the end members of solid solution series. Even elements showing extremely small concentration in the gas (about 1-10 ppb) were found to form own minerals. Some of these phases have not been described as minerals before, because these elements usually enter other phases. For example  $\text{ReS}_2$  is the first observation of a natural Re phase. The component  $\text{ReS}_2$  is usually incorporated in molybdenite ( $\text{MoS}_2$ ). Detailed SEM studies and microprobe analyses of the sublimate samples indicated the presence of native Al and Si, despite the oxygen fugacities were too high for these phases to be stable. To explain these observations the dynamic evolution of the thermodynamic equilibria have to be taken into account.

Field observations on the Kudriavy volcano of the Iturup island (Kuril Island Arc, Russian far east), have been performed by the members of the Laboratory of Hydrothermal Fluids of the Institute of Experimental Mineralogy (Chernogolovka, Russia), namely by Dr. M.A. Korzinsky, Dr. S.I. Tkachenko, and Prof. K.I. Shmulovich between 1988 to 1996. Being a former member of this group the aim of my work was to develop a thermodynamic model of the fumarolic activities on the Kudriavy volcano. In the first part of the first chapter the basic thermodynamic constrains on the low pressure fluid-rock-melts equilibria are discussed. In the second part the thermodynamic models of the mineral precipitation and the chemical evolution of the volcanic gases are described in detail.

## **II. An equation of state for complex mixtures of non-electrolytes**

In order to calculate the chemical equilibrium of geological systems the thermodynamic properties of minerals and fluids are needed. Any equilibrium requires that the chemical potential of each component is equal in all coexisting phases. If the temperature and pressure are chosen as the independent variables the chemical potential ( $\mu_i$ ) of a component  $i$  in a  $N$ -component fluid phase can be expressed by the following sum:

$$\mu_i(T, P, x_i) = \mu_i^o(T) + RT \ln(Px_i) + RT \ln(\phi_i^o(T, P)) + RT \ln(\gamma_i(T, P, x_1, x_2, \dots, x_N)) \quad (1)$$

where  $R$  is the universal gas constant,  $T$  the temperature,  $P$  the pressure,  $x_i$  the mole fraction of component  $i$  in the fluid,  $\phi_i^o$  the fugacity of the pure component  $i$  and  $\gamma_i$  the activity coefficient of the component  $i$  in the mixture. The standard chemical potential  $\mu_i^o(T)$  in eq. (1) describes the chemical potential of the pure fluid consisting of component  $i$  at a pressure of 0.1 MPa (1 bar) as a function of temperature as it would behave like an *ideal gas*. The ideal gas is characterised by molecules which do not interact with others and which do have a volume of zero. The temperature dependence of  $\mu_i^o(T)$  arises from the kinetic energy of molecular motion and from intra-molecular vibrations. It is usually described using the isobaric heat capacities ( $c_p$ ) which are available for many fluid components. In addition for simple molecules, the heat capacities can also be calculated using methods provided by quantum mechanics with an accuracy close to that of the experimental determinations.

As a first approximation, low density fluids can be treated like an ideal gas. The chemical potential of such a fluid can be calculated using the following simplified expression:

$$\mu_i(T, P, x_i) = \mu_i^o(T) + RT \ln(Px_i) \quad (2)$$

However, at conditions relevant to the Earth's crust and upper mantle, fluids are quite dense and therefore their behaviour deviates substantially from that of an ideal gas. These deviations are due to the intermolecular interaction. In order to account for such effects the fugacity coefficient  $\phi_i^o$  and the activity coefficient  $\gamma_i$  are introduced (eq. 1). By definition,  $\gamma_i$  is unity in a pure fluid ( $x_i = 1$ ). Therefore, for pure fluids the last term in eq. (1) becomes zero.  $\phi_i^o$  remains and describes the interaction of molecules of the same kind. In contrast,  $\gamma_i$  is attributed to the interaction of different components in fluid mixtures.

Fugacity and activity coefficients can be directly determined using experimental results of fluid-mineral equilibria or derived from partial molar volumes. In the latter case, however, the volumes must be known along an isotherm from zero to the pressure of interest. The fugacity coefficient of a component  $i$  in the mixture  $\phi_i = \phi_i^o \gamma_i$  is given by the following equation:

$$RT \ln(\phi_i(T, P, x_1, x_2, \dots, x_N)) = \int_0^P \left( \frac{\partial V(T, P, x_1, x_2, \dots, x_N)}{\partial n_i} - \frac{RT}{P} \right) dP \quad (3)$$

An integration can be performed using experimentally determined volumes. It is more convenient, however, to formulate an analytical function with temperature, pressure or volume and composition as variables and to perform the integration analytically. Such a function is called an *equation of state* (EOS).

An EOS can be any function accurately describing the experimental data. However, if the EOS is only empirical, it might be impossible to extrapolate it to high P-T conditions. Therefore it is more advantageous to use a theoretically justified EOS, which is based on the physical nature of fluids. Such EOS can be used in a substantially larger range of temperatures and pressures.

It was mentioned earlier that real gases deviate from the model of an ideal gas due to intermolecular interaction. Would the interaction potential be known, fugacity and activity coefficients could be, at least in principle, calculated using the laws of statistical mechanics. However, the interactions between polyatomic molecules are very complex and a true interaction potential would be too complicated for theoretical considerations. Therefore a model of intermolecular interaction must be simplified in such a way that it is simple enough for theoretical studies but in the same time still reflects the most important characteristics of the molecular interaction.

The first successful attempt to formulate an EOS based on intermolecular interaction is that of van der Waals in 1873. He argued that each molecule in the fluid occupies a finite volume which cannot be penetrated by other molecules and that the forces acting between molecules are proportional to the fluid density. These two assumptions lead to the following EOS:

$$P = \frac{nRT}{V - nb} - \frac{n^2 a}{V^2} \quad (4)$$

where  $n$  is the number of moles and  $a$ ,  $b$  are the van der Waals constants. The intermolecular interaction is described by these van der Waals constants. The parameter  $b$  corresponds physically to a hypothetical volume of the molecule and the  $a$  is a force constant. The van der Waals model is too simple to provide accurate quantitative results over wide  $P$ - $T$  ranges. However this equation is able to mimic qualitatively the main peculiarities of a fluid phase,

like liquid-vapour equilibria and the supercritical state. Since the discovery of the van der Waals equation there have been many attempts to improve it by introducing empirical modifications. These modifications usually include functional temperature and volume dependencies of the van der Waals constants.

Depending on the dominant types of the intermolecular interactions the molecules in a fluid can be classified into three groups:

(1) Ions. These are charged atoms and molecules (e.g.  $\text{Cl}^-$ ,  $\text{Na}^+$ ,  $\text{HCO}_3^-$ , etc.). The behaviour of such components is mainly governed by the Coulomb interaction forces. The ions are formed by dissolving the ionic salts in polar solvents. Such solutions are referred to as *electrolytes*.

(2) Polar compounds. These are polyatomic uncharged molecules with an uneven charge density distribution leading to a permanent dipole, like in  $\text{H}_2\text{O}$ ,  $\text{HCl}$ ,  $\text{NH}_3$ , etc. The nature of dipole-dipole interaction is also electrostatic, but in contrast to ions it depends substantially on the relative orientations of the molecules.

(3) Non-polar molecules. These are neutral molecules without the permanent dipole moment such as noble gases, nitrogen, methane, etc. The main contribution to the interaction of such molecules are *dispersion forces* (also called *London forces*, named after London, who first explained this phenomena in 1930). This type of interaction can be explained on the basis of quantum mechanics. In a system of two molecules, in each moment of time, the molecules have a certain but always changing dipole moment due to fluctuations in the electron cloud. As a result, each molecule induces a dipole moment in the surrounding molecules resulting in attractive forces. Many molecules of this group also possess a permanent quadrupole and/or higher order electric moments, responsible for additional intermolecular interaction.

Frequently, natural fluids are solutions of electrolytes or fluid mixtures of polar and non-polar molecules. The thermodynamic properties of charged species in electrolytes can be generally described by the Debye-Hückel theory. In contrast an universal approach for neutral species does not exist.

In the second chapter, an equation of state for solutions of non-electrolytes has been formulated, based on thermodynamic perturbation theory. This model considers dispersion forces and forces due to dipole-dipole and dipole-induced dipole interactions. The first part of this chapter deals with pure fluids, while in the second part the approach is extended to fluid mixtures. The EOS currently includes parameters for 98 different species and it can be used over a wide range of pressures and temperatures.

### III. Thermodynamics and structure of supercritical water

To develop an accurate thermodynamic model for a fluid it is necessary to understand its structure. In contrast to solids, constituents of fluids are mobile and do not occupy even on average definite places. However, not every relative orientation of molecules is favourable, so that molecular motion is not random, but substantially correlated. This correlation can be characterised by different statistical quantities like the *velocity autocorrelation function*, the *radial distribution function*, the *structure factor* and some other parameters used in solid state physics and as well crystallography.

Both experimental and theoretical methods can be applied to analyse fluid structures. The *structure factor* can be obtained from X-ray and neutron diffraction studies. Parameters of the intra-molecular and intermolecular interactions as well as the structure of molecular clusters can be derived from spectroscopic measurements. These measurements are rather complicated especially at high temperatures and pressures. In many cases, particularly in spectroscopy, the results are equivocal allowing various interpretations. Theoretical computer models can be used as an alternative. Certainly, molecular simulations can not fully substitute experimental measurements, because they need some results from experimental studies as input. Even the most powerful *ab initio* calculations imply a variety of approximations which lead to uncertainties. Nevertheless, such simulations provide a fast and reliable look inside fluid properties, which are sometimes much more detailed than one could expect from conventional experimental methods.

*Molecular dynamic* and *Monte Carlo* simulations are the two most popular techniques which are adopted in fluid modelling. In the first method the Newton equations of motion are solved for each of  $N$  particles in a fluid at constant volume and total energy of the system:

$$m_i \frac{d\vec{r}_i}{dt} = -\nabla_{\vec{r}_i} U, \quad i = 1..N \quad (5)$$

where  $m_i$  is the mass of  $i^{th}$  particle,  $\vec{r}_i$  the radius vector and  $U$  the potential energy of interaction. To accomplish the mathematical problem the so called periodic boundary conditions are applied in such a way, that the space is filled periodically by the images of the central simulation cell. Solving the specified equations one obtains the macroscopic thermodynamic parameters of the system like pressure and temperature as well as the

trajectories of molecular motion, which can be analysed to get the statistical quantities characterising the fluid structure.

In Monte Carlo simulations a *Markov chain* of molecular configurations is generated using random numbers which satisfies a particular statistical distribution. The Markov chain of states is a sequence of trials that satisfies the following two conditions: (a) the outcome of the trial belongs to a finite set of outcomes; (b) the outcome of each trial depends only on the outcome of the trial which immediately precedes it. For example at constant volume and temperature, starting from an arbitrary molecular configuration with the potential energy  $U_{old}$ , the new state is generated by translating and rotating the particles of a fluid at random. If the energy of the new configuration  $U_{new}$  is smaller than the  $U_{old}$ , the new configuration is immediately accepted. If  $U_{new}$  is larger than  $U_{old}$  then the new configuration will be accepted only with a probability which is proportional to  $\exp((U_{old} - U_{new})/kT)$ , where  $k$  is the Boltzmann constant and  $T$  the temperature. Otherwise, the new configuration is rejected and the old configuration is used again. Then the procedure is repeated.

Both molecular dynamics and Monte Carlo methods use various approximations for the potential energy of intermolecular interactions. The choice of intermolecular potentials is of principle importance, because it governs the accuracy of the calculations. Thus each potential model is a compromise between accuracy and simplicity.

In most typical geological fluids, H<sub>2</sub>O is the main component. Therefore to formulate a model for multicomponent mixtures, it is necessary to understand the behaviour of pure water. It is well established that the structure of liquid water at ambient conditions as well as the structure of ice is attributed to strong *hydrogen bonding*. The *hydrogen bond* is a particular type of intermolecular interaction which is observed between hydrogen and an electronegative atom of a different molecule. The physical nature of this effect consists of the fact, that the electron density around a hydrogen atom can be deformed. Therefore, such a hydrogen atom is partly charged and can constructively interact with other molecules. However, up to recently, the important role of hydrogen bonding at high temperatures have been mostly neglected. Molecular dynamic and Monte Carlo simulations have been applied to analyze the extend of hydrogen bonding and the structure of water in a temperature interval between 573 and 773K and densities of up to about 1 g/cm<sup>3</sup>. The results are summarized in two articles constituting the third chapter of the dissertation.

## **Natural Fluid Phases at High Temperatures and low Pressures**

## **Abstract**

Gas phases at low pressures and high magmatic temperatures have certain peculiar properties. The fluid is mainly water vapour, which is usually observed during discharging of crystal magmatic melts. At pressures about 100 bar these peculiar properties include: formation of near 'dry' salt melts as second fluid phase, very strong fractionation of hydrolysis products between vapour and melts, subvalence state of metals during transport processes, and high sensitivity of the gas to conditions of sublimate precipitation. Phase diagram analysis as well as results of field and laboratory experiments are presented in this article. The processes could be a model for industrial technologies to clean wastes from toxic, rare and heavy metals. Transport forms of some elements in volcanic gases are very similar to the species which were formed first in the protosolar nebula.

*Keywords:* gas phase; gas condensates; brines; solution transport; native elements

## 1. Introduction

Gas pollution is a serious problem in modern environments and will only increase in the next century. The principles of geochemical engineering, i.e. the organisation of industrial processes to protect our environment by the same way as natural processes (Schuiling, 1990), could be applied to clean industrial gases from heavy, toxic and rare elements, but we must know how these natural processes are regulated. The best way to investigate these processes is by studying volcanic gases which contain practically all elements, and these compositions can be used as a model for industrial gas pollution. This article is a short review of new field and laboratory results which were obtained from the Kudriavy volcano (andesitic Kuril Island Arc, Russian Far East) from 1988 to 1996, where very hot fumaroles of 170–940°C exist in a stationary regime dating from the last explosion in 1873. The main analytical and mineralogical data for the fumarole gases and sublimates are published by Korzhinsky et al. (1994, 1995, 1996) and Taran et al. (1995); some of the data are still in preparation. These high-temperature fumaroles have relatively constant compositions of 94–95 mol% of H<sub>2</sub>O, about 2 mol% each of various C and S species and 0.5 mol% HCl. A maximal H<sub>2</sub> concentration of 1.2 mol% was found in the hottest fumarole 940°C. Oxygen fugacities were found to fall within the ‘inner’ gas buffer, which mainly depend on the temperature of equilibrium between sulphuric species (SO<sub>2</sub>, H<sub>2</sub>S, S<sub>2</sub>), H<sub>2</sub> and H<sub>2</sub>O. This equilibrium is very near to the Ni–NiO buffer, which can be used for calculations. Calculation of oxygen fugacities using the ratios SO<sub>2</sub>/H<sub>2</sub>S and CO<sub>2</sub>/CO are in good agreement with direct measurements of  $f_{O_2}$  by solid state electrolyte cells (Rosen et al., 1993)

## 2. L–V equilibrium

Degassing of a magmatic melt at low pressure can take place if the magma chamber is in connection with the surface via gas conduits, and the pressure on the uppermost part of the chamber is not too large. Gas viscosity and, consequently, gasodynamic resistance are small and for conduits with a characteristic size of 1–10 cm, the Darcy equation indicates only a pressure of 5–20 bar on the magma surface at intermediate crust chambers, 2–3 km under the volcanic summit. Stable isotope data for D/H and <sup>18</sup>O / <sup>16</sup>O ratios support these estimations, as the boiling of meteoric water and beginning of mixing meteoric and magmatic water take place at 170–180°C, which corresponds to a pressure of 8–10 bar.

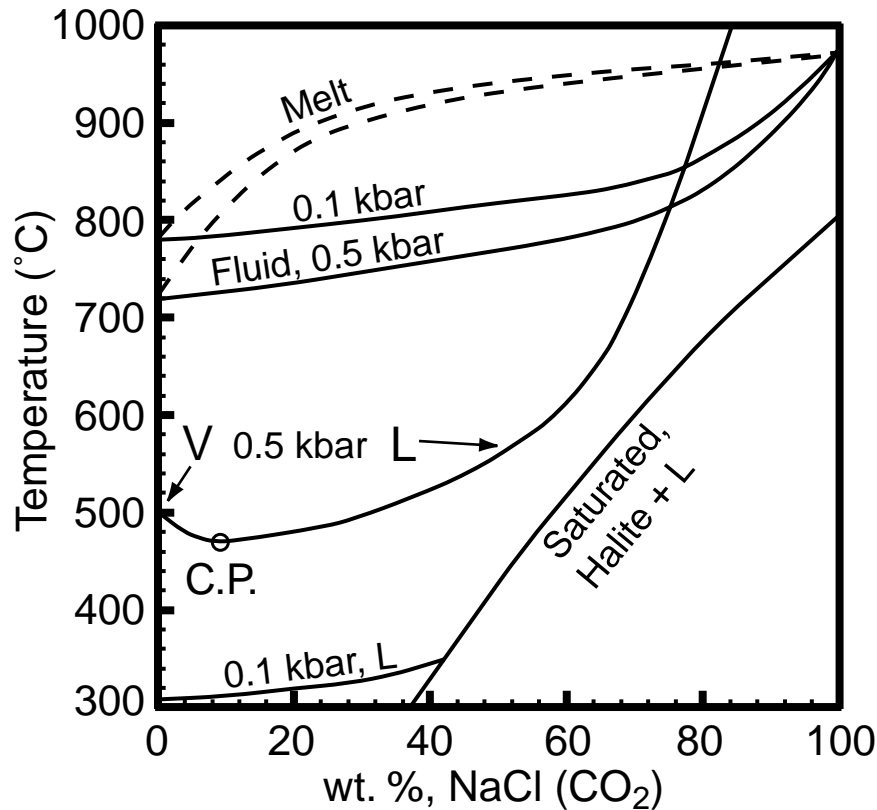


**Fig. 1.** Ratio of fluid components in the fluid and magmatic melt at 0.1 and 0.5 kbar and a simplified phase diagram for the  $\text{H}_2\text{O}$ – $\text{NaCl}$  system. If at low pressure the magmatic melt is in equilibrium with the fluids, then the composition of the brine is going along the saturation curve (Halite+L) and in fact three phases are stable (+V). Above  $800^\circ\text{C}$  the salt melt is practically dry.

At such low pressures and with magmatic temperatures of  $800$ – $1000^\circ\text{C}$ , the phase state and composition of the fluid have some specific properties. Two isobaric diagrams 100 and 500 bar are presented in Fig. 1. Both diagrams are a superposition of the melting diagrams showing the ratio  $\text{H}_2\text{O}/(\text{CO}_2 \text{ or } \text{NaCl})$  in the fluid and coexisting haplogranitic melts, and liquid–vapour–solid diagrams for the system  $\text{H}_2\text{O}$ – $\text{NaCl}$  (Bodnar et al., 1985; Bischoff and Pitzer, 1989). The melting diagrams for 0.5 and 0.1 kbar were obtained via the linear interpolation of data from Keppler (1989) for wet and dry melting haplogranite composition in a  $T$ – $\log P$  space. On the diagram we can see that at 0.5 kbar, magma degassing produces two fluid phases if the magma contains enough Cl, i.e. at a normal  $\text{H}_2\text{O}/\text{Cl}$  ratio near 10. During cooling of these fluid phases their compositions evolves along lines ‘L’ and ‘V’ up to the critical point (C.P.). At a pressure of 100 bar the vapour phase is practically pure water (at  $500^\circ\text{C}$  the NaCl concentration is below 0.02 wt.%) and therefore must be drawn along the ordinate axis. The liquid phase is undersaturated or saturated with respect to solid salt (halite). The diagram was drawn for pure NaCl; in fact, for a magmatic

melt that separates out a salt mix, the temperatures of saturation for the solid salts must be lower. Fluid phase equilibrium shows that at low pressures and high temperatures the normal process of magma degassing must produce two fluids — vapour and dry salt melt.

Field observations support this conclusion. The original melt from the Kudriavy volcano has a Cl content of 0.3 wt.% (melt inclusions, Tzareva, pers. commun., 1994). This is a quite normal concentration for andesitic melts. Water content is not known, but andesitic melts typically contain near 2–3 wt.% of H<sub>2</sub>O. The weight ratio of H<sub>2</sub>O/Cl in the melt is about 10. In gas samples collected from the Kudriavy volcano the mean ratio of H<sub>2</sub>O/Cl is 100–200, and therefore more than 90% of the chlorine is refined within the magma chamber as a salt melt. The viscosity of salt melts is approximately 4–6 orders of magnitude lower than that of andesitic melts and densities are approximately 0.5–0.6 of the andesitic melts. With so large differences in density and viscosity it would seem that salt melts would naturally collect on the surface of degassing magma as a separate phase. Semi-quantitative calculations for the Kudriavy volcano give a volume for the salt melt of approximately  $3 \cdot 10^6 \text{ m}^3$  after 114 years of passive stationary degassing.

It must be remarked that during the degassing process, the magma volume will decrease with the value of partial volume of the discharged gases mainly water from the melt and that this effect will result in additional space for the salt melt. After 114 years of degassing for the assumed primitive geometry of a spherical magmatic chamber with a diameter of 2 km, an ‘empty’ spherical segment with a volume of  $2 \cdot 10^7 \text{ m}^3$  will have been produced. The salt layer takes the form of a disk with a diameter of 1.3 km and a thickness of about 2 m. Of course, in the actual scenario we expect the collapse of overlying rocks. Also the shape of the salt melt will be quite irregular and locally much thicker. These conclusions may be incorrect for basaltic melts, since these melts usually contain 0.5 wt.% water and, at 1200–1300°C, the rate of evaporation (vapour pressure) of the salt can be too large to keep a salt melt on the top of the magma chamber. Formation of salt melts leads to ternary coexisting mobile phases: gas + salt-melt + silicate-melt, which are near equilibrium.

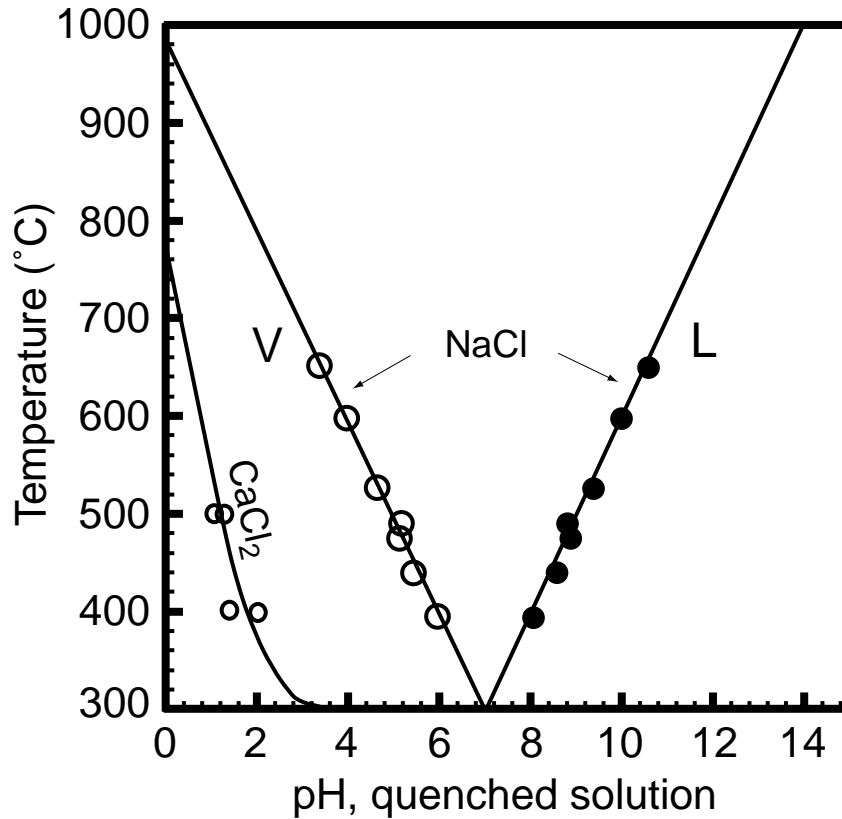


**Fig. 2.** Acid-base fractionation between the liquid and vapour phases in the systems  $\text{H}_2\text{O-NaCl}$  (Vakulenko et al., 1989) and  $\text{H}_2\text{O-CaCl}_2$  calculated from the data of Bischoff et al. (1996). The points for the  $\text{CaCl}_2$  system are our measurements of pH quenched vapour solutions from sampling in the system  $\text{H}_2\text{O-CaCl}_2$  (Tkachenko and Shmulovich, 1992).

### 3. Hydrolysis of the salt melt

At a liquid–vapour equilibrium, if the vapour phase is practically pure water, we should observe the effect of the fractionation of the hydrolysis products between coexisting phases. One such simple reaction is:  $\text{H}_2\text{O} + \text{NaCl} = \text{HCl} + \text{NaOH}$ . At high pressure (above 500 bar) this reaction has a strong shift to the left, but at magmatic temperatures and low pressures (below 100 bar) the process of fractionation begins to play an important role. The fugacities (or vapour pressures) of HCl and NaOH differ significantly, and HCl will go into the vapour phase and NaOH into the liquid phase. This is the principal reason for the acidity of volcanic gases. Experiments and field observations are in good agreement on this point. Fig. 2 presents an extrapolation of data from Vakulenko et al. (1989) by the equation for the pH of the quenched vapour phase:

$$\text{pH} = 9.891 - 9.943 \cdot T(^{\circ}\text{C}) \cdot 10^{-3}$$

Extrapolation from 350–650°C to 1000°C gives for the hottest fumarole on the Kudriavy volcano 940°C a pH of 0.544, which corresponds to 0.51 mol% HCl. The measured concentration of HCl in the condensed fumarole gas phase at the same temperature is 0.46 mol%. Of course, the salt melt is not pure NaCl and the concentrations of HCl from other hot fumaroles (500–900°C) lie between the hydrolysis curves for NaCl and CaCl<sub>2</sub> (Bischoff et al., 1996). This strong hydrolysis reaction and the fractionation products between coexisting fluid phases lead to the formation of contrasting acidity between hydrothermal solutions, i.e. acid springs associated with volcanic areas and albitization of granitic rocks during postmagmatic processes.

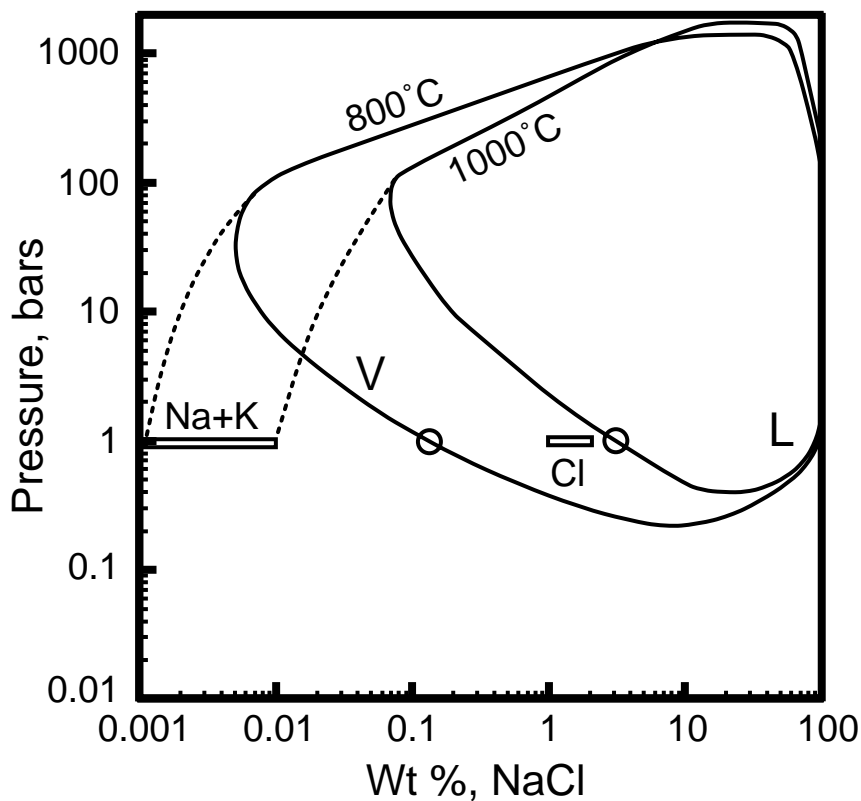


**Fig. 3.** Phase diagram for the system H<sub>2</sub>O–NaCl at 800 and 1000°C. The parts of the curves for pressure near and above 1000 bar from Bodnar et al. (1985), for a pressure near 100 bar are taken from Pitzer and Pabalan (1986). The circles represent ideal mixing between H<sub>2</sub>O and NaCl vapours. Rectangles represent the concentrations of alkali metals and Cl in the condensed gas phases from high temperature fumaroles on Kudriavy volcano.

This effect puts the problem of the description of the H<sub>2</sub>O – NaCl (–KCl, CaCl<sub>2</sub>) systems by the equation of state for binary systems. A diagram of liquid–vapour equilibrium for the H<sub>2</sub>O–NaCl system at 800 and 1000°C is shown in Fig. 3. At a pressure of 1 bar we can expect H<sub>2</sub>O and NaCl vapours to mix ideally. These points are shown by circles. But real Na

and K concentrations in condensed volcanic gases are 2–2.5 orders of magnitude lower than shown in the diagram for the binary system. Evolution of fluid phase compositions as a function of decreasing pressure follows the solid line from a pressure of above 1000 bar down to 200 bar. But below 100 bar the vapour composition is essentially nonbinary. Cation concentrations go along the dashed line, but Cl<sup>-</sup> behaves as if it were still in the binary system. The fluid phase ‘L’, the magmatic melt and the vapour are not so far from equilibrium at temperatures of 700°C and higher. It is obvious why condensed volcanic gases have a low pH, e.g. similar condensed gases from the Kudriavy volcano have a pH < 0. It is the same effect as was found for the system H<sub>2</sub>O–CaCl<sub>2</sub> (Bischoff et al., 1996) and was predicted by Khitarov (1954) nearly half a century ago.

#### **4. Sublimate minerals formation**

Long-time experiments for sublimate formation were done on the Kudriavy volcano. Maximal duration of the runs was nearly 1 month. The sublimates precipitated inside quartz glass tubes, 2/3 of which was exposed above the surface and 1/3 was buried below. In the tubes were found: halogenides (simple as NaCl and KCl), and more complicated (KPb<sub>2</sub>Cl<sub>5</sub>, marshite, CuI, and some fluorine minerals), oxides (SiO<sub>2</sub>, Al<sub>2</sub>O<sub>3</sub>, KReO<sub>4</sub>), sulphides, silicates and sulphates. Detailed description of sublimate mineralogy is beyond the scope of this article, but some remarks need to be made, principally from field observations. The discovery of the ore deposit of Re (Korzhinsky et al., 1994) demonstrates that sublimate minerals can precipitate from the gas phase even at very low metal concentrations. For example, the concentration of Re in the condensed vapour phase was never above 10 ppb, but ReS<sub>2</sub> covers the surface of each 2 rock sample in the zone of these deposits where fumarole temperatures were between 500 and 650°C. In the tubes particles of Au and Pt were found, despite the fact that bulk Au and Pt concentrations were below the detection limit of the ICP analysis - 1 ppb. The main rules for a process of sublimate precipitation were summarised by Schafer (1964, 1981), derived from experimental investigations of chemical reactions with transport through a gas phase. For sublimate minerals many parameters can play an important role, e.g. individual concentrations of both gas species and metallic components, temperature, oxidising state, nucleation of the phase, gas velocity, properties of the precipitation surface, etc.

Our field experiments and laboratory investigations of samples have demonstrated the following.

(1) Sublimate minerals usually form relatively large clusters, with many crystals connected together as a monomineral group. Not only the more abundant minerals form these types of clusters such as  $\text{SiO}_2$ ,  $\text{NaCl}$  and  $\text{KCl}$ , but also aegirin, molybdenite, wurzite,  $\text{KPb}_2\text{Cl}_5$ ,  $\text{K}_3\text{CdCl}_5$ , as well as a series of unknown phases form clusters. One of such unknown phases contains K, Mo and S (analysed by SEM-EDAX). The crystals have a cylindrical shape with near  $1\ \mu\text{m}$  diameter and  $20\text{--}40\ \mu\text{m}$  length, with hollow centres.

(2) While these sublimate phases readily precipitate in quartz glass tubes, graphite tubes remained clean even if they were exposed some days. Mullite ceramic tubes were usually destroyed by rain and wind, while metallic tubes corroded after short runs.

(3) Natural sublimates are mainly the products of reactions between primary phases precipitated from volcanic gases and acid rain. The acid rain was formed by mixing of the volcanic gas components  $\text{HCl}$ ,  $\text{SO}_2$  and  $\text{HF}$  with rain water.

Temperature zonality of the sublimate minerals was found in a number of tubes, but air cooling of the open part of the tubes at the very unstable weather on the Kuril Islands leads to variable temperature gradients inside the tubes and some mineral zones thus overlap. The same results (mixture of temperature zones) were produced by the filling of the tubes by sublimates, thereby decreasing heat flow. One of the tubes was fully blocked by sublimates, with mainly native sulphur at the cold end. More detailed investigations, in which the temperature is controlled, are needed to distinguish the separate precipitation of heavy, toxic and rare metals from the volcanic gases as a function of temperature.

Calculations of sublimate precipitation from real gas compositions usually correspond to the succession of minerals found inside the tubes within a relatively large temperature interval. This large interval is partly caused by air cooling.

## **5. Native elements**

Some native elements are quite common in rocks, e.g. noble metals, sulphur, iron, carbon, etc. In the Russian literature since 1981, many articles were published about quite unusual native metals (Al, Si, Mg, Bi, Pb) in kimberlites, trapps, granites and hydrothermal ore deposits (Novgorodova, 1983). Calculations concerning the stability fields of these metals lead to unrealistic fluid compositions (Novgorodova, 1996), which were practically pure methane or hydrogen. However, the many occurrences of these native metals indicate that the processes forming these minerals are much more common than can be explained from such exotic fluids.

We observed the formation of native Al, Si and Al–Si alloys directly inside the quartz glass tubes (Korzhinsky et al., 1995, 1996), where any contamination was excluded. The gas composition and oxygen fugacities of the gas jets were also measured (Rosen et al., 1993). Real conditions were found to be far from the equilibrium state. For example, for native Al to be stable the oxygen fugacities should be 31 orders of magnitude (!) below the measured value. The stability field for native Si is at an oxygen fugacity 23 orders of magnitude below the Ni–NiO buffer, which corresponds to the measured conditions in the gases. High H<sub>2</sub> contents in volcanic gases or hydrothermal fluids, which could stabilise such metals, were not observed. Therefore we need to find another explanation for the formation of these low oxidising metals. Perhaps, some of them indicate which gas species were present in the fluid at magmatic temperatures and relatively low pressures.

## 6. Vapour phase species

Calculations for metal transport by volcanic gases were done for the Momotombo (Quisefit et al., 1989), Augustin (Symonds et al., 1992) and St. Helens volcanoes (Symonds and Reed, 1993). From the database and software of Symonds and Reed (1993) the main species in those gases for rock-forming and ore elements include chlorides (MnCl<sub>2</sub>, CoCl<sub>2</sub>, CuCl, AgCl, KCl, NaCl, RbCl, CaCl<sub>2</sub>, CsCl), (hydr-)oxides (Fe(OH)<sub>2</sub>, H<sub>2</sub>WO<sub>4</sub>, H<sub>2</sub>MoO<sub>4</sub>), elements (Zn, Cd, Hg), sulphides (PbS, AsS, SbS, AuS), and fluorides (SiF<sub>4</sub>, AlOF<sub>2</sub>). These calculations agree with minerals of incrustations derived from fumarole jets except for Pb: this forms PbS galena in the incrustations, which is not one of the sulphide species in the gases.

Our calculations were done using the database IVTANTERMO (Glushko, 1978) and the gas composition of the hottest fumarole jet 940°C as the most representative magmatic gas. Calculations of gas species included 45 elements: H, O, Cl, F, S, C, Br, Li, Na, K, Rb, Cs, Be, Mg, Ca, Sr, Ba, Al, Ga, In, Tl, Si, Ge, Sn, Pb, As, Sb, Bi, Cu, Zn, Cd, Hg, Ti, Zr, V, Nb, Ta, Cr, Mo, W, Mn, Re, Fe, Co, and Ni. The existing database does not cover all possible species, especially for the rare elements. Therefore, the results are given for the more common mineral species, like sulphides, chlorides, etc.

### 6.1. Elements Li, Na, K, Rb, Cs

At temperatures above 600°C the most abundant transport form of these elements is in the form of metal–Cl. Concentrations of these chlorides depend on the source of the gas phase

and concentrations of the chlorides as defined by precipitation of LiCl, NaCl, KCl, etc. In high-temperature experiments ( $>700^{\circ}\text{C}$ ) NaCl and KCl are the most abundant mineral sublimates and they form the inner rim in the sampling tubes.

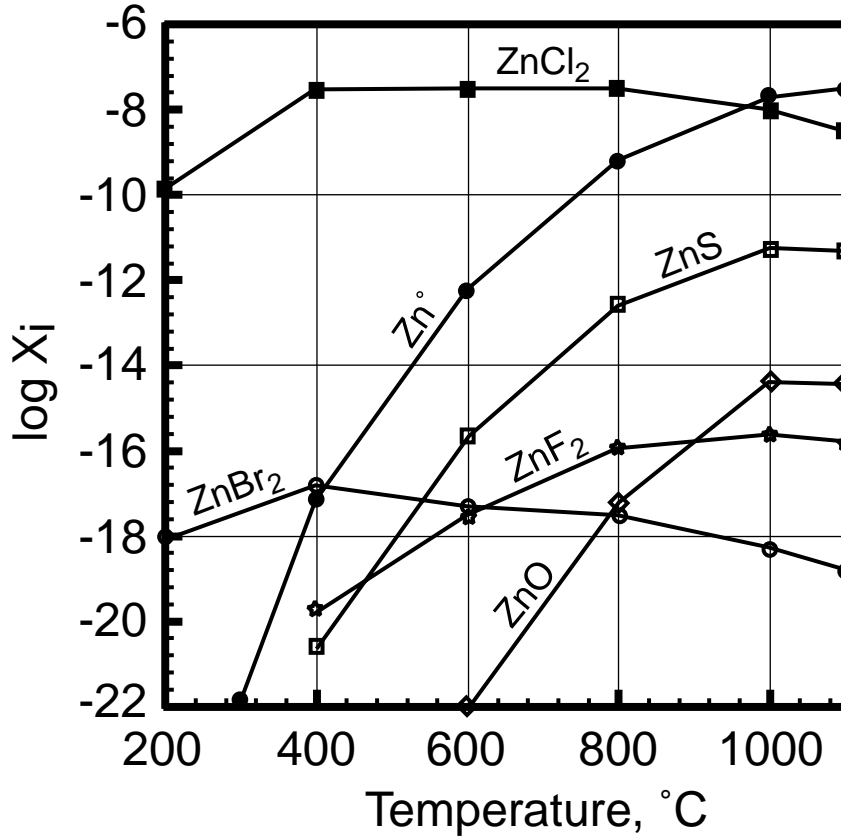


**Fig. 4.** Transport forms of Zn by volcanic gases at 1 bar and the bulk chemical composition of the gas from Taran et al. (1995, table 3, sample № F1292). At  $1000^{\circ}\text{C}$  and above,  $\text{Zn}^0$  is the main transport species.

## 6.2. Elements Cu, Zn, Cd, Pb

At  $T > 1100^{\circ}\text{C}$  the main transport form of Cu could be  $\text{Cu}^0$ , but below  $400^{\circ}\text{C}$  its main form is dimeric  $\text{Cu}_2\text{Cl}_2$ . Precipitation of Cu-bearing sublimates beginning below  $800^{\circ}\text{C}$  is consistent with experimental data. In the tube from a  $750^{\circ}\text{C}$  fumarole were found cubanite,  $\text{CuFe}_2\text{S}_3$ , and marshite, CuI. Iodine forms were not included in the calculations. It should be remarked here that the concentration of iodine in the fumarole gases is greater than the total concentration of all ore and rare elements. So, cation transport via iodine could be very important for mass transport at high temperatures and low pressures. Iodine transport is the usual transport mechanism in industrial processes for purification using a gas phase (Schafer, 1964). For Zn below  $1000^{\circ}\text{C}$  the main form is  $\text{ZnCl}_2$ , but above  $1000^{\circ}\text{C}$  Zn is transported as a

metal,  $Zn^0$ . This is illustrated in Fig. 4. Wurzite was a common sublimate mineral in our tubes, but the  $ZnS$  concentrations were smaller than  $ZnCl_2$  and  $Zn^0$  at all temperatures. The same behaviour was found for  $Cd$ , but here the change of transport form, from native metal to chloride, is at  $600^\circ C$ . According to calculations and observations, below this temperature  $Cd$  is precipitated as grinokite and  $K_3CdCl_5$ . For  $Pb$  above  $600^\circ C$  the dominant form is  $PbS$ , below  $600^\circ C$  the dominant form is  $PbCl_2$ .

### 6.3. Elements As, Sb, Bi, Hg

The transport forms of  $As$  change with temperature. Up to  $600^\circ C$   $As_4S_4$  and  $As_4O_6$  dominate in the gas phase. Above  $600^\circ C$  the main form is  $AsS$ , and only above  $1100^\circ C$  does the oxide,  $AsO$  dominate. The main transport forms of  $Sb$  change from  $SbF_3$  below  $300^\circ C$ , to  $Sb_4O_6$  up to  $600^\circ C$  and  $SbS$  above  $600^\circ C$ . At relatively low temperatures  $Bi$  and  $Hg$  are transported as chlorides.  $BiCl$  dominates below  $600^\circ C$ . However,  $HgCl_2$  is an artefact, since this form dominates below  $100^\circ C$ , where water will condense and a gas phase does not exist. At high temperatures  $Bi$  and  $Hg$  are transported as elements.

### 6.4. W and Mo

The concentrations of these metals in the fumarole gases are 3–60 ppb for  $W$  and 2–300 ppb for  $Mo$ . The main transport forms are  $WCl_2O_2$  at all temperatures, and  $MoCl_2O_2$  below  $700^\circ C$  and  $H_2MoO_4$  above. However the database for these elements is very limited.

### 6.5. Re, In and Tl

These elements are interesting because  $Re$  and  $In$  minerals were discovered in the natural sublimates as well as in ore deposits of  $ReS_2$ . The database is also limited for  $Re$ . For all temperatures  $ReClO_3$  was indicated to be the main form. But ore deposits contain  $Re$  sulphide and in the sampling tubes we only found  $KReO_4$ . Species of  $In$  are more simple. The dominant forms are  $InCl_3$  below  $350^\circ C$ ,  $InCl_2$  between  $350$  and  $600^\circ C$  and  $InCl$  at higher temperatures. In some condensed gas samples, very high concentrations of  $Tl$  were found. Usually concentrations are between 60 and 200 ppb, but in one fumarole at a temperature of  $605^\circ C$  we found concentrations of  $Tl$  near 4 ppm. At all gas temperatures the main transport form for  $Tl$  is  $TlCl$ .

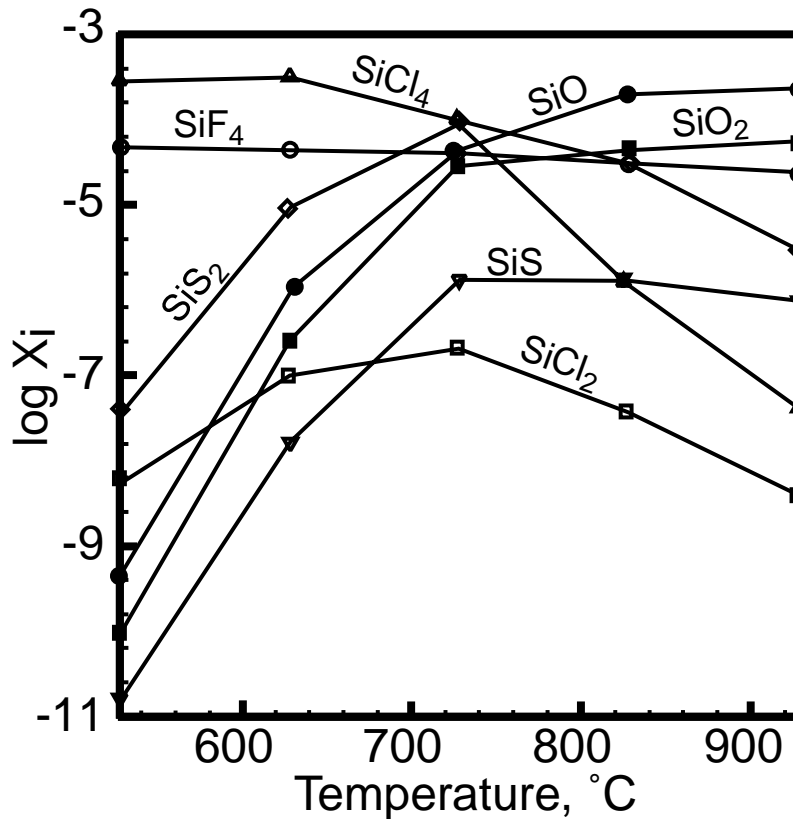


**Fig. 5.** Transport species of silicon at high temperatures and 1 bar (Shmulovich, et al., 1997) calculated for single homogeneous fluid phase using the database IVTANTERMO. Only seven species which have a concentration greater than  $10^{-10}$  are presented. At  $T > 750^\circ\text{C}$  the main transport species is silicon monoxide (SiO).

### 6.6. Si and Al

These elements are the most interesting since they were found as native elements in natural sublimates and in the sampling tubes. The result of thermodynamic modelling for the Si species in a gas phase at 1 bar is presented in Fig. 5 (Shmulovich, et al., 1997). At temperatures below  $750^\circ\text{C}$ , the main transport form is  $\text{SiCl}_4$ .  $\text{SiF}_4$  concentrations are an order of magnitude smaller. Above  $750^\circ\text{C}$  the main transport form is monoxide, SiO, and to a lesser extent  $\text{SiO}_2$ . Transport of this element in the subvalency state is quite usual for chemical transport reactions (Schafer, 1964), but as far as we know this has never been proposed for natural hydrothermal fluids. These results give the key to the understanding of the process of native element formation at high oxygen fugacity. As silicon monoxide does not have a solid state, the cooling of the gas must lead to the precipitation of excess Si. Normally, the  $\text{SiO}_2$  would be precipitated and at high temperatures we observe perfect crystal polymorphs of tridimite or cristobalite, sometime with aegirine needles. But, if salts were precipitated beforehand and formed salt melt drops on the wall of the sampling tube or gas conduits, the disproportionation reaction could be realised on the surface of the drops. The reaction  $2\text{SiO} =$

Si + SiO<sub>2</sub> can precipitate native Si if the Si is protected from oxidation via an oxygen-free medium. Under the protection of a salt melt or salt crystals the metal can remain unoxidized after cooling. We really observed these native metals (Al, Si) in salt ‘shirts’. Experiments with salt traps on the high-temperature fumaroles, analysed by electron microprobe after the salt mixture (NaCl + KCl) was washed out, showed a rest powder with a Si/O ratio of 1:1. The transport forms of Al from calculations is inconsistent with the sublimate mineralogy Fig. 6. At temperatures below 700°C the main form is NaAlF<sub>4</sub> (or KAlF<sub>4</sub>, dependent on

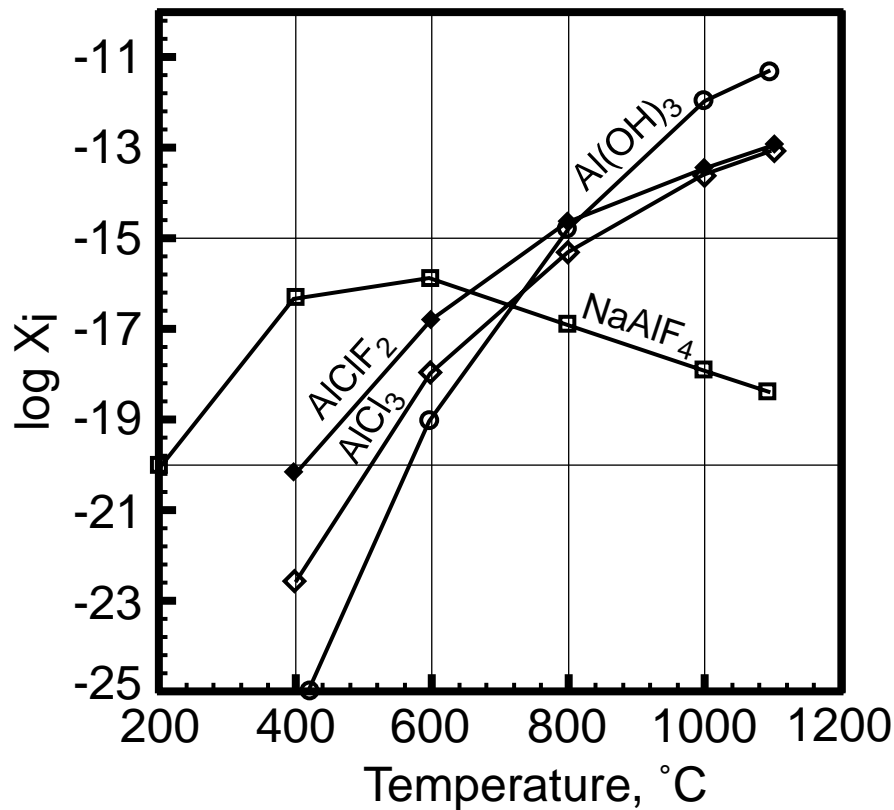


**Fig. 6.** The principal transport forms for Al in the fumarole gas, as in Fig. 3 and Fig. 4. Four main species of 134 which were included in a minimisation procedure are presented. Al has a normal valence of 3+ in all these species, none of which can precipitate the native metal.

the K/Na ratio), and above 700°C Al(OH)<sub>3</sub>. Our database contained 134 Al species, which were included in the procedure of minimisation of the Gibbs free energy (Shvarov, 1988). The diagram in Fig. 6 shows the four main forms; all others have negligible concentrations. The main Al transport forms in this diagram look quite reasonable but we could not get the native metals from these species. Yet we found more than fifteen Al particles in the sampling tubes as a natural sublimate on the Kudriavy volcano and many of them have been described in the literature (review in Novgorodova, 1983). Perhaps the precision of the thermodynamic

database that we used is not enough, or this process does not depend on the main forms but on Al species which have concentrations some orders of magnitude lower than the main species. This last version does not seem reasonable. Very rough calculations for NaCl and KCl suggest that 0.5% of the amount that theoretically goes through the tubes should precipitate. If  $\text{AlCl}^0$  has a concentration of 5 orders of magnitude below  $\text{Al(OH)}_3$ , it would be very difficult to determine the quantity of the disproportionation products.

## 7. Mass transport by gases

During the 1995 field season on the Kudriavy volcano COSPEC measurements were done by S. Williams and T. Fisher (Arizona State University, pers. commun., 1995). The bulk emission of magmatic gases was estimated at about 2000 metric tons per day. Surface mapping of the fumarole fields and measurement of gas velocities in the jets and in the steam areas have suggested that this value is an order of magnitude higher. However, these measurements have included meteoric as well as magmatic water. In fact, the correlation spectrometer (COSPEC) measured the diminution of sky ultraviolet radiation by  $\text{SO}_2$ , and the total emission of magmatic gases was calculated from the ratio of  $\text{SO}_2/\text{H}_2\text{O}$  in the hottest fumaroles which is more representative of magmatic gas. From analyses of condensed gases it follows that metal concentrations do not depend on the temperatures of the fumaroles as long as temperatures are above  $350^\circ\text{C}$ . This means, that calculations involving element exchanging could increase by one order of magnitude if we take into account the remobilization of elements by meteoric water.

The total quantity of the elements which were transported via the gas phase from the magma chamber after the last explosion in 1883 has been calculated as a minimal value and can be increased one order of magnitude. These values in metric tons are: for halogens Cl  $2 \cdot 10^7$ , Br  $1.5 \cdot 10^3$ , I  $4.5 \cdot 10^3$ ; for the ore metals Cu 45, Pb 620, Zn 500, Sn 80, W 25, Mo 90, Se 65, As 450, Hg 20, Tl 110 and Bi 60.

Of course, the majority of these elements and their compounds dissolve in ocean water and the contribution of passive volcanic gas emission to the atmosphere is not as important as that of industrial emission and catastrophic explosions. However, in order to understand the sequence of formation of ore deposits, we must also take into account L–V fractionation and gas transport as the model is developed.

## 8. Conclusions

Long-term investigations of sublimate precipitation of main and trace elements using optic, SEM and microprobe studies, analysis of volcanic gases and geochemical modelling of transport forms have been carried out on the Kudriavy volcano, which produces approximately 2000 tons/day of magmatic gases. The sublimates precipitated in quartz glass tubes as practically monomineral clusters. This process could be a model for industrial technologies to separate toxic, rare and heavy metals from waste. These low-density gases transport elements at high  $T$  and low  $P$  mainly as halogenides and/or as hydroxides. Some of the elements have a low valency state, and can be precipitated by regulation of the oxygen fugacity.

The transport forms for many elements which were produced by geochemical modelling of a real volcanic gas have very much in common with the list of first species which condensed out of the protosolar nebula at the beginning of the formation of our star (Word, 1976). In interplanetary space, at high temperatures (1200–2000 K) and low densities (low pressures), the same species were produced as the ones found in volcanic gases according to our calculations. This suggests that perhaps the process of sublimate formation could be used as an experimental model for the formation of more complex molecules and crystalline phases in the nebula as well.

## Acknowledgements

We are thankful for the support of the fieldwork on the Kudriavy volcano by the Russian Fund of Basic Investigations, the Russian Ministry of Sciences and Technology and, furthermore, the organising committee of the Geochemical Engineering Symposium for the opportunity to participate. Many thanks to Daniel Harlov and Hans Zijlstra for corrections of our terrible English.

## References

Bischoff, J.L., Pitzer, K.S., 1989. Liquid–vapor relations for the system NaCl–H<sub>2</sub>O: summary of the PTX surface from 300 to 500°C. *Am. J. Sci* 289, 217–248.

- Bischoff, J.L., Rosenbauer, R.J., Fournier, R.O., 1996. The generation of HCl in the system  $\text{CaCl}_2\text{-H}_2\text{O}$ : vapor–liquid relations from 380–500°. *Geochim. Cosmochim. Acta* 60, 7–16.
- Bodnar, R.J., Burnham, C.W., Sterner, S.M., 1985. Synthetic fluid inclusions in natural quartz, III. Determination of phase equilibrium properties in the system  $\text{H}_2\text{O-NaCl}$  to 1000° and 1500 bars. *Geochim. Cosmochim. Acta* 49, 1861–1873.
- Glushko, V.P. (Editor), 1978–1982. *Thermodynamic Properties of Individual Matters*. Moscow, v. 1–4, (Database IVTANTERMO).
- Keppler, H., 1989. The influence of the fluid phase composition on the solidus temperatures in the haplogranite system  $\text{NaAlSi}_3\text{O}_8\text{-KAlSi}_3\text{O}_8\text{-SiO}_2\text{-H}_2\text{O-CO}_2$ . *Contrib. Mineral. Petrol.* 102, 321–327.
- Khitarov, N.I., 1954. Chlorides of sodium and calcium as a possible source of acid media at depth. *Dokl. Akad. Nauk SSSR* 94 (3), 519–521.
- Korzhinsky, M.A., Tkachenko, S.I., Shmulovich, K.I., Taran, Y.A., Steinberg, G.S., 1994. Discovery of a pure rhenium mineral at Kudriavy volcano. *Nature* 369 (6475), 51–52.
- Korzhinsky, M.A., Tkachenko, S.I., Shmulovich, K.I., Steinberg, G.S., 1995. Native Al and Si formation. *Nature* 375 (6532), 544.
- Korzhinsky, M.A., Tkachenko, S.I., Bulgakov, R.F., Shmulovich, K.I., 1996. Condensate compositions and native metals in sublimates of high temperature gas streams of Kudriavy volcano, Iturup Island (Kuril Islands). *Geochem. Int.* 34 (12), 1175–1182.
- Novgorodova, M.I., 1983. *Native Metals in Hydrothermal Ores*. Nauka, Moscow, 287 pp.
- Novgorodova, M.I., 1996. Native magnesium and the problem of its genesis. *Geochem. Int.* 34 (1), 36–44.
- Pitzer, K.S., Pabalan, R.T., 1986. Thermodynamics of NaCl in steam. *Geochim. Cosmochim. Acta* 50, 1445–1454.
- Quisefit, J.P., Toutain, J.P., Bergametti, G., Javoy, M., Cheynet, B., Person, A., 1989. Evolution versus cooling of gaseous volcanic emission from Momotombo volcano, Nicaragua thermochemical model and observations. *Geochim. Cosmochim. Acta* 53, 2591–2608.
- Rosen, E., Osadchii, E., Tkachenko, S.I., 1993. Oxygen fugacity directly measured in fumaroles of the volcano Kudriavy Kuril Isles. *Chem. Erde* 53, 219–226.
- Schafer, H., 1964. *Chemische Transportreaktionen*. Verlag Chemie, Weinheim, Bergstr. (Russian version: Mir, Moscow).

- Schafer, H., 1981. Chemical transport reactions in gases and some remarks concerning melts and fluid phases. In: Chemistry and Geochemistry of Solutions at High Temperatures and Pressures, Proc. Nobel Sympos., Karlskoga, 1979, Phys. and Chem. Earth, pp. 409–417.
- Schuiling, R.D., 1990. Geochemical engineering: some thoughts on a new research field. *Appl. Geochem.* 5, 251–262.
- Shmulovich, K.I., Vakulenko, A.G., Shiryaev, A.A., 1997. Formation of Native Silicon in Sublimates of the Kudryavyi Volcano, Iturup Island, Kurils Islands, *Dokl. Ross. Akad. Nauk*, 354 (6), 800–803.
- Shvarov, Y.V., 1988. Calculation of equilibrium compositions of the hydrogeochemical system via Gibbs free energy minimization. In: Kraynov, S.R. (Ed.), *Methods of Geochemical Modeling and Forecasting in Hydrogeology* (in Russian). Nedra, Moscow
- Symonds, R.B., Reed, M.H., 1993. Calculation of multicomponent chemical equilibria in gas–solid–liquid system: calculation methods, thermochemical data, and application to studies of high-temperature volcanic gases with examples from Mount St. Helens. *Am. J. Sci.* 293, 758–864.
- Symonds, R.B., Reed, M.H., Rose, W.I., 1992. Origin, speciation and fluxes of trace element gases at Augustino volcano, Alaska: insights into magma degassing and fumarole processes. *Geochim. Cosmochim. Acta* 56, 633–657.
- Taran, Y.A., Hedenquist, J.W., Korzhinsky, M.A., Tkachenko, S.I., Shmulovich, K.I., 1995. Geochemistry of magmatic gases from Kudriavy volcano, Iturup, Kuril Islands. *Geochim. Cosmochim. Acta* 59, 1749–1761.
- Tkachenko, S.I., Shmulovich, K.I., 1992. Liquid–vapour equilibria in the system water–salt NaCl, KCl, CaCl<sub>2</sub>, MgCl<sub>2</sub> at 400–600°. *Dokl. Akad. Nauk SSSR* 326 (6), 1055–1059.
- Vakulenko, A.G., Alekhin, Y.V., Razina, M.V., 1989. Solubility and thermodynamic properties of alkali chlorides in steam. *Proc. II Int. Symp. Properties of Water and Steam*, Prague, pp. 395–401.
- Word, W.R., 1976. Formation of solar system. In: Avrett, E.A. Ed., *Frontiers of Astrophysics*. Harvard University Press, Cambridge, pp. 10–48.

**Evolution of Composition of High-Temperature Fumarolic Gases  
from Kudryavy Volcano, Iturup, Kuril Islands:  
Thermodynamic Modelling**

## **Abstract**

Based on the chemical analyses of gases and condensates from high-temperature fumaroles of the Kudryavy volcano, we performed a thermodynamic simulation of transportation and deposition of ore- and rock-forming elements in high-temperature volcanic gases within a temperature range of 1373-373 K at 1 bar pressure. The results of our numerical simulation of mineral deposition from gases are consistent with the data of field observations. Alkali and alkali earth metals, Ga, In, Tl, Fe, Co, Ni, Cu, and Zn are mainly transported as chlorides in the gas phase. Sulfide and chloride forms are characteristic of Ge, Sn, Pb, and Bi at intermediate and low temperatures. Be, Al, and Si migrate as fluorides and oxides, while As and Sb, as sulfides and oxides. More complex, oxyfluoride and oxychloride species are typical of Ti, Zr, V, Mo, W, and Re. Cd (at high temperatures) and Hg (within the whole temperature range) are transported in the neutral form. Our calculations revealed some general regularities in the variation of element species in the gas phase at a low (1 bar) pressure versus thermodynamic conditions.

High-temperature volcanic gases bear important information on the composition of volatile components in shallow-level magma chambers. At present, the composition of fumarolic gases from volcanoes in most of the geotectonic structures [1, 2, etc.] is well known. H<sub>2</sub>O, CO<sub>2</sub>, SO<sub>2</sub>, H<sub>2</sub>S, HCl, and HF are main constituents of these gases. The content of ore- and rock-forming elements in the condensates of volcanic gases usually ranges from 1 ppb to 10 ppm [3-7, etc.], which attests to their low solubility in the fluid and small coefficients of their fractionation between the silicate melt and the gas phase at low pressure. Studies of the volcanic sublimates [5, 7-11, etc.] resulted in the determination of their mineral composition and thermal conditions of deposition of different components from gases flowing in volcanic channels. However, knowledge of element species in volcanic gases is necessary for understanding the processes operated on the gas cooling, deposition of solid phases, and interaction between gases and surrounding rocks. The modern techniques for determining the modes of element occurrence in gases and liquids are based on spectrometry. These techniques are too complicated to be applied in the field investigations; that is why such data are usually obtained through thermodynamic calculations. The calculations performed for Momotombo [7], Augustine [12], and Mount St. Helens [13] volcanoes enabled to describe quantitatively the processes and reactions in the volcanic gas-rock-sublimate system and to determine the sources of different elements in the gas phase.

This paper presents the results of thermodynamic simulation of cooling of a high-temperature gas in the Kudryavy volcano. The study was aimed at:

1. Construction of a physico-chemical model for transportation and deposition of substances in the gas phase;
2. Comparison of the obtained results with the field data for checking the consistency of the thermodynamic data and the correlation between the thermodynamic model and natural process;
3. Calculation of the element species in the high-temperature fumarolic gases and determination of general regularities in the gas transport.

## **THERMODYNAMIC MODEL**

The following information is necessary for constructing a thermodynamic model that approximates the changes in the composition of fumarolic gases during their cooling and the deposition of solid phases from the supersaturated gases:

1. Complete chemical composition of the gases including major components and trace

- elements;
2. Initial and final parameters of gas conditions (temperature and pressure);
  3. Mechanisms of interaction of volcanic gases with the host rocks and newly formed mineral phases;
  4. Component composition of the gas phase. Set of possible solid phases in the system. Thermodynamic data for these compounds.

Table 1. Concentration of the major gas components from the highest temperature fumarole of the Kudryavy volcano [14], mol %

Sample	T, K	Lg[ $f_{O_2}$ ]	H <sub>2</sub> O	H <sub>2</sub>	CO <sub>2</sub>	CO	SO <sub>2</sub>	H <sub>2</sub> S	COS	S <sub>2</sub>	HCL	HF
F1292	1213	-10.93	94.61	1.15	1.78	0.034	1.79	0.18	0.0002	0.01	0.46	0.03

Chemical composition of the major gas components and trace-element contents in the condensate for the highest temperature (1213 K) fumarole are taken from [14] and presented in Tables 1 and 2a.

The latest, reliably known eruption of the Kudryavy volcano occurred in 1883 [15]; it was probably accompanied by an eruption of basaltic andesite lavas [16]. Consequently, we may assume that the melt in the shallow-level magma chamber of the Kudryavy volcano is also basaltic andesite in composition. Since the temperatures of water-saturated solidus for basaltic andesite and basalts are close [17], the temperature evolution of fumarolic gases in the volcano must occur within the range of 1373-373 K.

According to geophysical data (G.S. Shteinberg, personal communication), the shear-wave and compressional-wave attenuation is recorded at a depth of ~300 m beneath the crater of the Kudryavy volcano. It may attest to the presence of melt in a conduit at this depth. In the process of gas emanation from the melt surface, the total pressure is mainly determined by the hydrostatic pressure, i.e., by the height of the gas column. The pressure at 1 km depth, calculated from a barometric formula, is 2 bar. Therefore, without introduction of any substantial errors in the model, we may suppose that the cooling of the fumarolic gases occurs at a constant pressure of 1 bar. Due to the fact that the last eruption took place more than 100 years ago and the gas temperature has not changed significantly for the last 6 years [18], we may assume that the degassing goes on in a steady-state mode. Probably, the gas flows along well-formed conduits, whose walls are composed of altered rocks, the latter being in a local equilibrium with the gas flow. Therefore, any interaction between the gases and the wall rocks could be omitted, and, thus, the thermodynamic model becomes simpler.

Table 2. Trace elements in the gas and condensate

Element	a	b	c	Element	a	b	c	Element	a	b	c
<b>Si</b>	79100	0.0459	24	Cd	230	230	$1.9 \times 10^{-4}$	Sc	60	60	$2.4 \times 10^{-3}$
<i>Na</i>	6100	3856	1.94	Pb	1250	1250	$8 \times 10^{-4}$	Cr	130	128	$2 \times 10^{-2}$
B	33000	32998	$5 \times 10^{-6}$	Zr	980	975	$1 \times 10^{-2}$	W	30	30	$1 \times 10^{-4}$
<i>K</i>	5620	4605	$8.3 \times 10^{-4}$	Mo	200	200	$1.4 \times 10^{-4}$	Ge	27	27	$1.5 \times 10^{-4}$
<b>Al</b>	3900	0.0468	8.76	<i>Mn</i>	90	52	$2 \times 10^1$	<i>Li</i>	30	25	$1.5 \times 10^{-3}$
I	5400	5400	$5 \times 10^{-5}$	<b>Sr</b>	10	1	$4.4 \times 10^{-4}$	Sb	79	79	$1 \times 10^{-4}$
Br	750	750	$3 \times 10^{-4}$	Cu	270	269	$1 \times 10^{-4}$	Co	6	6	$4.5 \times 10^{-3}$
<i>Fe</i>	7300	5503	8.56	Sn	<sup>e</sup> 140	140	$1.5 \times 10^{-4}$	Te	10	10	$1 \times 10^{-7}$
<b>Ca</b>	2000	12	6.72	Bi	40	40	$7 \times 10^{-7}$	Hg	28	28	$9 \times 10^{-6}$
P	30800	30711	$1.4 \times 10^{-4}$	Se	170	170	$5 \times 10^{-6}$	Cs	10	10	$1 \times 10^{-4}$
<b>Mg</b>	500	120	4.5	Rb	45	43	$4.5 \times 10^{-3}$	Hf	10	10	$1 \times 10^{-4}$
As	1200	1200	$2 \times 10^{-4}$	<i>Ba</i>	150	142	$3 \times 10^{-2}$	Ce	2	2	$4.5 \times 10^{-4}$
Zn	3100	3081	$1.3 \times 10^{-2}$	<b>Ti</b>	160	1	$9 \times 10^{-1}$	Re	8	8	—
Tl	140	140	$2 \times 10^{-5}$	Ni	410	408	$1.6 \times 10^{-2}$	Th	1	1	$3 \times 10^{-4}$

Note: (a) The composition of gas condensate from the highest temperature fumarole of the Kudryavy volcano in ppb (1213 K, sample F1292 [14]); (b) the calculated equilibrium composition of gas condensate for sample F1292 in ppb (see description in the text); (c) average composition of terrestrial basaltic andesite after Vinogradov [24] in ppb. Boldfaced symbols refer to the elements occurring in the gas phase due to the presence of rock microparticles. Ordinary symbols depict elements transported as volatile compounds. Symbols of elements with an intermediate type of transportation are italicised.

Table 3. The species of gas solution included in the thermodynamic calculation [20].

H <sub>2</sub> O	AlO <sub>2</sub> H	BeF <sub>2</sub>	Ca(OH) <sub>2</sub>	CrO <sub>3</sub> H <sub>3</sub>	Fe	GeCl <sub>3</sub>	InCl	(LiOH) <sub>2</sub>	MoO	PbCl <sub>4</sub>	SbF <sub>3</sub>	SnF <sub>2</sub>	TiF <sub>4</sub>	WO <sub>3</sub>
CO <sub>2</sub>	Al(OH) <sub>3</sub>	Be <sub>2</sub> F <sub>4</sub>	Cd	CrO <sub>4</sub> H <sub>2</sub>	FeCl <sub>2</sub>	GeCl <sub>4</sub>	InCl <sub>2</sub>	LiH	MoO <sub>2</sub>	PbBr <sub>4</sub>	SbBr <sub>3</sub> *	SnF <sub>3</sub>	Tl	H <sub>2</sub> WO <sub>4</sub>
CO	NaAlF <sub>4</sub>	BeBr	CdBr <sub>2</sub>	Cs	FeCl <sub>3</sub>	GeF	InCl <sub>3</sub>	MgCl <sub>2</sub>	MoO <sub>3</sub>	PbO	SbO	SnF <sub>4</sub>	TlCl	WBr <sub>5</sub>
CH <sub>4</sub>	KAlF <sub>4</sub>	BeBr <sub>2</sub>	CdCl	Cs <sub>2</sub>	Fe <sub>2</sub> Cl <sub>4</sub>	GeF <sub>2</sub>	In <sub>2</sub> Cl <sub>6</sub>	(MgCl <sub>2</sub> ) <sub>2</sub> *	H <sub>2</sub> MoO <sub>4</sub>	PbS	Sb <sub>4</sub> O <sub>6</sub>	SnO	Tl <sub>2</sub> Cl <sub>2</sub>	WBr <sub>6</sub>
H <sub>2</sub> S	As	BeO	CdCl <sub>2</sub>	CsCl	FeF <sub>3</sub>	GeF <sub>3</sub>	InF	MgClF	MoS <sub>2</sub>	Rb	SbS	SnO <sub>2</sub>	TlF	WS <sub>2</sub>
HBr	As <sub>2</sub>	Be <sub>2</sub> O <sub>2</sub>	CdOH	Cs <sub>2</sub> Cl <sub>2</sub>	Fe(OH) <sub>2</sub>	GeF <sub>4</sub>	InF <sub>2</sub>	MgF <sub>2</sub>	NaCl	RbCl	Sb <sub>2</sub> S <sub>3</sub> *	SnS	Tl <sub>2</sub> F <sub>2</sub>	Zr
COS	As <sub>3</sub>	BeOH	CdO <sub>2</sub> H <sub>2</sub>	CsF	FeS*	GeBr	InF <sub>3</sub>	MgOH	Na <sub>2</sub> Cl <sub>2</sub>	Rb <sub>2</sub> Cl <sub>2</sub>	Sb <sub>2</sub> S <sub>4</sub> *	SrBr <sub>2</sub>	TlO	ZrCl
SO <sub>2</sub>	As <sub>4</sub>	BeO <sub>2</sub> H <sub>2</sub>	CoCl	Cs <sub>2</sub> F <sub>2</sub>	Ga	GeBr <sub>3</sub>	InO	Mg(OH) <sub>2</sub>	NaF	RbF	SiCl <sub>4</sub>	SrF <sub>2</sub>	Tl <sub>2</sub> O	ZrCl <sub>2</sub>
SO	AsF <sub>3</sub>	BeH	CoCl <sub>2</sub>	CsBr	GaCl	GeBr <sub>4</sub>	In <sub>2</sub> O	MgH	NaBr	Rb <sub>2</sub> F <sub>2</sub>	SiCl <sub>3</sub> F*	SrCl <sub>2</sub>	TlOH	ZrCl <sub>3</sub>
HS	AsO	BeS	CoCl <sub>3</sub> *	Cs <sub>2</sub> Br <sub>2</sub>	GaCl <sub>2</sub>	GeO <sub>2</sub>	InOH	Mn	NaOH	RbBr	SiF <sub>4</sub>	SrClOH	TlH	ZrCl <sub>4</sub>
HF	As <sub>4</sub> O <sub>6</sub>	Bi	Co <sub>2</sub> Cl <sub>4</sub>	Cs <sub>2</sub> O	GaCl <sub>3</sub>	GeS	InH	MnCl	NbCl <sub>5</sub>	Rb <sub>2</sub> Br <sub>2</sub>	SiFH	SrO <sub>2</sub> H <sub>2</sub>	VCl <sub>2</sub>	ZrF
HCl	AsH <sub>3</sub>	Bi <sub>2</sub>	CoH	CsOH	Ga <sub>2</sub> Cl <sub>6</sub>	GeS <sub>2</sub>	KCl	MnCl <sub>2</sub>	NbCl <sub>3</sub> O	RbOH	SiHF <sub>3</sub> *	TaCl <sub>5</sub>	VCl <sub>3</sub>	ZrF <sub>2</sub>
S <sub>2</sub>	AsS	BiO	CoO <sub>2</sub> H <sub>2</sub>	Cs <sub>2</sub> O <sub>2</sub> H <sub>2</sub>	GaF	Hg	K <sub>2</sub> Cl <sub>2</sub>	MnCl <sub>3</sub>	NbF <sub>5</sub>	RbH	SiH <sub>3</sub> F*	TaCl <sub>3</sub> O	VCl <sub>5</sub>	ZrF <sub>3</sub>
H <sub>2</sub>	As <sub>4</sub> S <sub>4</sub>	BiCl*	CrCl <sub>2</sub>	Cu	GaF <sub>2</sub>	HgCl*	KF	MnCl <sub>4</sub>	NbF <sub>3</sub> O	ReCl <sub>3</sub> **	SiOF <sub>2</sub> *	TaO <sub>2</sub>	VCl <sub>3</sub> O	ZrF <sub>4</sub>
O <sub>2</sub>	BaF <sub>2</sub>	BiF	CrCl <sub>3</sub>	CuCl	GaF <sub>3</sub>	HgCl <sub>2</sub>	KBr	MnF <sub>2</sub>	NbO <sub>2</sub>	ReCl <sub>5</sub> **	SiO	TaF <sub>3</sub> O	VO <sub>2</sub>	ZrS
Al	BaClOH	BiF <sub>3</sub> *	CrCl <sub>4</sub>	CuCl <sub>2</sub>	Ga <sub>2</sub> O	HgF*	KOH	MnF <sub>3</sub>	Ni	ReOCl <sub>4</sub> **	SiO <sub>2</sub>	TaF <sub>5</sub>	VF <sub>3</sub> O	ZrS <sub>2</sub>
AlCl	BaCl <sub>2</sub>	BiS	CrCl <sub>2</sub> O	Cu <sub>2</sub> Cl <sub>2</sub>	GaO	HgF <sub>2</sub>	LiCl	MnF <sub>4</sub>	NiCl	ReO <sub>3</sub> Cl**	SiS <sub>2</sub>	TiCl <sub>3</sub>	VF <sub>2</sub>	Zn
AlCl <sub>3</sub>	BaBr <sub>2</sub>	(BiS) <sub>2</sub> *	CrCl <sub>2</sub> O <sub>2</sub>	Cu <sub>3</sub> Cl <sub>3</sub>	GaOH	HgBr	Li <sub>2</sub> Cl <sub>2</sub>	MnBr <sub>2</sub> *	NiCl <sub>2</sub>	ReO <sub>2</sub> **	Sn	TiCl <sub>4</sub>	VF <sub>3</sub>	ZnCl
AlClF <sub>2</sub>	BaO <sub>2</sub> H <sub>2</sub>	Bi <sub>2</sub> S <sub>3</sub> *	CrF <sub>3</sub>	CuF <sub>2</sub>	GaH	HgBr <sub>2</sub>	Li <sub>3</sub> Cl <sub>3</sub>	MnClO <sub>3</sub>	NiOH	ReO <sub>3</sub> **	SnCl	TiOCl <sub>2</sub> *	VF <sub>5</sub>	ZnCl <sub>2</sub>
AlCl <sub>2</sub> F	Be	Ca	CrF <sub>4</sub>	CuBr*	Ga <sub>2</sub> S	HgO*	LiF	Mn(OH) <sub>2</sub>	Ni(OH) <sub>2</sub>	ReO <sub>7</sub> **	SnCl <sub>2</sub>	TiO	WCl <sub>4</sub>	ZnF <sub>2</sub>
AlF <sub>3</sub>	BeCl	CaCl <sub>2</sub>	CrO <sub>2</sub>	CuO	Ge	HgH*	Li <sub>2</sub> F <sub>2</sub>	MoCl <sub>4</sub>	Pb	Sb	SnCl <sub>3</sub>	TiO <sub>2</sub>	WCl <sub>6</sub>	ZnBr <sub>2</sub>
AlFO	BeCl <sub>2</sub>	CaF <sub>2</sub>	CrO <sub>2</sub> H <sub>2</sub>	CuH	GeCl	HgS*	LiBr	MoCl <sub>6</sub>	PbCl	Sb <sub>2</sub> *	SnCl <sub>4</sub>	TiOF <sub>2</sub> *	WCl <sub>2</sub> O <sub>2</sub>	ZnO
AlF <sub>2</sub> O	Be <sub>2</sub> Cl <sub>4</sub>	CaClOH	CrO <sub>3</sub> H <sub>2</sub>	CuS	GeCl <sub>2</sub>	In	LiOH	MoCl <sub>2</sub> O <sub>2</sub>	PbCl <sub>2</sub>	SbCl <sub>3</sub>	SnF	TiF <sub>3</sub>	WO <sub>2</sub>	ZnS

\* Thermodynamic data from the GASTHERM database [13]. \*\* Thermodynamic data from [21].

## CALCULATION TECHNIQUES AND THERMODYNAMIC DATA

The modelling has been performed using the GBGAS program (the author is Dr. D.V. Grichuk, Moscow State University) for calculating heterogeneous equilibria of gas solution with phases of constant composition. The program permits a calculation of gas composition in equilibrium with the phases of constant composition at a given temperature, pressure and bulk system composition. It is assumed for calculation that gas phase is always present in the system and the set of equilibrium phases of constant composition is estimated by minimisation of the system free energy. This program is capable of simultaneously operating with no more than 500 compounds of 50 elements, and no more than 400 compounds being gas species.

The isobaric cooling of the gas phase was modelled using the procedure of flow reactor [19]. In this technique, the continuous cooling of a thermodynamic system is approximated by a combination of isothermal steps (flow reactors). For each step, the mineral assemblage being in equilibrium with the gas phase is calculated at a given temperature and bulk system composition. This mineral assemblage (solid phase) is eliminated from the system and the equilibrium gas phase is taken as the bulk system composition for the next step of calculation, i.e., in a reactor of lower temperature. This procedure was applied for calculating the composition of equilibrium gas mixtures and distribution of volatile species and mineral assemblages originated during the cooling of the initial gas composition (Table 2b) from 1373 to 373 K. The calculation step was adopted at 20 K.

The calculations were fulfilled using the IVTAN-TERMO thermodynamic database [20]. Some additional data were taken from [13, 21, 22]. The calculation involved over 1700 gas species and 1500 solid phases for 82 elements.

Since the amount of the thermodynamic data substantially exceeded the value appropriate to the computer program, only the most important gas species for many elements were preliminarily chosen. The total concentrations of H, O, S, C, Cl and F, which form volatile compounds with trace elements and serve as transport agents in volcanic gas, are several orders of magnitude greater than the other element contents. Therefore, the trace elements, which do not form complex volatile compounds in the gas phase, were supposed to not mutually influence the distribution of gas species and could be considered, as the first approximation, independently of one another.

Such an approach made it possible to subdivide the whole task into a series of subtasks involving 18 elements with all their thermodynamic properties taken into account.

Correspondingly, the volatile species, whose concentration is several orders of magnitude lower than that of the major forms of element transportation in the whole range of studied temperatures, were excluded from further consideration. The final calculation involved 45 chemical elements and all important volatile species participating in their transportation (Table 3).

The minerals considered in the system (solid phases) must adequately approximate the natural process. All solid phases ever noted in the natural volcanic incrustations and sublimates, common minerals of rocks and ores, and the most probable solid phases of trace elements with the known thermodynamic properties were included into the calculation. The list of minerals and solid phases involved into the calculation is given in Table 4.

Table 4. The solid phases included in the thermodynamic model [20, 21]

Alabandite	Galena	Cassiterite	Molybdenite	Sulfur (s,l)	Celestite	CsCl	InCl <sub>3</sub>	ReCl <sub>5</sub>	TlCl
Anhydride	Halite	Quartz	Arsenic	Sylvite	Scheelite	Ga <sub>2</sub> S <sub>3</sub>	InF <sub>3</sub>	ReO <sub>2</sub>	ZnCl <sub>2</sub>
Andesine	Hausmannite	Cinnabar	Niccolite	Sphalerite	Spinel	GaCl <sub>3</sub>	InS	ReO <sub>3</sub>	ZrF <sub>4</sub>
Anortite	Hedenbergite	Covellite	Oligoclase	Tephroite	Enstatite	GaF <sub>3</sub>	KReO <sub>4</sub>	ReO <sub>3</sub> Cl	ZrO <sub>2</sub>
Antimonite	Hercynite	Corundum	Pyrite	Fayalite	Jacobsite	GaS	LiCl	ReOCl <sub>4</sub>	ZrS <sub>2</sub>
Arsenopyrite	Hematite	Crystobalite	Pyrolusite	Ferberite	BeCl <sub>2</sub>	GeO <sub>2</sub>	MnCl <sub>2</sub>	ReS <sub>2</sub>	
Orpiment	Greenockite	Labradorite	Pyrrhotite	Ferrosilite	BeF <sub>2</sub>	GeS	PbCl <sub>2</sub>	ReS <sub>3</sub>	
Barite	Gypsum	Magnetite	Powellite	Forsterite	BeO	GeS <sub>2</sub>	RbCl	SnCl <sub>2</sub>	
Bytownite	Hubnerite	Manganite	Realgar	Chalcocite	BeS	HgCl <sub>2</sub>	Re <sub>2</sub> O <sub>7</sub>	SrCl <sub>2</sub>	
Bornite	Diopside	Microcline	Rhodonite	Chalcopyrite	CdCl <sub>2</sub>	In <sub>2</sub> S <sub>3</sub>	Re <sub>2</sub> S <sub>7</sub>	SrWO <sub>4</sub>	
Bismuthine	Ilmenite	Millerite	Mercury (1)	Chromite	CoS	In <sub>5</sub> S <sub>6</sub>	ReCl <sub>3</sub>	Tl <sub>2</sub> S	

Due to the absence of thermodynamic data for a number of compounds occurring in the natural sublimates (for example  $K_3Zn_2(Cl, OH)_7$ ), it is not possible to reproduce exactly all of the natural mineral assemblages. Moreover, many mineral phases are known to be solid solutions. As the GBGAS program involves only the solid phases of constant composition into the calculation, it is assumed that the solid solution may be stable if the minerals representing the end members of this solid solution are obtained.

The deposition of sublimates in nature occurs under unstable temperature conditions [7, 23]. The deposition depends on both the dynamic conditions of transport and the kinetic factors of crystal nucleation and growth. That is why, in nature, the same elements in the same temperature zone may form several compounds, which contradicts to the thermodynamic phase rule and cannot be reproduced in a numerical model.

Due to the absence of thermodynamic data on the boron and iodine compounds, these elements were not included into the calculation, although B concentration in the gas is higher

than the content of all other trace elements and the I content is comparable with the total concentration of all ore elements.

When calculating, any precipitation of solid phase is registered, including its mole fraction in the system as low as  $1E-18$ . In the natural conditions, the deposition of solid phases at their very low concentrations in the system becomes impossible due to the kinetic factors. In addition, the mineral phase occurring in sublimates in small amounts may be missed in the microprobe analysis. Because of that, the description of the calculation results includes the data only for elements and compounds identified in the natural sublimates.

### THERMODYNAMIC ANALYSIS OF GAS AND CONDENSATE COMPOSITION

In order to develop a correct model of evolution of the volcanic gas composition, one has to determine whether the species of the gas phase are in thermodynamic equilibrium at the temperature of sampling. The processes of oxidation of gas species, condensation and/or boiling at the time of sampling, as well as errors of analysis result in errors in determination of the original gas composition. Therefore, the composition of most of the analysed volcanic gases is not in equilibrium at the temperature of sampling. However, if contamination is low and analytical errors are small, it is often possible to restore the proportions of major gas species corresponding to the last moment of thermodynamic equilibrium in the gas phase. Such a procedure applied for reconstruction of the Kudryavy volcano gas composition is comprehensively presented in [14]. For further calculations, we used the highest temperature gas composition (sample F1292) restored in [14] (Table 1, 2a), as the initial gas composition for major components.

Table 5. The composition of basaltic andesites of the Kudryavy volcano [16], wt %

<b>SiO<sub>2</sub></b>	<b>TiO<sub>2</sub></b>	<b>Al<sub>2</sub>O<sub>3</sub></b>	<b>FeO</b>	<b>MnO</b>	<b>MgO</b>	<b>CaO</b>	<b>Na<sub>2</sub>O</b>	<b>K<sub>2</sub>O</b>
55.2	0.58	19.96	6.52	0.15	2.93	7.81	2.56	0.7

The same technique of correcting the gas composition, unfortunately, cannot be applied to minor components, where analytical errors may influence the calculation results. It is suggested [5, 12, 13] that most of Ca, Al, Mg and some of Mn, Fe, Na, and K is transported in the gas phase as the finest solid dust particles. These particles are involved in samples of condensate together with the gas phase, which results in their overestimated contents. The true gas composition can be calculated for the condition of equilibrium between the fluid and

surrounding magmatic rocks at the conditions where melt occurs in shallow-level conditions. To achieve this, a computer modelling of dissolving the magmatic rock in the O-H-F-S-C1-C fluid at 1373 K and 1 bar pressure has been performed. The restored gas composition (Table 1) and the rock composition of the youngest lava flow (Table 5) from the Kudryavy volcano were taken as the initial data. The calculation was done for  $\log_{10}[\text{gas (mole)/dissolving rock (mole)}]$  ratio ranging from 12 to 1. The minerals, which buffer the component contents in the gas phase depending on a given bulk composition of the system, are presented in Table 6. At the maximum value of the gas/rock ratio, the gas remains unsaturated in all components. With an increase of major-element contents in the system, it becomes saturated in certain gas components and, later on, their concentrations are buffered by the corresponding quartz-bytownite-diopside-enstatite-magnetite assemblage. Obviously, the concentration of saturation depends on solid phase compositions and may differ by some orders of magnitude for different mineral assemblages. Note that the obtained buffering assemblage includes minerals Pl-Cpx-Opx-Mt-(Q), which basically corresponds to the mineralogical composition of andesite. Figure 1 depicts calculated values of the bulk major-element concentrations in the gas and their actual contents in the condensate (sample 22 in [14]). The concentrations of Si, Al, Ca, and Mg in the gas are several orders of magnitude higher than the saturation concentrations in equilibrium with the melt. The high Al, Ca, and Mg contents measured in the condensate are most likely accounted for by their transportation by gas as minor rock particles. The significant concentration of Si may result either from dust transport or interaction between the gas and quartz tubes of sampling device [1].

Table 6. The mineral assemblage which buffers element concentration in the gas phase as a function of the given bulk composition of the system.

Element	$\log_{10}[\text{gas(mol)/rock(mol)}]$										
	11	10	9	8	7	6	5	4	3	2	1
Si	Quartz										
Al	Al <sub>2</sub> O <sub>3</sub>			Bytownite							
Ca						Diopside					
Mg							Enstatite				
Fe									Magnetite		

Note: In the units of  $\log_{10}[(\text{gas phase})/(\text{dissolving rock})]$  at 1373 K temperature and 1 bar pressure. The corresponding equilibrium distribution of the elements in the gas phase is presented in Fig 1. Composition of the gas phase and the rock are given in Table 1 and 5 respectively.

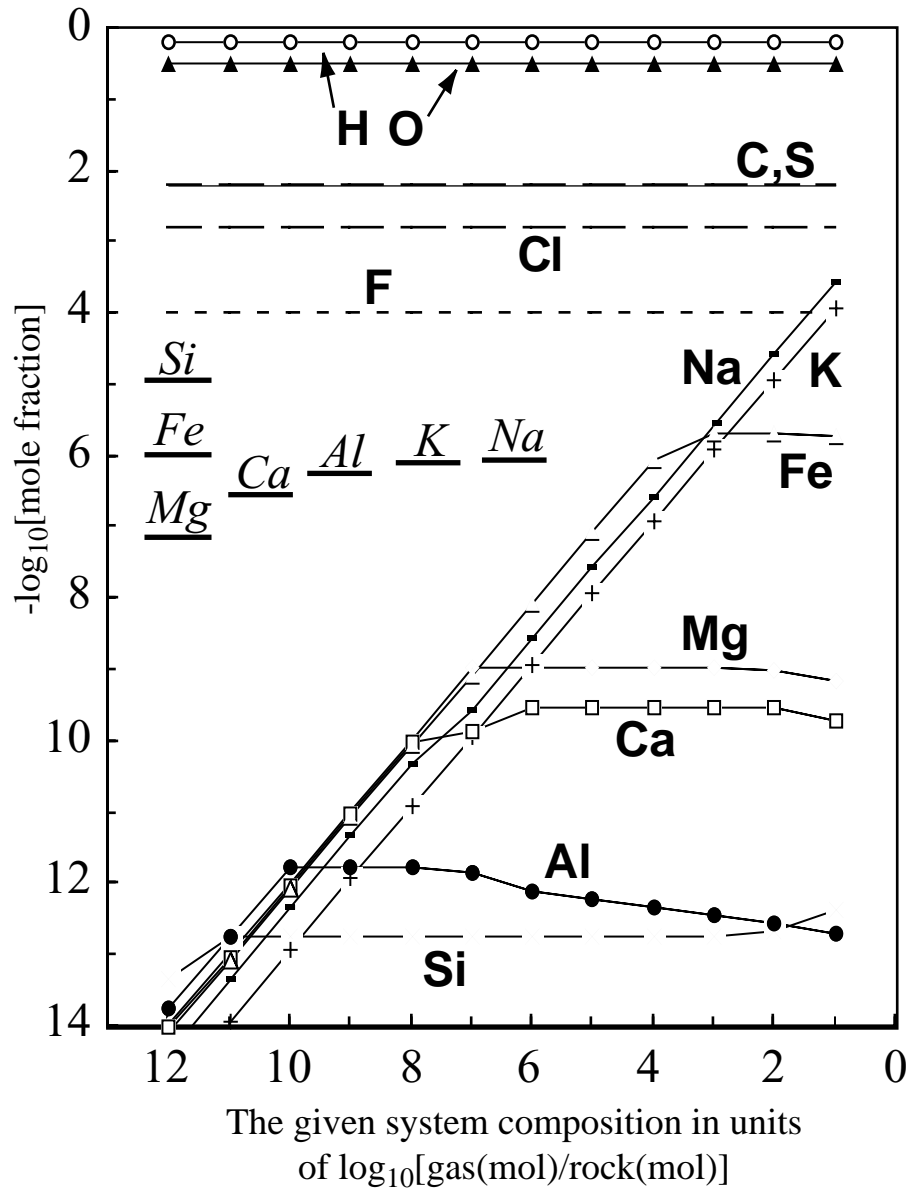


Fig. 1. The results of modelling of dissolving the Kudryavy volcano basaltic andesite in the gas phase at 1373 K temperature and 1 bar pressure. The boldfaced dashes designate mole fraction of rock-forming elements (italicized capital letters) in the volcanic gases from the highest temperature (1213 K) fumarole, according to data of chemical analysis. The curves represent change of the element concentration in the gas phase versus the given bulk composition of the system in the units of  $\log_{10}[\text{gas}(\text{mol})/\text{rock}(\text{mol})]$ . At the maximum value of this ratio the gas dissolves the rock completely. Upon the increase of rock proportion in the initial system composition, some elements of the gas phase become saturated. The equilibrium mineral assemblages buffering the gas composition in this case are given in Table 6.

In order to correct the minor-element composition of the gas, the contents of all elements were subtracted from the condensate composition in proportion to their concentrations in basaltic andesite, so that the Ca, Al, and Mg contents become equal to the

calculated concentrations of saturation. Due to the absence of data on trace element concentrations in the Kudryavy volcano rocks, the data on the mean contents of chemical elements in basic and intermediate rocks [24] (Table 2c) were used in the calculations. Then, the silica fraction in the gas was decreased to the estimated value. Table 2 shows the condensate composition taken from [14] (sample 22) and the calculated composition resulted from the subtraction procedure. The negative values obtained for Sr and Ti probably resulted from the deviation of the mean basalt composition from the real composition of solid particles entrapped by the condensate. Concentrations of 1 ppb were accepted for these elements. The data obtained on the equilibrium composition of condensate make it possible to define the source and speciation of different elements in the gas. The coincidence of the observed content of an element in the condensate with the estimated value means that this element was extracted from the magmatic melt and transported as a volatile compound. Otherwise, the element occurs in gas both as a volatile compound and as solid rock particles. The more the calculated concentration of an element differs from the initial one, the higher is the role of solid particles in transportation of this element.

The following conclusions could be derived from our calculations:

1. Si, Ti, Al, Mg, Ca, and Sr in the gas are generally transported as the solid particles of the wall rocks;
2. Fe, Mn, Na, K, Ba, and Li in gas are transported both as solid particles and volatile compounds;
3. B, I, Br, P, As, Zn, TI, Cd, Pb, Zr, Mo, Cu, Sn, Bi, Se, Ni, Cr, W, Sb, Te, Hg, Rb, and Cs are transported in gas largely as volatile compounds.

Our conclusions correlate well with the data obtained from a study of coefficients of element enrichment in gas [5].

## **COMPARISON OF THE CALCULATION RESULTS AND THE DATA FROM NATURAL OBJECTS**

A traditional mean to test a thermodynamic model is the comparison between the results of calculations and the field data. In this particular case, the comparison of the calculated temperature of mineral deposition with the data on the solid phase deposition from the Kudryavy volcano gases [23] (Fig. 2) is most efficient.

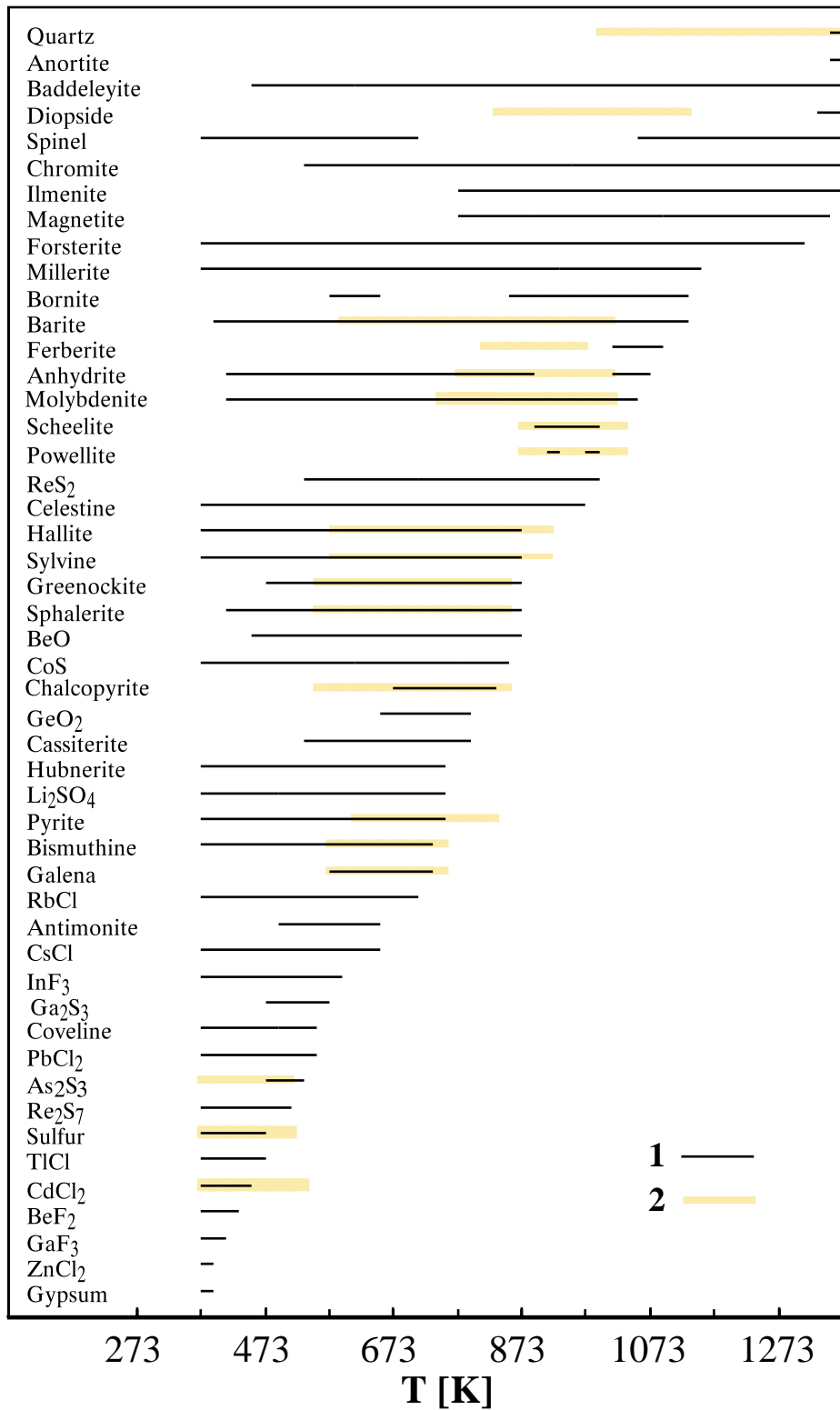


Fig. 2. Comparison of the calculated data on the mineral deposition from the gas phase at a decreasing temperature with the field observations [18, 23]. (1) Corresponds to the results of calculation, (2) shows the temperature interval of mineral deposition at natural conditions of Kudryavy volcano. The corresponding equilibrium compositions of the gas phase are presented on Fig. 3.

It should be noted that, due to the unstable temperature conditions while sampling natural sublimates [23], a discrepancy in the temperature range of mineral stability between the estimated values and those observed in nature must not be considered as a mistake up to 100 K. The sequence of mineral crystallisation with decreasing temperature is more informative.

### *Silicates*

According to the calculations, diopside is deposited within the temperature interval of 1323-1373K and is followed by forsterite at lower temperatures.

Natural silicates in the range of 1023-773K are represented by potassic feldspar, clinopyroxene of augite-hedenbergite composition, and aegirine. Silicates (wollastonite, grossular, sanidine) were also observed in the sublimates of a high-temperature zone in a quartz pipe [11]. However, it was inferred in [23] that the presence of potassic feldspar and pyroxenes could result from the transport and deposition of solid particles as discussed above. Probably, crystallization of these silicates in nature should be expected at higher temperatures.

### *W and Mo Minerals*

In our calculation, a joint deposition of scheelite and powellite (with the latter being predominant) was simulated within the range of 993-893 K. In the natural sublimates, scheelite, powellite, and their solid solutions also crystallized at temperatures of 1023-873 K.

From the calculation, molybdenite is stable at temperatures below 1043 K. In the natural sublimates, molybdenite was observed within the whole range of temperatures from 1023 to 443 K. Its maximum precipitation occurs at 973-673 K, where  $\text{MoS}_2$  is a major phase. The natural molybdenite contains small amounts of rhenium.

The hubnerite precipitation is simulated at temperatures below 763 K, while in the natural sublimates, wolframite with Mn admixture is formed at temperatures of 1023-723 K.

### *Barite and Anhydrite*

From the calculation, the deposition of barite occurs at temperatures below 1133 K. In the natural sublimates, small amounts of  $\text{BaSO}_4$  were registered in a wide range of temperatures from 1023 to 573K.

According to the calculation, anhydrite forms in the range of 1073-1013 and below 893 K. Within the range of 1013-893 K, anhydrite deposition ceases, because most of Ca precipitates in  $\text{CaWO}_4$  and  $\text{CaMoO}_4$ . In nature, small amounts of anhydrite were found in the temperature range of 1023-773 K, together with scheelite and powellite.

#### *Halite and Sylvite*

According to the calculation, halite and sylvite crystallize together within the range of 873-373 K. The KCl concentration in the sublimates is higher than that of NaCl, excluding the temperature interval from 853 to 873 K. Under natural conditions, deposition of halite and sylvite was noted within the whole temperature range of 1023-443 K, with the maximum content at 923-673 K. A neutron activation analysis revealed that Na concentration in the sublimates (and, correspondingly, NaCl as the major Na-bearing phase) at temperatures of 1023-823 K is higher than that of K (KCl).

#### *Fe and Cu Minerals*

According to the calculation, magnetite is stable at temperatures of 1353-773 K, while in the natural sublimates only hematite was found in the range of 1023-823 K. In the gas sublimates from other volcanoes, either magnetite [5, 7, 10] or magnetite and hematite [9, 25] were observed. Forms of iron oxide deposition depend on the redox conditions in the gas phase. The oxygen fugacity in the Kudryavy volcano gases at these temperatures is close to the NNO buffer [14, 26, 27], which excludes the deposition of hematite in an equilibrium process. The possible reasons for forming  $\text{Fe}_2\text{O}_3$  under natural conditions are discussed in [23]. The  $f_{\text{O}_2}$  values obtained in our calculation are between the NNO and HM mineral buffers. Therefore, magnetite can be the only possible equilibrium form of iron oxide deposition in thermodynamic calculation.

In our simulation, bornite precipitates at 1133-853 K and 653-573 K; chalcopyrite, at temperatures of 833-673 K; pyrite, below 773 K; and coveline, below 553 K. In the natural sublimates, the iron and copper minerals are deposited in the following sequence: pyrite - at 973-513 K with the maximum at 793-593 K; chalcopyrite - at 973-473 K with the maximum at 843-573 K; unidentified complex Cu-Fe-Zn-Cd-Sn sulfides were found in vents with temperatures below 593 K.

### *Zn and Cd Minerals*

Sphalerite and greenockite are both stable at temperatures of 873-473 K. In our model, it means the presence of their solid solution. In the natural sublimates, the ZnS-CdS solid solution with an admixture of iron and indium forms within the range of 923-493 K with the maximum at 823-553 K.

According to the calculation chlorides of these metals are stable at temperatures below 473 K. In nature, CdCl<sub>2</sub> was found at a temperature below 523 K. At the same time, Cd was present in a complex chloride (Na, K)<sub>3</sub>CdCl<sub>5</sub> and Zn in K<sub>3</sub>Zn<sub>2</sub>(Cl, OH)<sub>7</sub>.

### *Pb, As and Bi Minerals*

From the calculation, galena (PbS) crystallizes in the temperature range of 753-573 K. At a lower temperature, lead is deposited in cotunnite (PbCl<sub>2</sub>). Bismuth forms bismuthine (Bi<sub>2</sub>S<sub>3</sub>) at temperatures from 743 to 373 K. Natural compounds of these metals are represented by: galena with a minor admixture of bismuth in the range of 873-473 K and with the maximum content at 723-553 K; cotunnite in the interval of 773-373 K with the maximum at 793-473 K; varieties of Pb-Bi sulfides at 643-443 K; and bismuth chloride at 603-583 K. In natural sublimates, a significant amount of complex chloride (KPb<sub>2</sub>Cl<sub>5</sub>) was found. This compound was not included into the calculation due to lack of thermodynamic data.

According to the calculations, orpiment was deposited between 553 and 473 K. In natural sublimates, nonstoichiometric compounds of sulfur and arsenic were found in this temperature interval.

The estimated temperature of minerals precipitation agree well with the corresponding data on their deposition from natural fumaroles. This means that our model takes into account fully and accurately the major species which play a leading role in transportation and deposition of elements by the high-temperature magmatic gases.

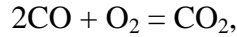
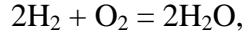
## **FORMS OF ELEMENT TRANSPORT**

### *Major Gas Components (Fig. 3.1)*

Concentrations of major gas components at different temperatures are plotted in Fig. 3.1. As the temperature decreases the H<sub>2</sub>O content increases from 0.944 to 0.966 mole

fractions. CO<sub>2</sub>, the second important volcanic gas, follows a similar tendency, i.e., with the temperature decrease its concentration increases from 0.0176 to 0.0183 mole fractions.

The H<sub>2</sub> and CO concentrations drop sharply during cooling in accordance with the reactions:



the change in the equilibrium constant with the temperature decrease results in the shift of the equilibrium toward H<sub>2</sub>O and CO<sub>2</sub> formation.

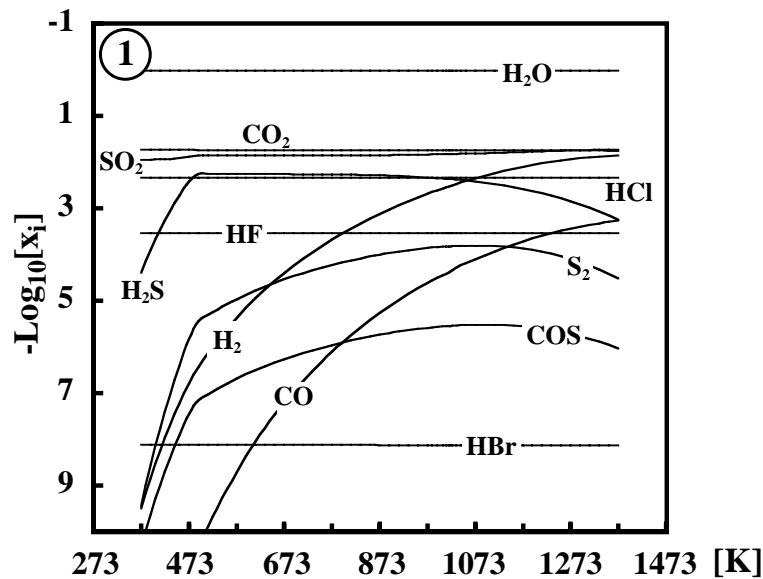
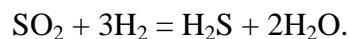


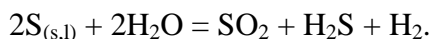
Fig. 3. Results of calculation of the temperature evolution of the gas phase during cooling. The calculated equilibrium composition of the gas phase (Table 2b) is taken as the initial bulk system composition. The graphs show the relationship between mole fraction of the major species in the gas phase (  $-\log_{10}[\text{mole fraction}]$  ) and the temperature (K). The change of equilibrium mineral assemblages is presented in Fig. 2. The total decrease of an element content in the gas phase is due to deposition of the solid phases containing this element. See description of the modelling technique in the text.

Sulfur in the gas exists in two major species: SO<sub>2</sub> and H<sub>2</sub>S. The calculated SO<sub>2</sub> concentration in the Kudryavy volcano gas gradually decreases from 0.0186 to 0.0112 mole fractions with the temperature decrease, but remains higher than the H<sub>2</sub>S fraction over the whole temperature range. The H<sub>2</sub>S content grows with gas cooling down to 473 K and then drops dramatically. These variations in SO<sub>2</sub> and H<sub>2</sub>S contents at temperatures above 573 K are controlled by the reaction [28]:



At lower temperatures, where elementary sulfur is stable, the equilibrium is governed by the

reaction:



The halogens: Cl, F, Br, and, possibly, I are transported in volcanic gases in the form of their compounds with hydrogen: HCl, HF, and HBr. Their concentrations in gas are almost constant over the whole temperature range, 0.0046, 0.00029, and  $7.45 \times 10^{-9}$  mole fractions, respectively. Such behaviour of HCl, HF, and HBr is due to the fact that they do not take part in redox reactions, and that the amount of precipitated solid halogen-bearing phases is incommensurably small as compared with their concentrations in the gas.

With a temperature decrease, the CH<sub>4</sub>, COS, and S<sub>2</sub> contents pass their maxima at high temperatures (1213 K for CH<sub>4</sub> and 1073 K for COS and S<sub>2</sub>), and then their concentrations gradually decrease. These components are subordinate and their contents are controlled by proportions of the major gas constituents H<sub>2</sub>O, CO<sub>2</sub>, SO<sub>2</sub>, H<sub>2</sub>S, and H<sub>2</sub>.

At high temperatures, the calculated oxygen fugacity lies within the interval of the QFM and NNO mineral buffers and shifts to the HM mineral buffer at lower temperatures. A similar relationship between the  $f_{O_2}$  and temperature was also revealed from the data on gas composition [14] and the direct measurements of  $f_{O_2}$ , by electrolytic sensor in the Kudryavy volcano fumaroles at various temperatures [27], which proves the correctness of our calculations.

*Elements of the First Group, Li, Na, K, Rb, Cs (Fig. 3.2), and Cu (Fig. 3.3)*

MeCl species are the main forms of the transport of the major subgroup's elements. (MeCl)<sub>2</sub> dimers play an equal role at lower temperatures. At temperatures above 873 K, the contents of these elements are determined by their initial concentrations in the gas. At lower gas temperatures, chlorides of these metals (LiCl, NaCl, KCl, RbCl, and CsCl) precipitate and the equilibrium with chlorides determines the contents of these elements in the gas phase.

Copper in the volcanic gas behaves similarly as the elements of the major subgroup. At high temperatures, the copper is transported as a simple chloride CuCl, but below 673 K, (CuCl)<sub>2</sub> dominates. Further cooling results in a more active polymerisation of CuCl molecules and in predominance of copper transportation in the form of (CuCl)<sub>3</sub> trimer. The transportation of copper at high temperatures in the form of monochloride was proven by spectrometric measurements [29] carried out on the Kilauea volcano.

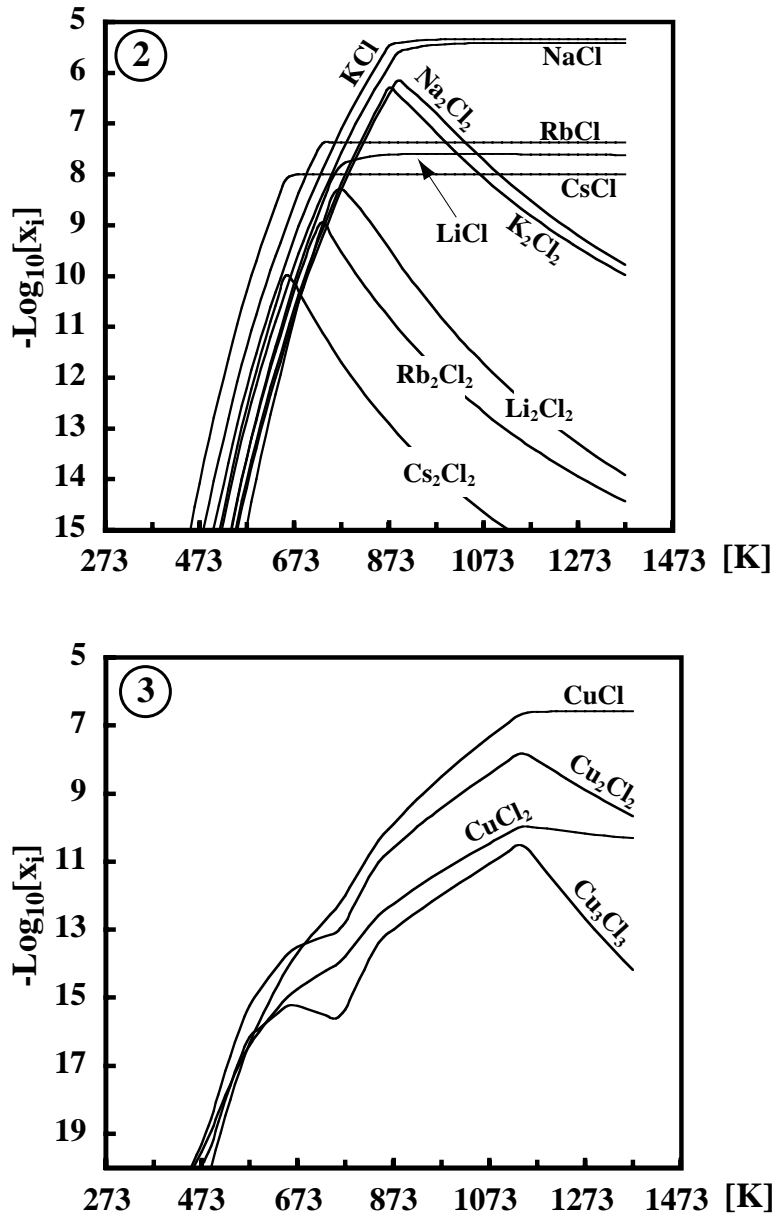


Fig. 3. Continued

Elements of the Second Group, Be, Mg (Fig. 3.4), Ca, Sr, Ba (Fig. 3.5), Zn, Cd, and In (Fig. 3.6)

The forms of beryllium transportation in gas phase change with decreasing temperature. Within the range of 1373-623 K, the major beryllium compound is hydroxide  $\text{Be}(\text{OH})_2$ , which is replaced by beryllium fluoride  $\text{BeF}_2$  at lower temperatures.

Above 1373 K, magnesium, like beryllium, is transported as hydroxide  $\text{Mg}(\text{OH})_2$ . Upon cooling to 623 K, magnesium chloride  $\text{MgCl}_2$  dominates and then it is replaced by  $(\text{MgCl}_2)_2$  at lower temperatures.

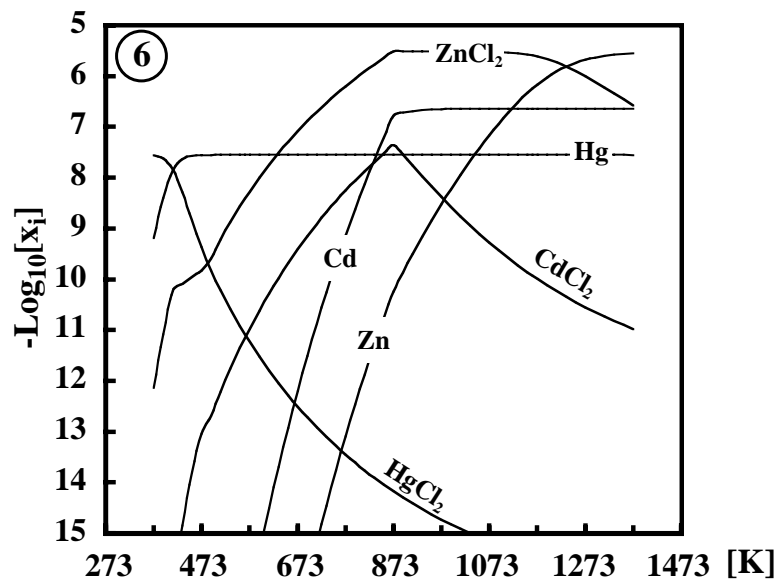
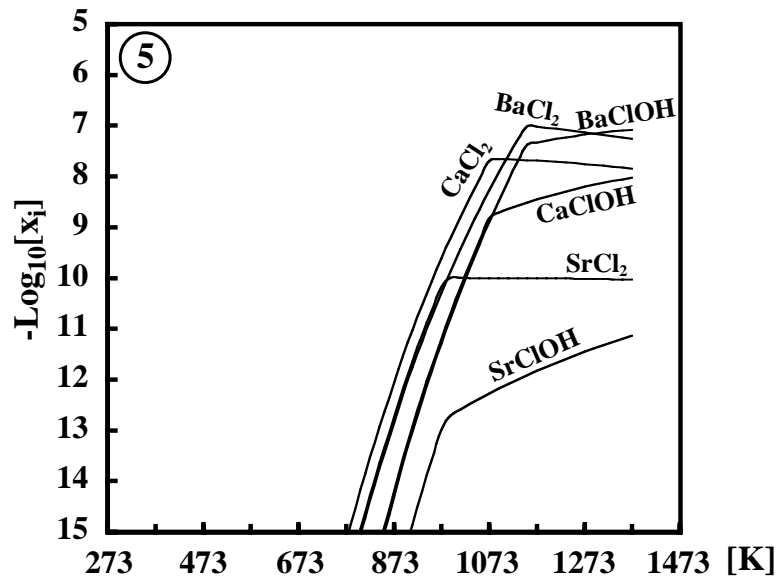
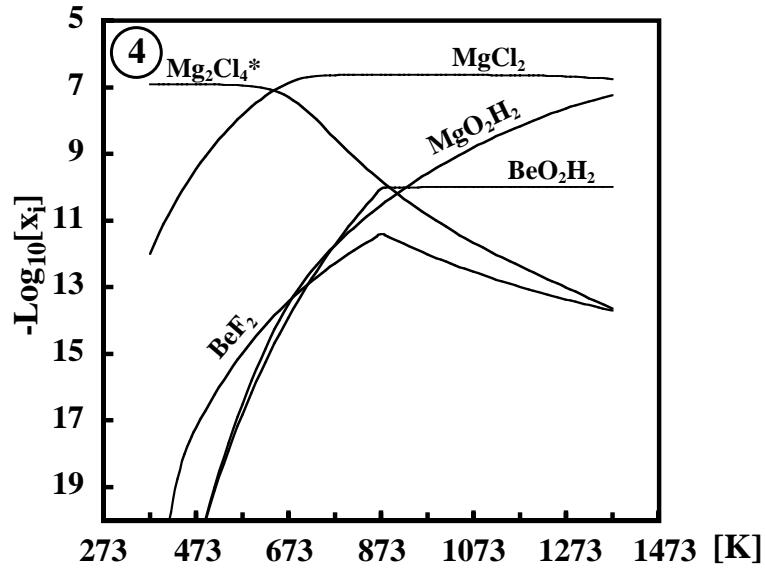


Fig. 3. Continued

Ca, Sr, and Ba are transported in identical forms in the whole temperature interval: above 1273 K, MeClOH species predominate, and at lower temperatures, these elements are transported in the form of simple chloride MeCl<sub>2</sub>. Extrapolation of the calculated data suggests that Me(OH)<sub>2</sub> species could also play a significant role in Ca, Sr, and Ba transport at temperatures above 1373 K.

Elements of a subgroup of the second group, namely, Zn, Cd, and Hg, form similar species within the whole temperature range. At a high temperature, they are transported largely neutral Me<sup>0</sup> species and at a lower temperature, as simple chloride MeCl<sub>2</sub>. The change in speciation occurs at 1223 K for Zn, 823 K for Cd, and 433 K for mercury.

*Elements of the Third Group Al (Fig.3.7), Ga, In, and Tl (Fig. 3.8)*

Aluminum is transported in different forms in the gas phase. At temperatures above 1123 K, the aluminum hydroxide Al(OH)<sub>3</sub> prevails. In the temperature interval of 1073-1123 K, there are several species of approximately equal importance: AlCl<sub>2</sub>F, AlClF<sub>2</sub>, and AlF<sub>3</sub>. At temperatures below 1073 K, the KAlF<sub>4</sub> and the NaAlF<sub>4</sub> species become the major forms for aluminum transport. It depends on the Na/K ratio in the gas which one of those species plays the main role in this process. The above ratio is determined either by the composition of the degassing melt and the coefficients of Na and K fractionation between the melt and gas, or melt and two fluid phases (equilibrium of silicate melt with water-salt liquid and vapor), which is believed [30] to occur in degassing from the Kudryavy volcano.

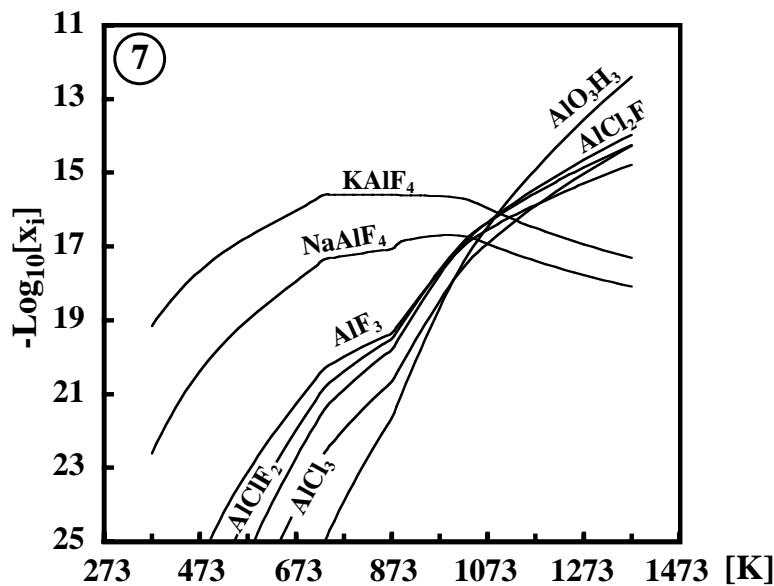


Fig. 3. Continued

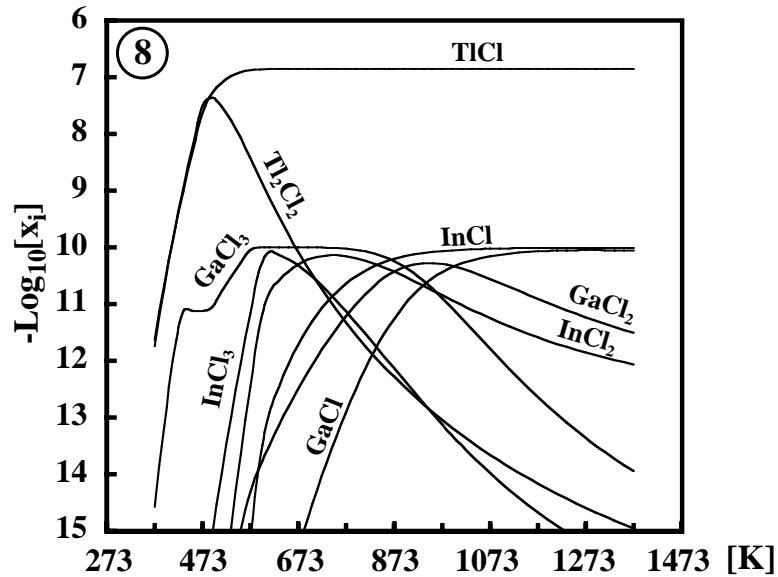


Fig. 3. Continued

Therefore, those species are equally important and each of them could dominate in a certain geologic setting. Gallium, indium, and thallium are transported as chlorides in the whole temperature range and, as the temperature decreases, the transport forms change according to the sequence  $\text{MeCl} \rightarrow \text{MeCl}_2 \rightarrow \text{MeCl}_3$ . The temperature of replacement of the major species is the highest for gallium, lower for indium, and the lowest for thallium.

*Elements of the Fourth Group, Si, Ge (Fig. 3.9), Sn, Pb (Fig. 3.10), Ti, and Zr (Fig. 3.11)*

At temperatures above 1223 K, silicon in the gas phase is transported as  $\text{SiO}$  and  $\text{SiO}_2$  oxides, and monoxide can be up to ten times more abundant than dioxide with increasing temperature. Within the interval of 1173-1223 K, the  $\text{SiO}_2$ ,  $\text{SiO}$ ,  $\text{SiOF}_2$ , and  $\text{SiF}_4$  species play almost equal roles in silicon transport. When the temperature decreases, the  $\text{SiF}_4$  species prevails. When discussing the origin of native silicon in the Kudryavy volcano sublimates [31], it was demonstrated by the thermodynamic calculations using the program by A. Shiryaev that the  $\text{SiO}$  species plays a leading role in the silicon transport by high-temperature gases.

At high temperatures, germanium is transported mainly as sulfide  $\text{GeS}$  and, at lower temperatures, as chloride  $\text{GeCl}_4$ . The change of the predominant species takes place at 723 K, where the  $\text{GeF}_2$ ,  $\text{GeCl}_2$ , and  $\text{GeS}_2$  species are almost equally important in Ge transportation as well.

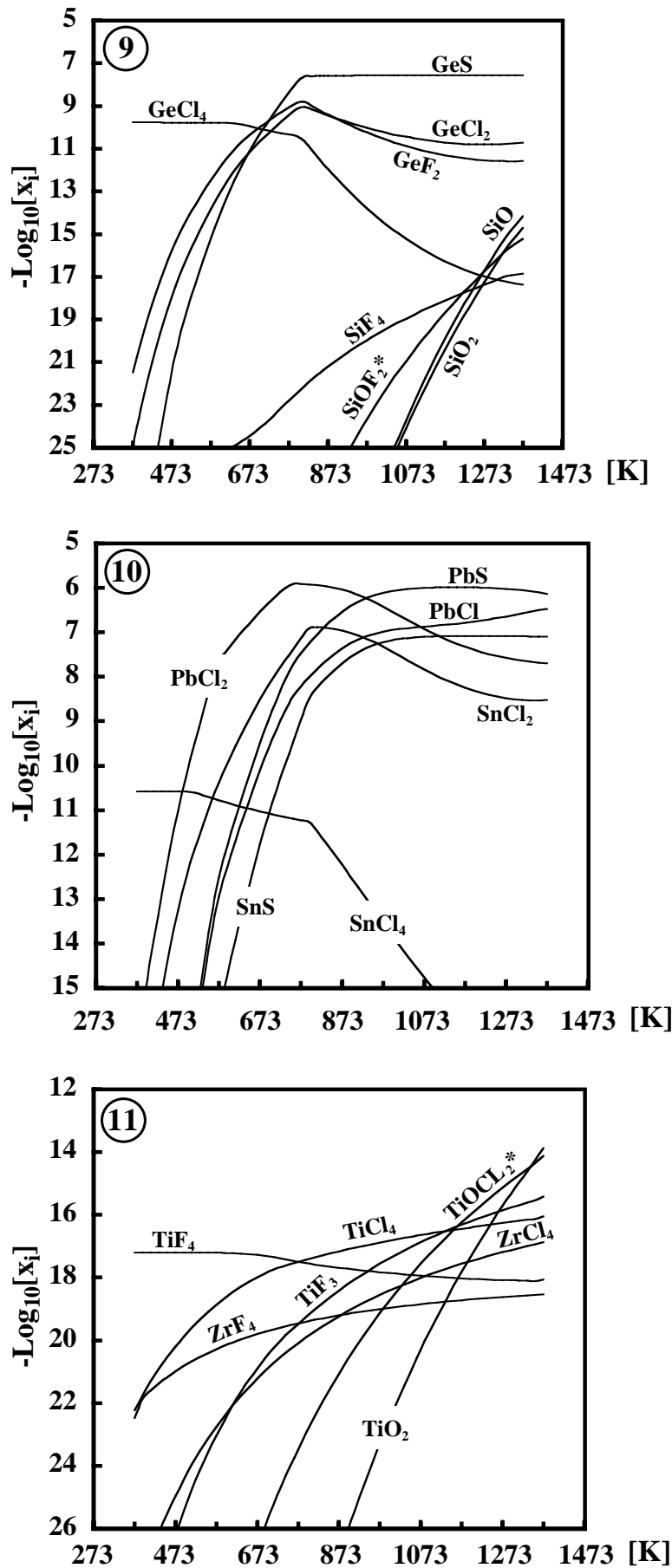


Fig. 3. Continued

Sn and Pb are close in the peculiarities of their transportation in gas. At high temperatures, they are transported in the form of sulfides PbS and SnS, and at intermediate temperatures, as bivalent chlorides PbCl<sub>2</sub> and SnCl<sub>2</sub>. At low temperatures Sn is transported as tetravalent chloride SnCl<sub>4</sub>. The importance of PbCl<sub>4</sub> species also increases at lower temperatures. The temperatures of replacement of the prevailing transportation forms are rather close for Sn and Pb (about 973 K).

Forms of Ti transportation in the gas are various. The sequence of replacement of the major forms with decreasing temperature is: TiO<sub>2</sub> → TiOCl<sub>2</sub> → TiF<sub>3</sub> → TiCl<sub>4</sub> → TiF<sub>4</sub>. Zirconium is transported as chloride ZrCl<sub>4</sub> in the range of 1373-853 K and as fluoride ZrF<sub>4</sub> at lower temperatures.

*Elements of the Fifth Group, As (Fig. 3.12), Sb (Fig. 3.13), Bi(Fig. 3.14), V, Nb, Ta(Fig. 3.15)*

As and Sb have similar forms of transportation in the gas phase. Above 1293 K, As is transported in gas as oxide AsO. As the temperature decreases, the oxide is replaced by sulfide AsS, which remains major gas species down to 873K. In the interval of 1373-873 K, Sb is transported as sulfide, but at higher temperatures, a more important role of SbO species should be expected, similarly to the arsenic transportation as AsO. The prevailing species in the cooling gas change as follows: As<sub>4</sub>O<sub>6</sub> at 873-723 K, As<sub>4</sub>S<sub>4</sub> at 723-473 K, and AsF<sub>3</sub> below 473 K. A respective sequence for Sb species is as follows: Sb<sub>4</sub>O<sub>6</sub> at 873-573 K, and SbF<sub>3</sub> below 573 K. Unfortunately, we had no thermodynamic data for the Sb<sub>4</sub>S<sub>4</sub> species, which could prevail in the interval of 873-473 K, similarly to the As<sub>4</sub>S<sub>4</sub> species.

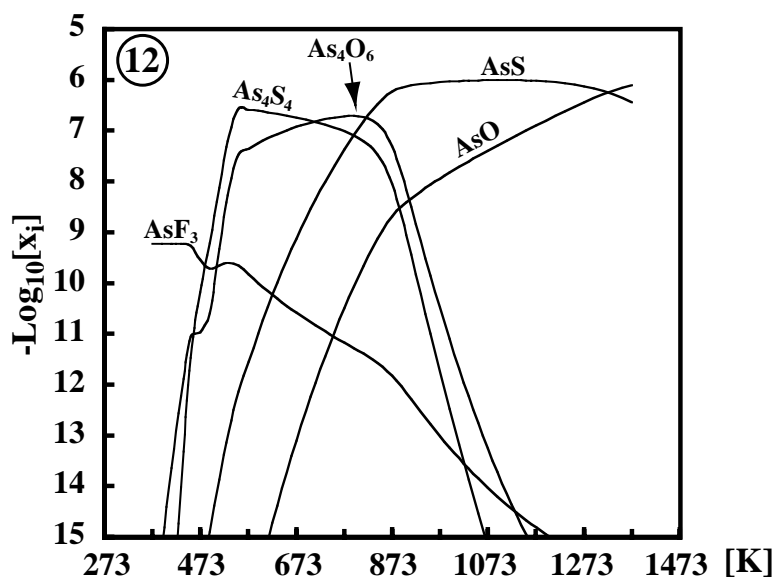


Fig. 3. Continued

Bismuth is transported in the neutral  $\text{Bi}^\circ$  species at temperature above 1173 K, then, in sulfide  $\text{BiS}$  in the interval of 1173-923 K, and as monovalent chloride  $\text{BiCl}$  below these temperatures.

Vanadium is transported as dioxide  $\text{VO}_2$  at temperatures above 1353 K, as fluoride  $\text{VF}_2$  in the interval 1353-973 K, and as oxychloride  $\text{VOCl}_3$  at lower temperatures. With the temperature decrease, the abundance of  $\text{VOF}_3$  species in the gas grows and if the F/Cl ratio rises (at the final stages of magma crystallization), these species may become dominant.

Niobium and tantalum are transported as oxychlorides  $\text{MeOCl}_3$  at temperatures above 873 and 773K, respectively, and as oxyfluorides  $\text{MeOF}_3$ , at lower temperatures.

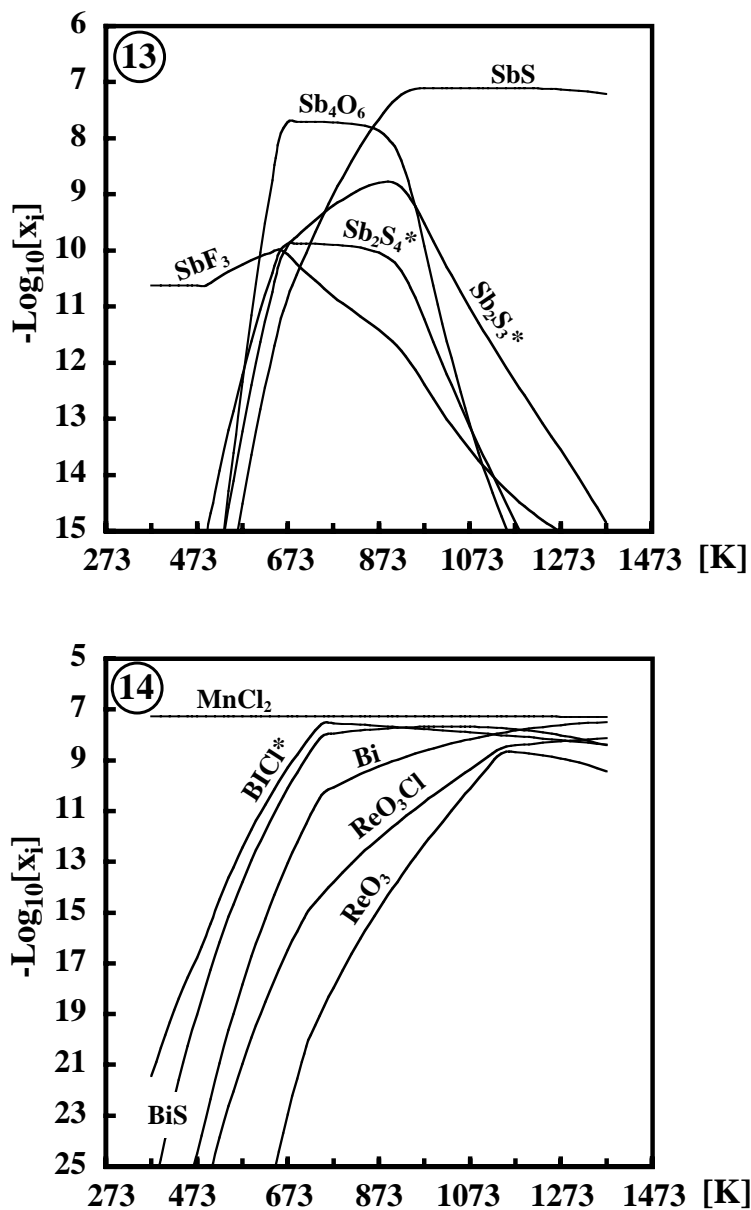


Fig. 3. Continued

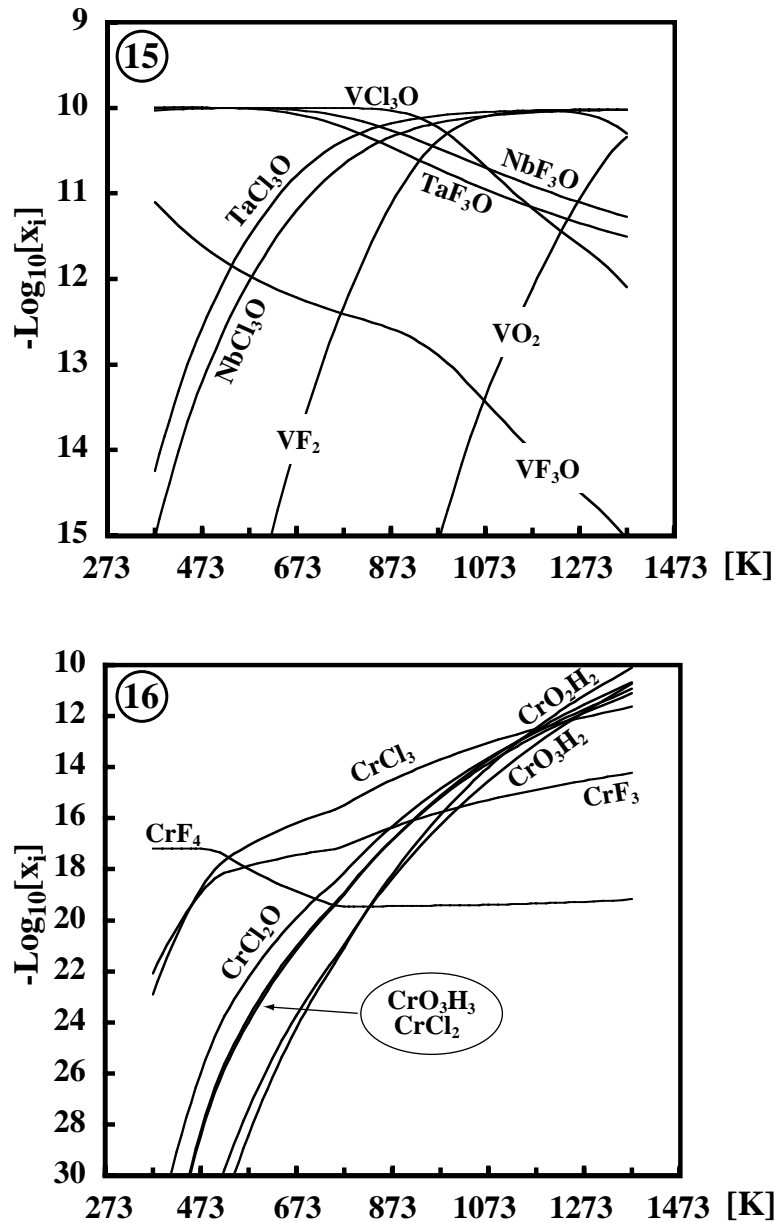


Fig. 3. Continued

*Elements of the Sixth Group, Cr (Fig. 3.16), Mo, and W (Fig. 3.17)*

Bivalent chloride  $\text{CrCl}_2$ , oxychloride  $\text{CrCl}_2\text{O}_2$ , and the  $\text{CrO}_2\text{H}_2$  species are practically equally important in chromium transport at temperature above 1123 K. Trivalent chloride is the main species between 1123 and 523 K and, tetrafluoride  $\text{CrF}_4$  at lower temperatures. Molybdenum is transported in the gas phase as molybdic acid  $\text{H}_2\text{MoO}_4$  at temperatures above 1053 K and as dioxychloride  $\text{MoO}_2\text{Cl}_2$  at lower temperatures. Dioxychloride  $\text{WO}_2\text{Cl}_2$  is the major form of tungsten transportation in the whole temperature range.

*Elements of the Seventh Group, Mn and Re (Fig. 3.14)*

MnCl<sub>2</sub> chloride is the major Mn transport form within the whole studied temperature interval. Rhenium is transported as oxychloride ReOCl<sub>3</sub>, however, between 1033 and 1273 K, ReCl<sub>3</sub> species plays a significant role.

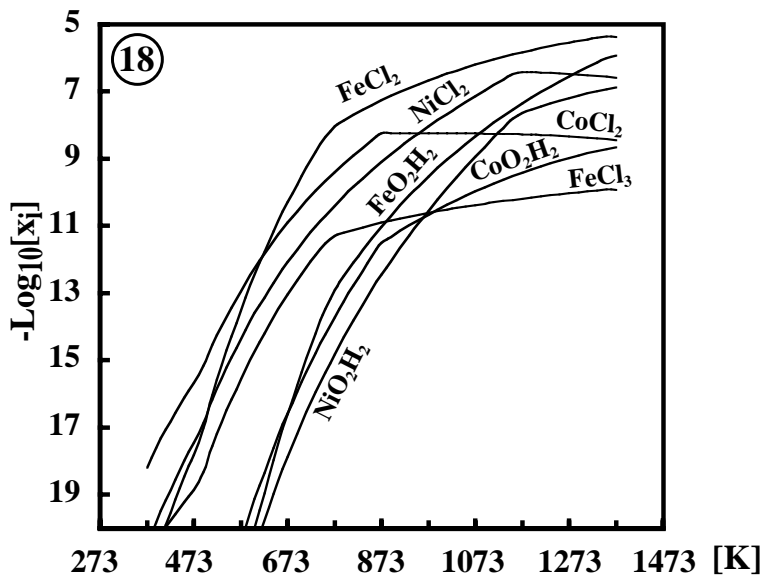
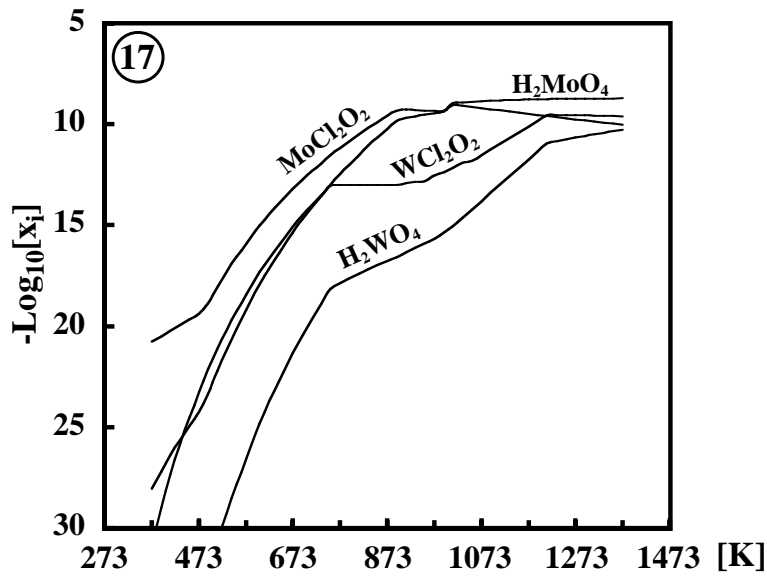


Fig. 3. Continued

*Elements of the Eighth Group, Subgroup of Iron, Fe, Co, and Ni (Fig. 3.18)*

As we expected, the elements of the iron subgroup have similar transportation forms. These elements are transported as bivalent chlorides  $\text{MeCl}_2$  in the whole temperature range. The role of hydroxides  $\text{Me}(\text{OH})_2$  is higher at temperatures above 1273 K, while at lower temperatures, a more oxidized trivalent iron transported as  $\text{FeCl}_3$  becomes more important.

**GENERAL REGULARITIES OF GAS TRANSPORT**

The calculation demonstrated that behaviour of all the elements is governed by common regularities, the knowledge of which enables to predict the element species that have not been included into the calculation due to the lack of thermodynamic data.

All of the elements tend to form simpler species (i.e., with decreasing number of atoms in a molecule) at higher temperatures. Sometimes, this dependence is not obvious, and the same major species prevails over the whole temperature interval; then the regularity is true for the second important species. For elements of constant valence, this tendency is manifested in the gradual polymerization of molecules with decreasing temperature. Alkali metals which are transported at high temperatures as a simple chloride  $\text{MeCl}$  present a typical example of such behaviour. With a temperature decrease they polymerize to dichloride  $(\text{MeCl})_2$ . Similar properties were exhibited by Mg, Cu, and Tl. Elements of variable valence form more complex molecules by increasing the valence of their cations at lower temperatures. This is exemplified by Zn, Cd and Hg showing replacement of neutral  $\text{Me}^0$  species by  $\text{MeCl}_2$  chloride with the temperature growth. The changes in Ga and In species correspond to the sequence of  $\text{MeCl} \rightarrow \text{MeCl}_2 \rightarrow \text{MeCl}_3$ .  $\text{MeCl}_2$  is substituted by  $\text{MeCl}_4$  for Sn and Ge, while SiO is replaced by  $\text{SiO}_2$ . According to the calculation, Al, Cr, W, Mo, and Re are transported as complex species at the highest temperatures of the studied interval. Consequently, we may expect the occurrence of simpler molecules at even higher temperatures.

The analysis of element speciation reveals that, at the lower temperatures, most of the elements are transported as halogenides. At high temperatures, the predominant forms are sulfides ( $\text{SnCl}_4 \rightarrow \text{SnS}$ ;  $\text{PbCl}_2 \rightarrow \text{PbS}$ ;  $\text{AsF}_3 \rightarrow \text{AsS}$ ;  $\text{SbF}_3 \rightarrow \text{SbS}$ ), oxides ( $\text{SiF}_4 \rightarrow \text{SiO}_2 \rightarrow \text{SiO}$ ;  $\text{TiF}_4 \rightarrow \dots \rightarrow \text{TiO}_2$ ), hydroxides ( $\text{FeCl}_2 \rightarrow \text{Fe}(\text{OH})_2$ ;  $\text{CrF}_4 \rightarrow \dots \rightarrow \text{Cr}(\text{OH})_2$ ), and monatomic species ( $\text{ZnCl}_2 \rightarrow \text{Zn}$ ;  $\text{CdCl}_2 \rightarrow \text{Cd}$ ;  $\text{BiCl} \rightarrow \dots \rightarrow \text{Bi}$ ). Similar regularities were discovered in the mineral equilibria [32]. Studies of exchange reactions showed an increase in

stability of minerals with more covalent bonds, as compared to those with more ionic bonds, with the temperature growth. In general, the stability of compounds with ionic bonds decreases and stability of compounds with covalent bonds increases with increasing temperature. The degree of compounds' ionicity may be estimated by the ionization energy. According to [33, 34], the ionization energies for compounds of Sn, Si, and Pb are as follows:

SnCl <sub>4</sub>	12.4 eV	SiO <sub>2</sub>	11.7 eV	PbS	8.6 eV
SnS	9.7 eV	SiO	11.4 eV	PbCl	7.5 eV

The last three species should occur at higher temperature, which is confirmed by the calculation. According to Fig. 3.10, the transformation of PbS → PbCl could occur at temperature above 1373 K.

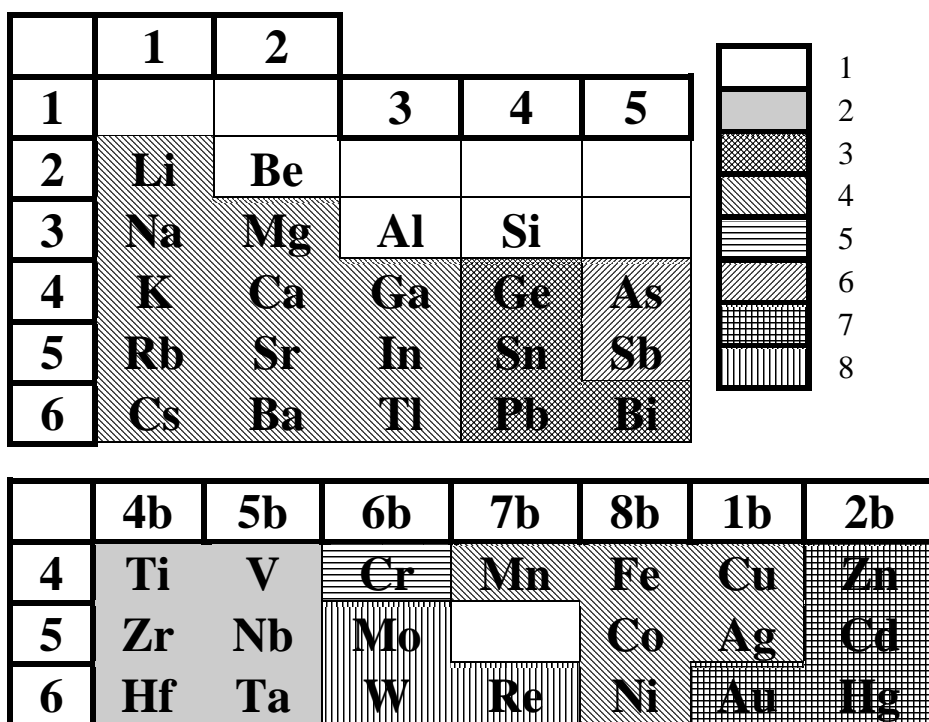


Fig. 4. The combined table of major regularities of the element transportation in the gas phase. (1) Fluorides, oxides, and hydroxides, (2) fluorides, chlorides, and oxides, (3) sulfides and chlorides, (4) chlorides, (5) hydroxides, chlorides, and fluorides, (6) sulfides and fluorides, (7) monatomic compounds and chlorides, (8) oxides, chlorides, and hydroxides.

Let us review now the changes in transportation forms of different elements belonging to the same period or group in the Mendeleev's periodic table. Obviously, the elements of the same subgroup (either main or side) in the periodic system have similar transportation forms and regularities of their modification in connection with the temperature variations. The

heavier elements change their major (similar) transportation forms at lower temperatures. For example, for zinc, cadmium, and mercury the  $\text{Me}^0 \rightarrow \text{MeCl}_2$  transformation occurs at respective temperatures of 1273, 873, and 453 K. The transformation of gallium and indium species occurs in the sequence  $\text{MeCl} \rightarrow \text{MeCl}_2 \rightarrow \text{MeCl}_3$  in the intervals of 1023-873 K and 793-653 K, respectively. A similar dependence is also typical of some elements from the other groups: Pb-Sn-Ge, Ti-Zr, and Sb-As. Such regularities are less pronounced for elements belonging to different groups of the same period.

Considering the relationships between the element species and position of these elements in the long period version of the Mendeleev's periodic table (Fig. 4), we can draw the following conclusions. In the major subgroup, elements located in the top right-hand part of the table (Be, Al, and Si) are transported in the form of fluorides and oxides. Elements in the right part of the table (As, Sb) are transported in the form of sulfides and oxides. The bottom left-hand corner is occupied by elements with chloride transportation forms (Li, Na, K, Rb, Cs, Mg, Ca, Sr, Ba, Ga, In, and Tl). Elements of intermediate location in the table (Ge, Sn, Pb, and Bi) have both sulfide and chloride transportation forms. Elements of the side group may be described as follows. The top left-hand part is occupied by elements with the fluoride and chloride transportation forms (Ti, Zr, and V). When moving to the right, these forms are replaced by oxyfluorides and oxychlorides (Nb, Ta, Cr, Mo, W, and Re), then chlorides (Fe, Co, Ni, Cu, and Zn) and, finally, Hg is transported as a neutral species in almost the whole range of temperatures examined.

Therefore, the transportation forms for all the elements are in close relation with their position in the Mendeleev's periodic table. The behaviour of the volatile forms of elements, similarly to the behaviour of the elements themselves, is controlled by general regularities, the knowledge of which enables to forecast the dependence of transportation forms on temperature for elements not included into the calculation.

For example, considering the position of silver and gold in the periodic table, we may expect that their properties, on the one hand, must be close to those of copper and, on the other hand, to the properties of zinc, cadmium, and mercury. We may suppose that gold and silver will be transported as neutral species and chlorides of a  $\text{MeCl}$  type. A calculation of the element transportation forms in the gases from Mount Saint Helens volcano [13] revealed that silver is transported as  $\text{AgCl}$ , which agrees with our assumption. On the other hand, according to the calculation, sulfide  $\text{AuS}$  was the major transportation form for gold [13]. This could be resulted from the absence of gold chloride species in the applied database [13]. However, this species may play the major role in Au transportation. This example demonstrates that the

completeness and reliability of thermodynamic data involved in calculation are the most important prerequisites for an adequate approximation to natural processes with calculations of this kind.

## CONCLUSIONS

(1) Based on the data on the composition of gases and condensates, a thermodynamic modelling of a high-temperature cooling gas from the Kudryavy volcano has been performed. Transportation and deposition forms have been calculated for most ore and rock-forming elements.

(2) The calculated mineral stability and the temperatures of deposition of most minerals correspond well to the data on their crystallization from volcanic gases. Consequently, the model takes into account rather completely and correctly those forms of the element transportation and deposition, which play the leading role in their transportation by high-temperature fumarolic gases.

(3) The alkali and alkali earth metals, Ga, In, Tl, Fe, Co, Ni, Cu, and Zn are mainly transported as chlorides in the gas phase. Ge, Sn, Pb, and Bi occur as sulfide and chloride species, at intermediate and low temperatures. Be, Al, and Si are transported as fluorides and oxides, while As and Sb, as sulfides and oxides. More complex, oxyfluoride and oxychloride transportation forms are dominant for Ti, Zr, V, Mo, W, and Re. Cd at a high temperature and Hg in the whole temperature range are transported as neutral species.

(4) Forms of transportation of all elements in gas are closely related to the position of these elements in the Mendeleev's periodic table. The behaviour of the volatile element forms, like the behaviour of the elements themselves, is controlled by the following general regularities: (a) all the elements follow a tendency of simplifying the major transportation forms, i.e., decreasing the number of atoms in the molecule at higher temperatures. For elements of a constant valence, this tendency is manifested in gradual polymerization of their molecules as the temperature decreases; (b) as the temperature rises, the stability of compounds with ionic bonds decreases, but that of compounds with covalence bonds increases; (c) similar species transformations takes place at lower temperatures for heavier elements.

## ACKNOWLEDGEMENTS

We are grateful to D. V. Grichuk, staff member of the Geochemistry Department of

the Moscow State University for making available the GBGAS software as well as for his help in the interpretation of the results and for valuable remarks when preparing this paper.

## REFERENCES

1. Symonds, R.B., Rose, W.I., Gregg, J., et al, Volcanic Gas Studies: Methods, Results and Applications, in Review in Mineralogy, vol. 30: Volatiles in Magmas, Carroll, M.R. and Holloway, J.R., Eds., 1994, pp. 1-66.
2. Giggenbach, W.F., Chemical Composition of Volcanic Gases, in Monitoring and Mitigation of Volcano Hazards, Scarpa, R. and Tilling, R.I., Eds. Berlin: Springer, 1996, pp. 221-256.
3. Stoiber, R.E. and Rose, W.I., The Geochemistry of Central American Volcanic Gas Condensates, Geol. Soc. Am. Bull., 1970, vol. 81, pp. 2891-2912.
4. Gemmell, J.B., Geochemistry of Metallic Trace Elements in Fumarolic Condensates from Nicaraguan and Costa Rican Volcanoes, J. Volcanol. Geotherm. Res., 1987, vol. 33, pp. 161-181.
5. Symonds, R.B., Rose, W.I., Reed, M.H., et al, Volatilization, Transport and Sublimation of Metallic and Non-Metallic Elements in High Temperature Gases at Merapi Volcano, Indonesia, Geochim. Cosmochim. Acta, 1987, vol. 51, pp. 2083-2101.
6. Symonds, R.B., Rose, W.I., Gerlach, T.M., et al., Evaluation of Gases, Condensates, and SO<sub>2</sub> Emission From Augustine Volcano, Alaska: the Degassing of a Cl-Rich Volcanic System, Bull. Volcanol., 1990, vol. 52, pp. 355-374.
7. Quisefit, J.P., Toutain, J.P., Bergametti, G., et al., Evolution versus Cooling Gaseous Volcanic Emissions from Momotombo Volcano, Nicaragua: Thermochemical Model and Observations, Geochim. Cosmochim. Acta, 1989, vol. 53, pp. 2591-2608.
8. Symonds, R.B., Scanning Electron Microscope Observations of Sublimates from Merapi Volcano, Indonesia, Ceochem. J., 1993, vol. 26, pp. 337-350.
9. Le Guern, F. and Bernard, A., A New Method for Sampling and Analyzing Volcanic Sublimates - Application to Merapi Volcano, Java, J. Volcanol. Geotherm. Res., 1982, vol. 12, pp. 133-146.
10. Bernard, A. and Le Guern, F, Condensation of Volatile Elements in High-Temperature Gases of Mount St. Helens, J. Volcanol. Geotherm. Res., 1986, vol. 28, pp. 91-105.
11. Le Guern, F, Cheynet, B., and Faivre-Pierret, R.X., Characterization and Modeling of the Complete Volcanic Gas Phase, Geochem. J., 1993, vol. 27, pp. 323-336.
12. Symonds, R.B., Reed, M.H., and Rose, W.I., Origin, Speciation, and Fluxes of Trace-

- Element Gases at Augustine Volcano, Alaska: Insights into Magma Degassing and Fumarolic Processes, *Geochim. Cosmochim. Acta*, 1992, vol. 56, pp. 633-657.
13. Symonds, R.B. and Reed, M.H., Calculation of Multicomponent Chemical Equilibria in Gas-Solid-Liquid Systems: Calculation Methods, Thermochemical Data, and Applications to Studies of High-Temperature Volcanic Gases with Examples from Mount St. Helens, *Am. J. Sci*, 1993, vol. 293, pp. 758-864.
  14. Taran, Yu.A., Hedenquist, J.F., Korzhinskii, M.A., et al., Geochemistry of Magmatic Gases From Kudryavy Volcano, Iturup, Kuril Islands, *Geochim. Cosmochim. Acta*, 1995, vol. 59, pp. 1749-1761.
  15. Gorshkov, G.S., *Vulkanizm Kuril'skoi ostrovnoi dugi (Volcanism of the Kurile Island Arc)*, Moscow: Nauka, 1967.
  16. Ostapenko, V.F., Petrology of Calderas of the Kurile Islands: Medvezhii and Zavaritskii Calderas, in *Geologiya igeofizika okeanov (Geology and Geophysics of the Oceans)*, Mater. Sakhalin. Issled. Inst., 1970, vol. 25, pp. 159-176.
  17. Pawley, A.R. and Holloway, J.R., Water Sources for Subduction Zone Volcanism: New Experimental Constrains, *Sciences*, 1993, vol. 260, pp. 664-667.
  18. Tkachenko, S.I., High-Temperature Fumarolic Gases, Condensates, and Sublimates of the Kudryavy Volcano, Iturup Island, Kurile Islands, Cand. Sc. (Geol.-Mineral.) Dissertation, Chernogolovka: Inst. Exp. Miner., 1996.
  19. *Melody geokhimicheskogo modelirovaniya i prognozirovaniya v gidrogeologii (Methods of Geochemical Modeling and Prediction in Hydrogeology)*, Moscow: Nedra, 1988.
  20. *Termodinamicheskie svoistva individual'nykh veshchestv (Thermodynamic Properties of Individual Compounds)*, Moscow: Nauka, 1978-1982, vols. 1-4.
  21. Baryshnikov, N.V. and Zelikman, D.T., Thermodynamic Properties of Re Chlorides and Oxides, *Izv. tyssh. Uchebn. Zaved., Tsvetn. Metal*, 1962, no. 6, pp. 98-110.
  22. Robie, R.A., Hemingway, B.S., and Fisher, J.R., Thermodynamic Properties of Minerals and Related Substances at 298.15 K and 1 bar Pressure and at Higher Temperatures, *Bull. U.S. Dep. Interior. Geol. Surv. Washington: U.S. Gov. Print. Off* 1978, vol. 1452.
  23. Tkachenko, S.I., Porter, R.R., Korzhinskii, M.A., et al., Study of Processes of Ore and Mineral Formation from the High-Temperature Fumarolic Gases on the Kudryavy Volcano, Iturup Island, Kurile Islands, *Geokhimiya*, 1999, vol. 37, no. 4, pp. 410-422.
  24. Vinogradov, A.P., Average Abundances of Chemical Elements in the Main Types of Igneous Rocks, *Geokhimiya*, 1962, no. 7, pp. 555-571.
  25. Toutain, J.P., Person, A., Cheminee, J.L., et al, *Mineralogie des sublimes du Volcan Poas*

- (Costa Rica), C. R. Acad. ScL, Set: II: ScL Terre Planetes, 1985, vol. 15, pp. 769-772.
26. Rosen, E., Osadchii, Eu., and Tkachenko, S., Oxygen Fugacity Directly Measured in Fumaroles of the Volcano Kudrjavii (Kuril Isles), Chem. Erde, 1993, vol. 53, pp. 219-227.
  27. Osadchii, E.G., Lunin, S.E., Korzhinskii, M.A., et al, Measurement of  $f_{O_2}$  and  $f_{S_2}$  by Electrochemical Sensors in High-Temperature Fumaroles of Active Volcanoes, Geokhimiya, 1997, no. 1, pp. 74-81.
  28. Giggenbach, W.F., Redox Processes Governing the Chemistry of Fumarolic Gas Discharges from White Islands, New Zealand, Appl Geochem., 1987, vol. 2, pp. 143-161.
  29. Murata, K.J., Occurrence of CuCl Emission in Volcanic Flames, am. J. ScL, 1960, vol. 258, pp. 769-772.
  30. Shmulovich, K.I., Formation of Salt Melts during Magmatic Degassing in an Open System: Evidence from the Kudryavii Volcano, Iturup Island, the Kurils, Doki Ross. Akad. Nauk, 1999, vol. 365, no. 3, pp. 361-365.
  31. Shmulovich, K.I., Vakulenko, A.G., and Shiryaev, A.A., Formation of Native Silicon in Sublimates of the Kudryavii Volcano, Iturup Island, Kurils Islands, Dokl Ross. Akad. Nauk, 1997, vol. 354, no. 6, pp. 800-803.
  32. Purchuk, L.L. and Ryabchikov, I.D., Fazovoe sootvetstvie v mineral'nykh sistemakh (Phase Correspondence in Mineral Systems), Moscow: Nedra, 1976.
  33. Fizicheskie velichiny: Spravochnik (Physical Values: A Handbook), Grigor'ev, I.S. and Meilikhov, E.Z., Eds., Moscow: Energoatomizdat, 1991.
  34. Energii razryva khimicheskikh svyazei. Potentsialy ionizatsii i srodstvo k elektronu (Energy of Disruption of Chemical Bonds. Ionization Potentials and Electron Affinity), Kondrafeva, V.N., Ed., Moscow: Nauka, 1974.

# **Perturbation Theory Based Equation of State for Polar Molecular Fluids:**

## **I. Pure Fluids**

**ABSTRACT**

Based on the thermodynamic perturbation theory an equation of state (EOS) for molecular fluids has been formulated which can be used for many fluid species in geological systems. The EOS takes into account four substance specific parameters, which are the molecular dipole moment, the molar polarizability and the two parameters of the Lennard-Jones potential. For the most important fluids these parameters are available from experimental measurements. In lack of direct experimental determinations, as a first approximation, for a pure fluid these parameters can also be evaluated using the critical temperature and the critical density in addition to the dipole moment for polar molecules with reasonable accuracy. The EOS has the appropriate asymptotic behaviour at high pressures and temperatures. Currently parameters for 98 inorganic and organic compounds are available. In this article the EOS for pure fluids is presented. In a further communication the EOS is extended to fluid mixtures (Churakov and Gottschalk, submitted to GCA).

Table 1. Notation and symbols

$\alpha, \alpha^*$	molecular polarizability, reduced polarizability
$\varepsilon, \sigma$	parameters of Lennard-Jones potential
$\varphi$	fugacity coefficient
$\mu, \mu^*$	dipole moment, reduced dipole moment
$\rho, \rho^*$	density, reduced density
$\rho_c, \rho_c^*$	critical density, reduced critical density
$A$	Helmholtz free energy
$J, K$	integrals over the pair and triple distribution functions
$N_A$	Avogadro's number
$P$	pressure
$P_c, P_c^*$	critical pressure, reduced critical pressure
$T$	temperature,
$T_c, T_c^*$	critical temperature, reduced critical temperature
$U$	internal energy
$Z$	compressibility
$r$	distance
$f$	fugacity
$u$	potential energy

## 1. INTRODUCTION

Fluids are important for many geological and petrological processes in the Earth's crust and mantle. For the evaluation of such processes the thermodynamic properties of these fluids are needed. The required free energies, i.e. fugacities, of the fluid components at high pressure and temperature are usually derived using equations of state (EOS). Several approaches are currently used to derive equations of state. For geological purposes these are sophisticated modifications to the van der Waals equation (e.g. Holloway, 1976; Jacobs and Kerrick, 1981; Kerrick and Jacobs, 1981; Halbach and Chatterjee 1982; Holland and Powell, 1991; Grevel and Chatterjee, 1992; Anderko and Pitzer, 1993a, 1993b; Duan et al., 1995b), virial equations of state (e.g. Saxena and Fei, 1987, 1988; Duan et al., 1992a, 1992b; Sterner and Pitzer, 1994) and other equations based on the thermodynamic perturbation theory (e.g. Shmulovich et al., 1982; Ree, 1984). In all these EOS the required coefficients are determined primarily using experimental results (e.g. *PVT*-data, phase equilibria). As an alternative to experimental results, fluid properties can be derived by computer simulations considering molecular interaction potentials (e.g. Brodholt and Wood, 1990, 1993a, 1993b; Belonoshko

and Saxena 1991a, 1991b, 1992; Duan et al., 1992c, 1995a, 1996, 2000; Kalinichev and Heinzinger, 1995; Destigneville et al., 1996).

All types of EOS mentioned are based on physical models and require various coefficients. If the physical description used by an EOS is perfect all required coefficients will have an exact physical meaning. Molecular interactions are manifold, however. Types of interactions involve repulsion due to a finite size of the molecules, attraction between permanent and induced dipoles, quadrupole and higher multipoles, and in addition dispersion forces. In the case of charged molecules coulomb interaction forces must be taken into account. Therefore any EOS uses simplifications by grouping sets of similar interactions into specific terms and therefore the precise physical significance of the required coefficients fades or is even lost. Fitting experimental data to an EOS reveals then in many cases coefficients with complicated functional dependencies with respect to temperature and either pressure or volume and are therefore often described using empirical functions such as polynomials. The use of arbitrary functions with questionable or no physical meaning transforms these EOS into empirical equations. Such empirical approaches generally offer relatively simple explicit expressions which are very attractive from a computational point of view. However, the determination of the coefficients of such EOS requires a large experimental database over the entire  $P$ - $T$  range for which the equation is intended to be used. Generally, it can not be safely extrapolated. Furthermore, because of the applied simplifications, these EOS are often unable to reproduce available experimental data with the required accuracy. The accuracy can be improved by introducing additional totally empirical parameters, which will dramatically degrade the reliability of any extrapolation. All EOS based on the van der Waals equation of state are therefore more or less empirical.

An alternative to EOS derived from the van der Waals equation are equations based on the perturbation theory. In general an EOS based on the perturbation theory is an equation which connects the macroscopic properties of a fluid (volume, temperature, pressure) to the parameters of intermolecular interaction. The general idea of the thermodynamic perturbation theory can be described as follows (e.g. Gray and Gubbins, 1984).

The potential of intermolecular interaction  $u$  of a real fluid can be always expressed as the sum of a model dependent interaction potential  $u_0$  (the reference potential) and the residual potential  $u_1$  which considers the differences of an interaction in the real fluid and the reference model. For any given  $u$  and  $u_0$ , a parametrical potential depending on a perturbation parameter  $\lambda$  can be formulated:

$$V(\lambda) = u_0 + \lambda(u - u_0) = u_0 + \lambda u_1 \quad (1)$$

It follows that  $V(0) = u_0$  and  $V(1) = u$ . The configurational part of the Helmholtz free energy  $A$ , i.e. the part of energy depending only on intermolecular or interatomic interaction forces, for a thermodynamic system of  $N$  molecules can be expressed at constant  $T$  and  $V$  by eq. (2) using the configurational integral  $z$  (eq. 3) which is the integral over all possible configurations  $\Gamma$  of  $N$  molecules.

$$A = -RT \ln(z) \quad (2)$$

$$z = \int \exp\left(-\frac{u(\Gamma)}{RT}\right) d\Gamma \quad (3)$$

If in eq. (3)  $u$  will be substituted by the parameterized potential  $V(\lambda)$  (eq. 1), the Helmholtz free energy  $A$  can be expressed as a power series of the perturbation parameter  $\lambda$ :

$$A(\lambda) = A_{\lambda=0} + \lambda \left( \frac{\partial A}{\partial \lambda} \right)_{\lambda=0} + \frac{\lambda^2}{2!} \left( \frac{\partial^2 A}{\partial \lambda^2} \right)_{\lambda=0} + \frac{\lambda^3}{3!} \left( \frac{\partial^3 A}{\partial \lambda^3} \right)_{\lambda=0} + \dots \quad (4)$$

As a first approximation the second and higher order terms can be neglected. Noting that  $u = V(\lambda=1)$ , the first order approximation of the Helmholtz free energy for the system of  $N$  molecules interacting with the potential  $u$  can be obtained as

$$A = -RT \ln(z_0) + z_0^{-1} \int u_1 \exp\left(-\frac{u_0}{RT}\right) d\Gamma = A_0 + A_1 \quad (5)$$

$$z_0 = \int \exp\left(-\frac{u_0}{RT}\right) d\Gamma \quad (6)$$

Thus the energy  $A$  of a thermodynamic system with the potential  $u$  can be expressed as the sum of the energy  $A_0$  of the reference system of molecules with the interaction potential  $u_0$  and the perturbation term  $A_1$ . The approximation requires, however, that  $u_1$  is small and the reference potential  $u_0$  is therefore close to the interaction potential in the real fluid. The accuracy can be improved, if the higher order terms in eq. (4) will be considered.

Strict application of the perturbation theory requires that the integral representing the term  $A_1$  in eq. (5) is solved. Some approaches (e.g. Anderko and Pitzer, 1993a, 1993b; Duan

et al, 1995b) avoid this complication, by combining  $A_0$  for the reference system with an empirical approximation for the perturbation term  $A_1$  without assumptions on the character of the intermolecular interaction in the fluid. But an EOS formulated in such a way becomes again empirical in character and the capability of extrapolation will be lost. One aim of this study is to formulate an EOS which is suitable for extrapolations to high pressures and temperatures. Therefore we insist on using a type of equation like eq. (5) for the formulation of the EOS which is based on the strict physical model of intermolecular interaction. Because it is an approximation we realize that this model may also deviate from the interaction of real molecules under extrapolation which will lead to deviations of the calculated thermodynamic properties. However these deviations are expected to be at least small, because the model is based on physical assumptions.

Most available experimental data are for pure fluids. *PVT*-data for fluid mixtures are rare and extraction of fluid properties of fluid mixtures requires interpolation. As a first approximation the van der Waals one-fluid theory is commonly used and parameters of pure fluids are combined algebraically. Their application requires, however, that for each involved fluid component the EOS is exactly of the same type. Most published EOS are for one or only few fluid components and the EOS from different communications are rarely of the same type. Therefore these EOS can not be used to derive fluid properties in complex mixtures which have not been studied experimentally. In addition the mixing rules generally used are not strictly in accordance with statistical mechanics. Dohrn and Prausnitz (1990) showed in a systematic study of different fluid mixtures that van der Waals mixing rules may predict an unrealistic physical behaviour such as increasing volume with pressure. Nevertheless one of the aims of this study was to formulate an EOS which is suitable for as many components as possible, so that this EOS can be applied in a further step to complex fluid mixtures (Churakov and Gottschalk, submitted to GCA).

In the following an EOS is formulated using the perturbation theory with the Lennard-Jones potential as the reference system. The EOS is applied to 98 pure inorganic and organic fluid components and has the following attractive features. It needs a minimum number of fitting parameters and its asymptotic behaviour at high pressure and temperature is physically correct. As far as the form of the EOS is identical for all 98 considered fluid components the EOS can be easily extended to the complex fluid mixtures using mixing rules. Fluid mixtures will be covered in a second communication (Churakov and Gottschalk, submitted).

## 2. THERMODYNAMIC MODEL

In this section only the principal aspects of the proposed EOS are discussed. Details for the computational implementation can be found in the Appendix II.1.

The main contribution to the potential interaction energy between two polar molecules  $i$  and  $j$  (eq. 7) is given by the sum of the Lennard-Jones potential (eq. 8), the potential due to dipole-dipole (eq. 9) and to dipole-induced dipole interaction (eq. 10) which is the generalized Stockmayer potential (e.g. Hirschfelder et al., 1964).

$$u_{ij} = u_{ij}^{LJ} + u_{ij}^{dip-dip} + u_{ij}^{ind-dip} \quad (7)$$

$$u_{ij}^{LJ} = 4\epsilon_{ij} \left[ \left( \frac{\sigma_{ij}}{r_{ij}} \right)^{12} - \left( \frac{\sigma_{ij}}{r_{ij}} \right)^6 \right] \quad (8)$$

$$u_{ij}^{dip-dip} = \mu_i \mu_j \frac{-2 \cos \theta_i \cos \theta_j + \sin \theta_i \sin \theta_j \cos(\phi_i - \phi_j)}{r_{ij}^3} \quad (9)$$

$$u_{ij}^{ind-dip} = - \frac{\alpha_i \mu_j^2 + \alpha_j \mu_i^2}{r_{ij}^6} \quad (10)$$

Here  $r$  is the distance between the centres of two molecules,  $\theta$  and  $\phi$  are the angles defining the relative orientation of its dipoles,  $\sigma$  and  $\epsilon$  are the specific parameters of interaction of the Lennard-Jones potential,  $\alpha$  is the average polarizability of a molecule and  $\mu$  its dipole moment. Although, eqs. (7)-(10) also hold for interactions between different molecules, in this part of the communication only interactions between molecules of the same type are considered. In the case of interaction of two non-polar molecules the potentials  $u_{ij}^{dip-dip}$  and  $u_{ij}^{ind-dip}$  are both zero and therefore only  $u_{ij}^{LJ}$  remains.

These potentials (eqs. 7-10) can be used to derive an EOS for molecular fluids based on perturbation theory (e.g. Gray and Gubbins, 1984). Because the thermodynamic properties of the Lennard-Jones potential are well known, it is convenient to take the Lennard-Jones potential as the reference system and consider all contributions from other interactions (dipole-dipole, dipole-induced dipole) as perturbations, i.e. deviations from the properties of Lennard-Jones fluid.

The molar residual Helmholtz free energy  $A^{res}$ , the contribution due to deviations from the ideal gas behaviour (no molecular interaction and zero volume of molecules) can be generally expressed in form of a power expansion:

$$A - A^{ideal} = A^{res} = A_0 + A_1 + A_2 + A_3 + \dots \quad (11)$$

In the following the truncated expression is used

$$A^{res} = A^{LJ} + A_1^{dip-dip} + A_2^{dip-dip} + A_3^{dip-dip} + A_1^{ind-dip} \quad (12)$$

where  $A^{LJ}$  is residual Helmholtz free energy of a Lennard-Jones fluid as the reference system,  $A_1^{dip-dip}$ ,  $A_2^{dip-dip}$  and  $A_3^{dip-dip}$  are the first, second and third order perturbation contributions of the dipole-dipole interaction and  $A_1^{ind-dip}$  is the first order perturbation contribution of the induced dipole-dipole interaction. Because of its much smaller contribution in comparison to the dipole-dipole contribution the induced dipole-dipole interaction is already truncated after the first term.

The explicit expressions for a pure fluid are (e.g. Gubbins and Twu, 1978):

$$A_1^{dip-dip} = 0 \quad (13)$$

$$A_2^{dip-dip} = -\frac{2\pi N_A^2 \rho \mu^4}{3kT \sigma^3} J \quad (14)$$

$$A_3^{dip-dip} = \frac{32\pi^3 N_A^3 \rho^2}{135(kT)^2} \left(\frac{14\pi}{5}\right)^{1/2} \frac{\mu^6}{\sigma^3} K \quad (15)$$

$$A_1^{ind-dip} = -4\pi N_A^2 \rho \frac{\alpha \mu^2}{\sigma^3} J \quad (16)$$

Here,  $\rho$  is the density of the fluid,  $\mu$  is the dipole moment and  $\alpha$  is the polarizability of the respective molecule. Due to symmetry of the interaction, the term  $A_1^{dip-dip}$  is zero. The symbols  $J$  and  $K$  are integrals over the pair and triple distribution functions of the reference Lennard-Jones fluid, which depend on temperature, density and the Lennard-Jones parameters  $\sigma$  and  $\varepsilon$ . For  $J$  and  $K$  the approximations of Stell et. al (1972) and of Gubbins and Twu (1978) were used, respectively (see Appendix).

In order to improve the convergence of the perturbation expansion Stell et al. (1972, 1974) recommended to use a [0,1] Padé approximation for the dipole-dipole interaction, which gives the final expression for Helmholtz free energy of system as:

$$A^{res} = A^{LJ} + A_2^{dip-dip} \left( 1 - \frac{A_3^{dip-dip}}{A_2^{dip-dip}} \right)^{-1} + A_1^{ind-dip} \quad (17)$$

Thermodynamic properties of the reference Lennard-Jones system were calculated with the modified Weeks-Chandler-Andersen perturbation theory (Weeks et al., 1971; Andersen et al., 1972). Accordingly the Lennard-Jones contribution to the Helmholtz free energy can be expressed by:

$$A^{LJ} = A^{HS} + A^{HTA} + A^{RPA} \quad (18)$$

Here  $A^{HS}$  is the free energy of a hard sphere system,  $A^{HTA}$  is the high temperature approximation and  $A^{RPA}$  the random phase approximation. The approaches proposed by Carnahan and Starling (1969), Tereshchenko et al. (1981) and Miyano and Masuoka (1984) were used, respectively. For the details see the discussion by Verlet and Weis (1972a, 1972b) and for the practical implementation the Appendix II.1.

The perturbation expansion discussed above provides a formulation for the Helmholtz free energy  $A=A(T,\rho)$  of the system as function of temperature and density. Other thermodynamic quantities of interest can be derived by differentiation, (e.g. the compressibility factor  $Z$ , the internal energy  $U$  and the fugacity coefficient  $\phi$ ):

$$Z = 1 + \rho \frac{\partial(A^{res}/(RT))}{\partial \rho} \quad (19)$$

$$U = -T^2 \frac{\partial(A/T)}{\partial T} \quad (20)$$

$$\ln \frac{f}{P} = \ln \phi = \frac{A^{res}}{RT} - \ln(Z) + Z - 1 \quad (21)$$

A list of other important derivatives can be found in the literature (e.g. Prausnitz et al., 1999).

### 3. LIMITATIONS OF THE PROPOSED EOS

The EOS presented above includes the following simplifications. First the molecules are treated as Lennard-Jones spheres with a permanent point-dipole moment. But typical polyatomic molecules possess also quadrupole and higher order moments leading to dipole-quadrupole, quadrupole – quadrupole, induced dipole – quadrupole and other interactions. The polarizability of complex molecules depends substantially on their orientation with respect to the applied electric field, while the EOS takes only the average isotropic polarizability into account. Additional interactions between some molecules will occur if the intermolecular distance is short and the electron shells overlap. Contributions of such forces to the total interaction energy could be significant for some molecule species.

Furthermore, the intermolecular interactions were treated to be pair additive. In real fluids, the interaction of three and more molecules differs from the sum of the pairwise interactions. But this difference is substantial only, if all interacting molecules will be close together. In low density fluids the probability of simultaneous collision of more than two molecules is low, therefore higher order interactions can be neglected at such conditions. In order to use the pair additive model at high densities, triple and higher order interactions must be included in the pair interaction term which is called the effective pairwise potential. While such effective pairwise potentials lead to an accurate description of the fluids at the high and intermediate densities, for low densities these are less accurate.

Another problem is that the perturbation expansion is only reasonable if the properties of the target fluid are close to the reference system. In our particular case this requires that the energy due to dipole-dipole interaction is small relative to the contribution due to Lennard-Jones interaction. Computer experiments showed (Stell et al., 1972) that the perturbation expansion in the proposed form will be very accurate if the square of the reduced dipole moment

$$\mu^{*2} = \mu^2 / (\epsilon \sigma^3) \quad (22)$$

is lower than 3, less accurate in the range of  $3 < \mu^{*2} < 4$  and inaccurate for values greater than 4. The squares of typical reduced dipole moments of slightly polar compounds like CO and HCl are smaller than 3, but for strong dipoles like H<sub>2</sub>O it is in the range of  $3 < \mu^{*2} < 4$  or even larger. The dipole moment of molecules changes with temperature, density and fluid composition while it is treated here, with the exception of H<sub>2</sub>O, as constant.

#### 4. DERIVATION METHODS OF THE POTENTIAL PARAMETERS FOR PURE FLUIDS

The EOS described above requires the four parameters  $\varepsilon$ ,  $\sigma$ ,  $\mu$ ,  $\alpha$  for each pure fluid, to be evaluated using experimental data. If thermodynamic data (*PVT*-data, phase equilibria) for a considered fluid are available, it is always advantageous to fit  $\varepsilon$ ,  $\sigma$ ,  $\mu$  and  $\alpha$  directly to these experimental results. As an alternative these potential parameters can be derived from other experimental sources. Values for the electric dipole moment  $\mu$ , and the polarizability  $\alpha$  of molecules in fluids are readily available from spectroscopy measurements. The parameters of the Lennard-Jones potential  $\varepsilon$  and  $\sigma$  can be derived from the experimental determination of the second-virial-coefficient or from fluid viscosities. Both methods are suffering from the same limitations, however. Parameters derived from experimental second-virial-coefficient data or fluid viscosities usually fail to describe the fluid properties at liquid like densities or vapour-liquid equilibria (see van Leeuwen, 1994 for a more detailed discussion).

Because of these limitations it seems advantageous to derive the values of the required parameters from phase equilibria. Liquid-vapour equilibria of pure fluids or critical properties are readily available. Potoff and Panagiotopoulos (1998) determined critical properties for a Lennard-Jones fluid from computer simulations. They reported general values for the reduced (dimensionless) critical temperature ( $T_c^{*LJ} = kT_c / \varepsilon$ ), critical density ( $\rho_c^{*LJ} = \rho_c \sigma^3$ ) and critical pressure ( $P_c^{*LJ} = P_c \sigma^3 / \varepsilon$ ) of 1.312, 0.316 and 0.1279, respectively. Using these values, the critical temperature  $T_c$  and applying the corresponding-states theory (e.g. Prausnitz et al., 1999) for pure fluids  $\varepsilon$  can be obtained with eq. (23),

$$\varepsilon = \frac{kT_c}{T_c^{*LJ}} \quad (23)$$

and  $\sigma$  can be derived either by eqs. (24) or (25) using the critical density

$$\sigma^3 = \frac{\rho_c^{*LJ}}{\rho_c} \quad (24)$$

or the critical pressure

$$\sigma^3 = \frac{P_c^{*LJ}}{P_c} \varepsilon \quad (25)$$

For real fluids eqs. (24) and (25) provide slightly different values for  $\sigma$ . This difference can be thought as a measure of the validity of the Lennard-Jones model. The best agreement is observed for noble gases. For simple non-polar molecules the difference in the obtained  $\sigma$  from critical pressure and density does not exceed 1-2%. For non-polar molecules which possess a strong quadrupole moment (e.g. CO<sub>2</sub>) this deviation is in the range of 4-5%. For highly polar molecules this difference is up to 10%, indicating that the derivation using the Lennard-Jones approximation is unacceptable for such fluids.

For polar molecular fluids an effective method of determination of the Stockmayer potential parameters (Lennard-Jones plus dipole-dipole interaction), was introduced by van Leeuwen (1994). This method requires the knowledge of the critical temperature  $T_c$  and density of the boiling liquid  $\rho_{L,0.75}$  at the temperature  $0.75 T_c$ . Based on results of computer simulations the specific properties of a Stockmayer fluid were expressed as a function of the square of the reduced dipole moment  $\mu^{*2}$ :

$$T_c^{*ST} = 1.313 + 0.2999\mu^{*2} - 0.2837\ln(\mu^{*2} + 1) \quad (26)$$

$$\rho_{L,0.75}^{*ST} = 0.7197 - 0.00362\mu^{*2} + 0.00666\mu^{*4} - 0.00142\mu^{*6} + 0.0000863\mu^{*8} \quad (27)$$

where  $\rho_{L,0.75}^{*ST}$  is the reduced density at  $0.75 T_c$ :

$$\rho_{L,0.75}^{*ST} = \sigma^3 \rho_{L,0.75} \quad (28)$$

$\mu^{*2}$  can be obtained from eq. (29) which is a combination of eqs. (22), (23), (27) and (28) if a value for  $\mu$  is available.

$$\mu^{*2} = \frac{T_c^{*ST}}{kT_c} \frac{\rho_{L,0.75}}{\rho_{L,0.75}^{*ST}} \mu^2 \quad (29)$$

Knowing  $\mu^{*2}$ ,  $\varepsilon$  and  $\sigma$  can be calculated from eqs. (23, 26, 27, 28).

If the liquid density  $\rho_{L,0.75}^{*ST}$  at  $T^*=0.75$  is unknown, the critical density or pressure can be used instead and eq. (27) is replaced by either eq. (30) or (31) (van Leeuwen, 1994):

$$\rho_c^{*ST} = 0.3009 + 0.00785\mu^{*2} - 0.0198\mu^{*4} \quad (30)$$

$$P_c^{*ST} = 0.127 + 0.0023\mu^{*2} \quad (31)$$

The reduced dipole moment  $\mu^{*2}$  is then calculated by eq. (32) or (33), respectively.

$$\mu^{*2} = \frac{T_c^{*ST}}{kT_c} \frac{\rho_c}{\rho_c^{*ST}} \mu^2 \quad (32)$$

$$\mu^{*2} = \left( \frac{T_c^{*ST}}{kT_c} \right)^2 \frac{P_c}{P_c^{*ST}} \mu^2 \quad (33)$$

The parameters  $\varepsilon$  and  $\sigma$  are then calculated in the same way as shown above. The latter approach, however, is less accurate (van Leeuwen, 1994).

It should be remembered that the corresponding state theory approach can be applied only to non-polar molecules ( $\mu=0$ ). For such fluids the terms  $A_2^{dip-dip}$ ,  $A_3^{dip-dip}$ ,  $A_1^{ind-dip}$  in eq. (12) are zero. However, the polarizabilities of non-polar molecules are non-zero.

The approach of van Leeuwen (1994) for polar molecules requires further assumptions. According to this method the potential interaction energy of two molecules of the same kind is given by sum the of the Lennard-Jones and the dipole-dipole interaction. The dipole-induced dipole interaction is neglected ( $A_1^{ind-dip}=0$ ) and implicitly included in the Lennard-Jones and dipole-dipole terms, i.e. the molecular polarizability  $\alpha$  must be set to zero. The dipole-induced dipole interaction becomes relevant for mixtures of polar and non-polar molecules (Churakov and Gottschalk, submitted to GCA).

## 5. RESULTS AND DISCUSSION

### 5.1. Polar gases

#### 5.1.1. $H_2O$

Water is the most common component in natural fluids. It is also one of the fluids for which it is very difficult to describe the thermodynamic properties accurately. First of all, the critical point of pure water (647.1 K, 22.1 MPa) is in the P-T range of geological processes. It is known that perturbation theory fails to describe properties of fluid near the critical point (e.g. Gray and Gubbins, 1984). Additionally the near critical region is difficult to define rigorously. A detailed review of the anomalous behaviour of water near the critical point is

given by Johnson and Norton (1991). They have shown that the anomalous behaviour of  $\text{H}_2\text{O}$  at the critical point extends as far as 100-150 °C above the critical temperature in a density range of approximately 0.15-0.5  $\text{g}/\text{cm}^3$ . Because of the complex behaviour of  $\text{H}_2\text{O}$  at these conditions it can not be expected beforehand that the proposed EOS works satisfactorily in this region. Furthermore the large dipole moment of water molecules is close to the tolerance limit of the proposed model ( $\mu^{*2} = 4.79$ ). On the other hand, pure  $\text{H}_2\text{O}$  is an excellent example to check the applicability of the proposed EOS. If the EOS reproduces the properties of  $\text{H}_2\text{O}$  in a satisfactorily manner, then it gives us some confidence that it can be used for other less polar fluids with lower critical temperatures, too.

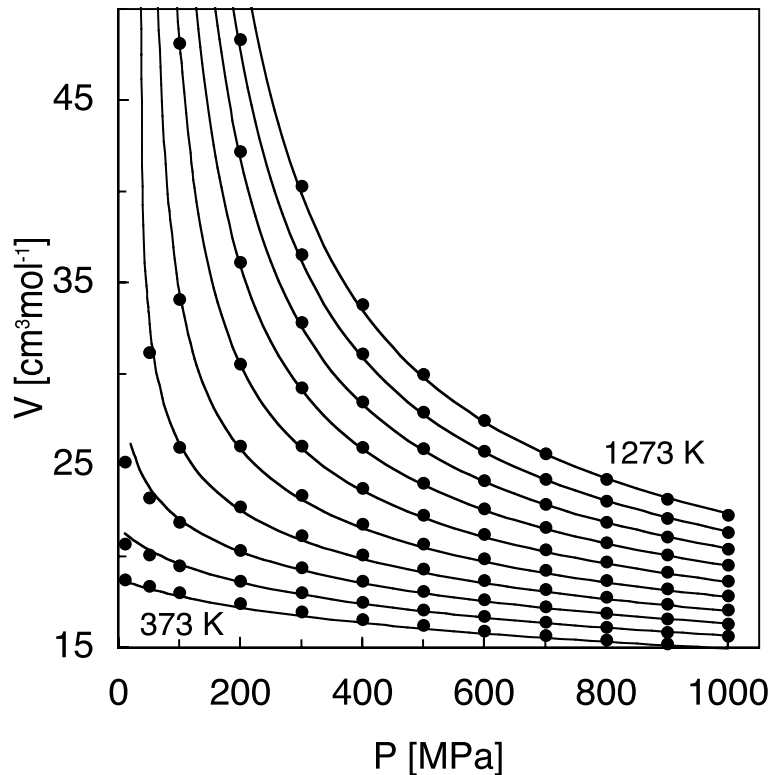


Fig. 1. The molar volumes of  $\text{H}_2\text{O}$  as predicted by the presented EOS (curves) compared to the values (points) derived using the EOS from Saul and Wagner (1989). Each line in the plot corresponds to an isotherm in the range of 373.15 to 1273.15 K in 100 degree increments.

Instead of using the original experimental thermodynamic data to derive the parameters for our EOS, the EOS of Saul and Wagner (1989) was used to provide  $PVT$  data for water. This EOS reproduces the experimental data of  $\text{H}_2\text{O}$  up to 1273 K and 2500 MPa

with sufficient accuracy. The parameters were determined by minimising the pressure deviation in the range 0-1000 MPa and 373-1273 K.

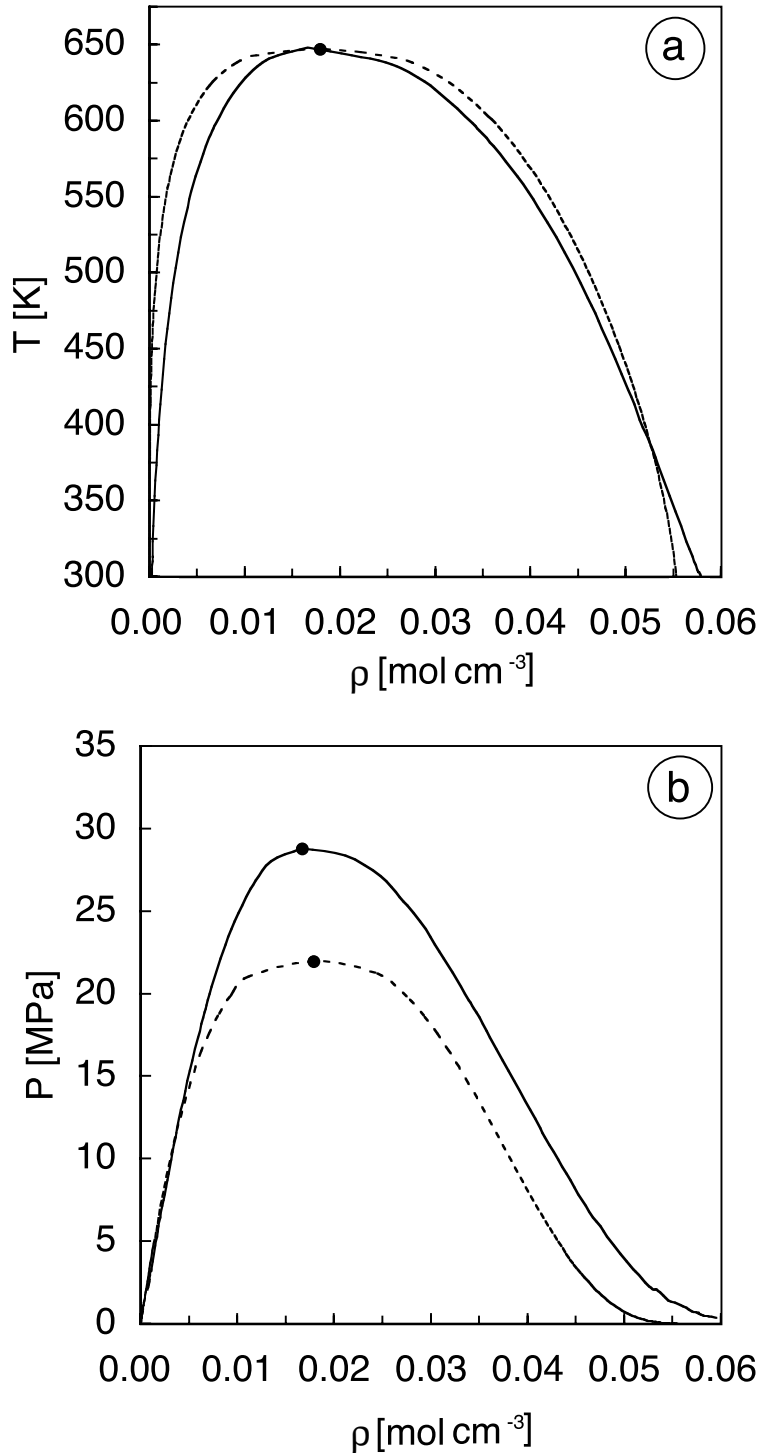


Fig. 2. Vapour-Liquid equilibria of H<sub>2</sub>O as predicted by the EOS (solid curves) and experimental saturation data (dotted curves).

For temperatures above 773.15 K the P-V-T properties of water can be accurately reproduced assigning constant values of the EOS parameters:

$$\sigma [\text{\AA}] = 2.926 \quad (34)$$

$$\varepsilon/k [\text{K}] = 264.604 \quad (35)$$

$$\mu [\text{D}] = 2.09457 \quad (36)$$

At lower temperatures, this set of parameters provides unsatisfactory results. It was possible, however, to extend the application range of the EOS by introducing a temperature dependency of the dipole moment  $\mu$  and the Lennard-Jones parameter  $\sigma$ , while the parameter  $\varepsilon$  remains constant identical to the high temperature value. A simple quadratic function is used which reaches smoothly the high temperature parameters at 773.15 K. The following relations for  $\mu$  and  $\sigma$  for  $T < 773.15\text{K}$  were derived:

$$\sigma [\text{\AA}] = 2.926 - 2.0996 \cdot 10^{-7} \times (T - 773.15)^2 \quad (37)$$

$$\mu [\text{D}] = 2.09457 - 2.5887 \cdot 10^{-6} \times (T - 773.15)^2 \quad (38)$$

In Fig. 1 the molar volumes of water predicted by the EOS and the values provided by Saul and Wagner (1989) are plotted between 373-1273 K. The agreement is good except for the direct vicinity of the liquid-vapour equilibrium (LVE) and the near critical region. The deviations are emphasised in Figs. 2a,b which show the calculated the LVE in comparison to the saturation properties of real H<sub>2</sub>O. The derived EOS reproduces accurately the critical density and the critical temperature (Fig. 2a) while the critical pressure (Fig. 2b) is overestimated by 6.4 MPa. Due to this discrepancy the density of the saturated vapour is overestimated and the density of the coexisting liquid is underestimated. However, Fig. 1 shows that at sufficient distance from these conditions the EOS provides accurate PVT-properties.

The observed deviations have an influence on those thermodynamic quantities, however, which are calculated using integrals of the volume or pressure (e.g. Gibbs free energy or fugacity). Therefore any Gibbs free energy calculated for low temperatures and pressures above 50 MPa will have constant offset from the correct value. At the critical

temperature and at pressures above 50 MPa the Gibbs free energy of H<sub>2</sub>O calculated by our EOS is about 0.9 kJ/mole too large in comparison to Saul and Wagner (1989). At lower temperatures the difference progressively increases. The following expression can be used to correct the Gibbs free energy of H<sub>2</sub>O below 773.15 K and above 50 MPa:

$$G_{corr}[\text{kJ/K mol}] = 5.68644 \cdot 10^{-5} \times (T - 773.15)^2 \quad (39)$$

It is up to the user to decide if the correction should be applied or not. Eq. (39) can be always used to improve the accuracy of the Gibbs free energy of the water provided by the EOS. If the deviation is acceptable, however, it is advantageous to ignore the correction. The EOS loses its self-consistency if  $G_{corr}$  is used and it can not be properly applied to vapor-like phase.

Table 2. Experimentally measured densities of water compared to the predictions from various EOS. The experimental values of Withers et al. (2000) are based on fluid inclusion measurements. In the first column, the measured densities of the fluid inclusions in corundum at ambient conditions are given, the next column shows the data corrected to the thermal expansion and compressibility of the host mineral (see original paper for details).

P	T	Withers et al. (2000)		EOS		
		Density (measured)	Density (corrected)	Brodholt & Wood (1993)	Saxena & Fei (1987)	this work
[GPa]	[K]	[g cm <sup>-3</sup> ]	[g cm <sup>-3</sup> ]	[g cm <sup>-3</sup> ]	[g cm <sup>-3</sup> ]	[g cm <sup>-3</sup> ]
3.50	1173.15	1.17	1.17	1.20	1.27	1.19
2.50	983.15	1.15	1.14	1.15	1.21	1.15
3.00	1373.15	1.11	1.09	1.10	1.19	1.10
1.40	983.15	1.00	0.99	0.99	1.05	1.00
3.00	1273.15	1.12	1.11	1.12	1.20	1.12
1.85	983.15	1.07	1.06	1.07	1.13	1.07
3.50	1373.15	1.16	1.15	1.15	1.24	1.14
2.50	1373.15	1.05	1.04	1.04	1.13	1.04
4.00	1373.15	1.19	1.18	1.19	1.28	1.18
3.00	1173.15	1.15	1.14	1.15	1.22	1.14

To evaluate the behaviour of the EOS at high pressures and temperatures the calculated densities from the derived EOS are compared to the experimental measurements by Withers et al. (2000) and to the EOS by Brodholt and Wood (1993a) and Saxena and Fei (1987). The agreement between the EOS presented here and the experimental values is always within the uncertainties of the measurements. While the data of Withers et al. (2000) were not used in the fitting procedure, the successful predictions in the range from 1 to 4 GPa provides some confidence into the ability to use the EOS for extrapolation at high pressures.

5.1.2.  $NH_3$ 

Like  $H_2O$ ,  $NH_3$  also has a strong dipole moment. Accurate  $PVT$ -relationships are available up to 700 K and 1000 MPa (Tillner-Roth et al., 1993).  $NH_3$  is a good example to check accuracy of the method proposed by van Leeuwen (1994) to derive parameter of the Stockmayer potential. The densities calculated using the potential parameters reported by van Leeuwen (1994):  $\sigma = 3.261 \text{ \AA}$ ,  $\epsilon/k = 262.2 \text{ K}$ ,  $\mu = 1.47 \text{ D}$  are compared with those from Tillner-Roth et al. (1993) in the temperature and pressure range of 573–700 K and 0–1000 MPa (Fig. 3a). The maximum deviations in the density are below 2%. This is not the best set of parameters, however, because the deviations are systematically positive. But it is important to emphasize that only two experimental values, the critical temperature  $T_c$  and the density of liquid  $\rho_{L,0.75}$ , are involved in the determination of  $\epsilon$  and  $\sigma$ . For such a simple method the agreement is excellent. Moreover, it can be expected that for less-polar or strictly linear molecules these deviations will be even smaller. Using available  $PVT$ -data, the parameters can obviously be improved. The parameters obtained by least-square fit are  $\sigma = 3.294 \text{ \AA}$ ,  $\epsilon/k = 200 \text{ K}$ ,  $\mu = 1.849 \text{ D}$ . The observed maximum density deviation is below 0.5 % (Fig. 3b). In comparison to the parameters derived by van Leeuwen (1994) the values of the parameter  $\sigma$  are quite similar whereas based on  $PVT$ -data the dipole moment is higher and  $\epsilon$  is smaller.

Table 3. Parameters of Stockmayer interaction potential for various molecules (van Leeuwen, 1994).

	$\epsilon/k$ [K]	$\sigma$ [ $\text{\AA}$ ]	$\mu$ [D]	$\alpha$ [ $\text{\AA}^3$ ]
$N_2O$	235.7	3.658	0.161	0.0
NO	137.0	3.094	0.159	0.0
$H_2S$	277.2	3.680	0.97	0.0
$SO_2$	302.7	3.903	1.633	0.0
COS	286.9	4.099	0.715	0.0
CO	101.2	3.623	0.11	0.0
$PH_3$	302.7	3.903	0.55	0.0
HCN	149.7	3.796	2.984	0.0

5.1.3.  $N_2O$ , NO,  $H_2S$ ,  $SO_2$ , COS, CO,  $PH_3$ , HCN, and various organic compounds

The Stockmayer potential parameters of these eight polar gases (Table 3) were determined by van Leeuwen (1994) using vapour-liquid equilibria. These values are incorporated in the model without any changes. Van Leeuwen (1994) also reported parameters for additional 53 organic compounds. These parameters are repeated in Table 4 for convenience.

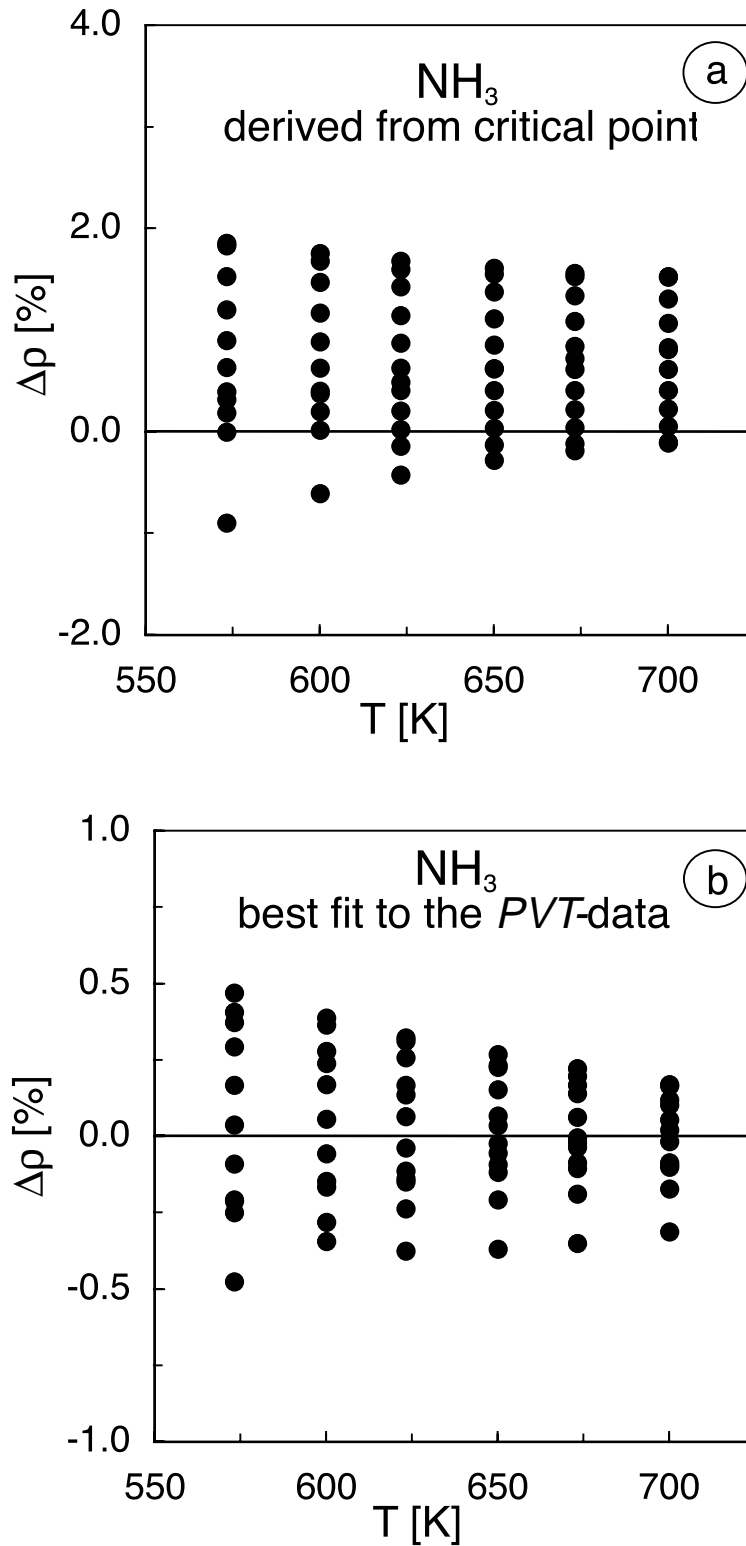


Fig 3. Deviations of the densities of  $\text{NH}_3$  from the experimental  $PVT$ -results (Tillner-Roth et al., 1993) as predicted by the EOS using the parameters a) proposed by van Leeuwen (1994) and b) fitted to the experimental results.

Table 4. Parameters for further molecules (van Leeuwen, 1994).

	$\epsilon/k$ [K]	$\sigma$ [Å]	$\mu$ [D]	$\alpha$ [Å <sup>3</sup> ]		$\epsilon/k$ [K]	$\sigma$ [Å]	$\mu$ [D]	$\alpha$ [Å <sup>3</sup> ]
CCl <sub>2</sub> O (phosgene)	342.3	4.548	1.17	0.0	C <sub>2</sub> H <sub>4</sub> O (ethylene ether)	324.7	4.079	1.89	0.0
CH <sub>4</sub> O (methanol)	359	3.803	0.71	0.0	C <sub>4</sub> H <sub>8</sub> O (tetrahydrofuran)	403.4	4.856	1.63	0.0
C <sub>2</sub> H <sub>6</sub> O (ethanol)	373.3	4.299	0.73	0.0	CH <sub>5</sub> N (methylamine)	315.1	3.91	1.29	0.0
C <sub>3</sub> H <sub>8</sub> O (n-propanol)	398.1	4.691	0.69	0.0	C <sub>2</sub> H <sub>7</sub> N (dimethylamine)	329.8	4.444	1.03	0.0
C <sub>3</sub> H <sub>8</sub> O (2-propanol)	376.8	4.699	0.66	0.0	C <sub>3</sub> H <sub>9</sub> N (trimethylamine)	329.4	4.918	0.63	0.0
C <sub>4</sub> H <sub>10</sub> O (n-butanol)	421.8	5.047	0.66	0.0	C <sub>2</sub> H <sub>7</sub> N (ethylamine)	342.1	4.431	1.22	0.0
C <sub>4</sub> H <sub>10</sub> O (2-butanol)	401.1	5.037	0.66	0.0	C <sub>4</sub> H <sub>11</sub> N (diethylamine)	377.2	5.212	0.91	0.0
C <sub>4</sub> H <sub>10</sub> O (2-methyl-1-propanol)	410.4	5.041	0.64	0.0	C <sub>6</sub> H <sub>15</sub> N (trimethylamine)	407	5.798	0.83	0.0
C <sub>4</sub> H <sub>10</sub> O (2-methyl-2-propanol)	378.1	5.061	0.67	0.0	CH <sub>3</sub> NO <sub>2</sub> (nitromethane)	290.4	4.347	3.57	0.0
C <sub>6</sub> H <sub>6</sub> O (phenol)	524.9	5.079	1.45	0.0	C <sub>2</sub> H <sub>3</sub> N (acetonitrile)	175.7	4.284	3.92	0.0
C <sub>3</sub> H <sub>6</sub> O (acetone)	326.2	4.691	2.88	0.0	C <sub>3</sub> H <sub>3</sub> N (acrylonitrile)	244.3	4.606	3.87	0.0
C <sub>4</sub> H <sub>8</sub> O (2-butanone)	370.4	5.036	2.8	0.0	C <sub>5</sub> H <sub>5</sub> N (pyridine)	453.3	4.956	2.25	0.0
C <sub>5</sub> H <sub>10</sub> O (2-pentanone)	402.5	5.38	2.72	0.0	CH <sub>4</sub> S (methyl mercaptan)	343.7	4.19	1.52	0.0
C <sub>5</sub> H <sub>10</sub> O (3-pentanone)	401.9	5.345	2.72	0.0	C <sub>2</sub> H <sub>6</sub> S (dimethyl sulphide)	375.1	4.637	1.5	0.0
C <sub>5</sub> H <sub>10</sub> O (3-methyl-2-butanone)	393.9	5.338	2.77	0.0	C <sub>2</sub> H <sub>6</sub> S (ethyl mercaptan)	371.2	4.659	1.56	0.0
CH <sub>2</sub> O (formaldehyde)	206.5	3.731	2.33	0.0	CH <sub>3</sub> F (fluoromethane)	186.7	3.766	1.82	0.0
C <sub>2</sub> H <sub>4</sub> O (acetaldehyde)	268.3	4.248	2.69	0.0	CH <sub>2</sub> F <sub>2</sub> (difluoromethane)	213	3.881	1.96	0.0
C <sub>3</sub> H <sub>6</sub> O (propionaldehyde)	335.5	4.648	2.52	0.0	CHF <sub>3</sub> (trifluoromethane)	199.6	4.007	1.62	0.0
C <sub>2</sub> H <sub>4</sub> O <sub>2</sub> (acetic acid)	435.6	4.356	1.74	0.0	C <sub>2</sub> H <sub>5</sub> F (fluoroethane)	253.3	4.268	1.94	0.0
C <sub>2</sub> H <sub>4</sub> O <sub>2</sub> (methyl Formate)	352.6	4.374	1.77	0.0	C <sub>2</sub> H <sub>4</sub> F <sub>2</sub> (1,1-difluoroethane)	248.5	4.429	2.3	0.0
C <sub>3</sub> H <sub>6</sub> O <sub>2</sub> (ethyl formate)	371.9	4.806	0.94	0.0	C <sub>2</sub> H <sub>3</sub> F <sub>3</sub> (1,1,1-trifluoroethane)	221.2	4.535	2.28	0.0
C <sub>4</sub> H <sub>8</sub> O <sub>2</sub> (n-propyl formate)	402.9	5.159	0.7	0.0	CH <sub>3</sub> Cl (chloromethane)	279.8	4.097	1.94	0.0
C <sub>3</sub> H <sub>6</sub> O <sub>2</sub> (Mmethyl acetate)	376.3	4.781	0.67	0.0	CHCl <sub>3</sub> (trichloromethane)	406.5	4.829	1.05	0.0
C <sub>4</sub> H <sub>8</sub> O <sub>2</sub> (ethyl acetate)	390.3	5.153	0.78	0.0	C <sub>2</sub> H <sub>4</sub> Cl <sub>2</sub> (1,1-dichloroethane)	381.7	4.9	2.06	0.0
C <sub>2</sub> H <sub>6</sub> O (dimethyl ether)	297.1	4.386	0.3	0.0	C <sub>6</sub> H <sub>5</sub> Cl (chlorobenzene)	476.3	5.319	1.69	0.0
C <sub>3</sub> H <sub>8</sub> O (methyl ethyl ether)	329.5	4.793	0.23	0.0	C <sub>2</sub> H <sub>5</sub> Br (bromoethane)	370.2	4.684	1.79	0.0
C <sub>4</sub> H <sub>10</sub> O (diethyl ether)	353.4	5.166	0.13	0.0					

## 5.1.4. HF, HBr

The parameters for HF and HBr were evaluated (Table 5) from vapour-liquid properties at  $0.75 T_c$ , according to the method of van Leeuwen (1994). Densities of liquid HBr and HF are available from Strunk and Wingate (1954) and Frank and Spalhoff (1957), respectively. The molecular dipole moments of these molecules are taken from Lide (1993).

Table 5. Parameters of the Stockmayer potential for non-polar molecules derived from densities at  $0.75 T_c$  or critical densities, critical temperatures (Ambrose, 1993) and dipole moments (Lide, 1993; if not stated otherwise) using the approach of van Leeuwen (1994).

	$T_c$ [K]	$\rho_{L,0.75}^{*ST} \times 10^2$ [mole cm <sup>-3</sup> ]	$\rho_c^{*ST} \times 10^2$ [mole cm <sup>-3</sup> ]	$\epsilon/k$ [K]	$\sigma$ [Å]	$\mu$ [D]	$\alpha$ [Å <sup>3</sup> ]
HBr	363.2	2.3480 <sup>†</sup>		272.4	3.705	0.827	0.0
HF	461.0	4.3029 <sup>‡</sup>		237.0	3.058	1.826	0.0
NO <sub>2</sub>	431.2		1.2392	328.1	3.431	0.316	0.0
HCl	324.7		1.2346	230.9	3.455	1.109	0.0
HI	424.0		0.7536	322.5	4.050	0.448	0.0
C <sub>3</sub> H <sub>6</sub> (propene)	364.9		0.5525	277.7	4.490	0.366	0.0
C <sub>4</sub> H <sub>8</sub> (Isobutene)	417.9		0.4184	318.0	4.927	0.503	0.0
SiClF <sub>3</sub>	307.7		0.4785 <sup>††</sup>	233.5	4.715	0.686*	0.0
SiCl <sub>2</sub> F <sub>2</sub>	369.0		0.4049 <sup>††</sup>	280.3	4.984	0.7329*	0.0
SiCl <sub>3</sub> F	438.6		0.3521 <sup>††</sup>	333.8	5.218	0.49	0.0

<sup>†</sup> Strunk and Wingate (1954)

<sup>‡</sup> Frank and Spalhoff (1957)

<sup>††</sup> Simmorock K.H. et al. (1986)

\* Dipole moment from *ab-initio* quantum mechanic calculations (see text for details)

 5.1.5. NO<sub>2</sub>, HCl, HI, C<sub>3</sub>H<sub>6</sub> (Propene), C<sub>4</sub>H<sub>8</sub> (Isobutene), SiFCl<sub>3</sub>

Parameters of the EOS of these polar gases were determined from critical point data (van Leeuwen, 1994). Critical properties of the compounds and molecular dipole moments are taken from Ambrose (1993) and Lide (1993). The determined EOS parameters are reported in Table 5.

 5.1.6 SiF<sub>3</sub>Cl, SiF<sub>2</sub>Cl<sub>2</sub>

Up to our knowledge, direct experimental measurements of molecular electric dipole moments of SiF<sub>3</sub>Cl, SiF<sub>2</sub>Cl<sub>2</sub> are not available. Therefore the values were determined by *ab-initio* quantum mechanic (QM) molecular orbital calculations. The calculations were performed with the B3LYP-method (Becke-3-parameter density functional) and the 6-311+G(3df,2p) basis set using the Gaussian94 package (see Forresman and Frish, 1996 for

details). Dipole moments predicted from QM-simulations are typically larger than experimental values and must be considered as approximations. For example, the experimental dipole moment of  $\text{SiFCl}_3$  reported by Lide (1993) is 0.49 D, while the value predicted using B3LYP// 6-311+G(3df.2p) calculations is 0.586 D. The other parameters (Table 5) were determined from critical data given by Ambrose (1993) and Simmorock et al. (1986).

## 5.2. Non-polar gases

### 5.2.1. $\text{CO}_2$

Molecules of carbon dioxide have no permanent dipole moment and must therefore be described in our means by using only the Lennard-Jones interaction potential. However,  $\text{CO}_2$  possesses a very strong quadrupole moment which makes it difficult to derive an accurate EOS based on such simple interaction potentials. A successful attempt to obtain parameters for an EOS, similar to the one used here, was made by Shmulovich et al. (1982). To improve the accuracy of the EOS, the parameters  $\sigma$  and  $\varepsilon$  were made a function of temperature. Because of physical reasons the functional form of the temperature dependency of  $\varepsilon$  was chosen to approach a constant value asymptotically at high temperatures. At high temperatures due to molecule rotations the contribution of the quadrupole interaction becomes minor in comparison to the Lennard-Jones interaction and  $\text{CO}_2$  starts to behave like spherically symmetric molecules. As far as the presented EOS is different from the equation of Shmulovich et al. (1982) in respect to the  $A^{RPA}$ -term (eq. 18), the  $\sigma$  and  $\varepsilon$  parameters had to be refitted using the experimental  $PVT$ -measurements of pure  $\text{CO}_2$  (Shmonov and Shmulovich, 1974):

$$\sigma [\text{\AA}] = 3.646 + 7.567 \times 10^{-5} T \quad (40)$$

$$\varepsilon / k [\text{K}] = 96.168 + 203.72 \exp(-1.3877 \times 10^{-3} T) \quad (41)$$

The molar volumes calculated using the EOS are compared to the experimental data of Shmonov and Smulovich (1974) in the Fig. 4. Both sets are in reasonable agreement.

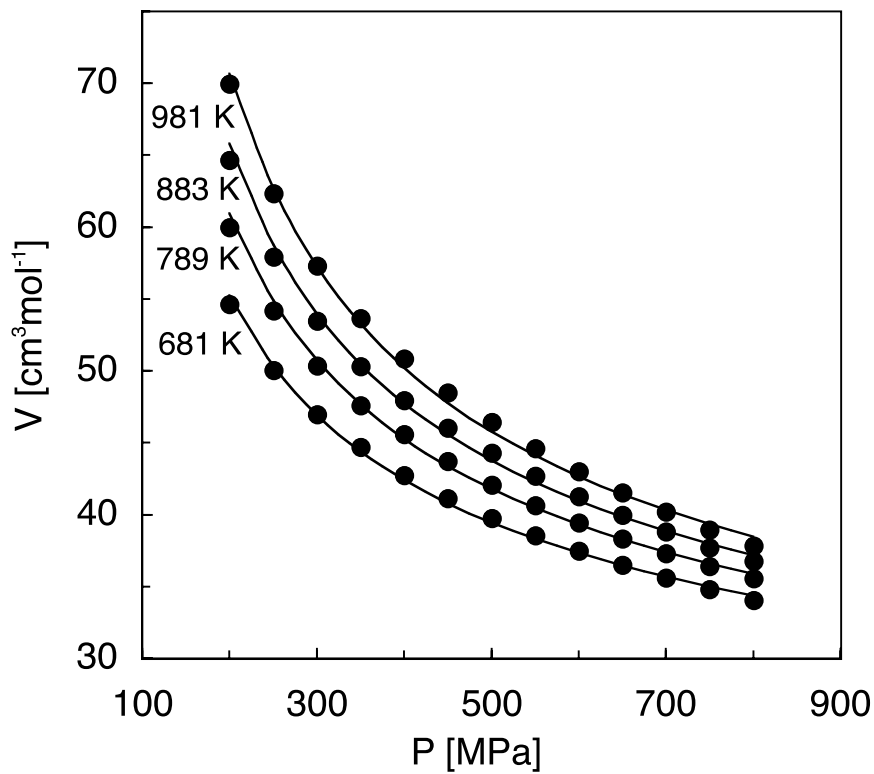


Fig. 4. The molar volumes of carbon dioxide as predicted by the EOS compared to the experimental data of Shmonov and Shmulovich (1974).

### 5.2.2. $N_2$

The  $PVT$ -relationships for nitrogen are known up to very high pressures and temperatures (e.g. Jacobsen et al., 1986). The properties of this fluid can be used to check the accuracy of the method to determine Lennard-Jones parameters for non-polar fluids using its critical properties. The EOS parameters derived from critical temperature and density of  $N_2$  are:  $\epsilon/k = 96.2$  K and  $\sigma = 3.615$  Å. Fig 5. illustrates that in the ranges of 573-1773K and 100-1000 MPa the calculated volumes of nitrogen are in excellent agreement with the data of Jacobsen et al. (1986).

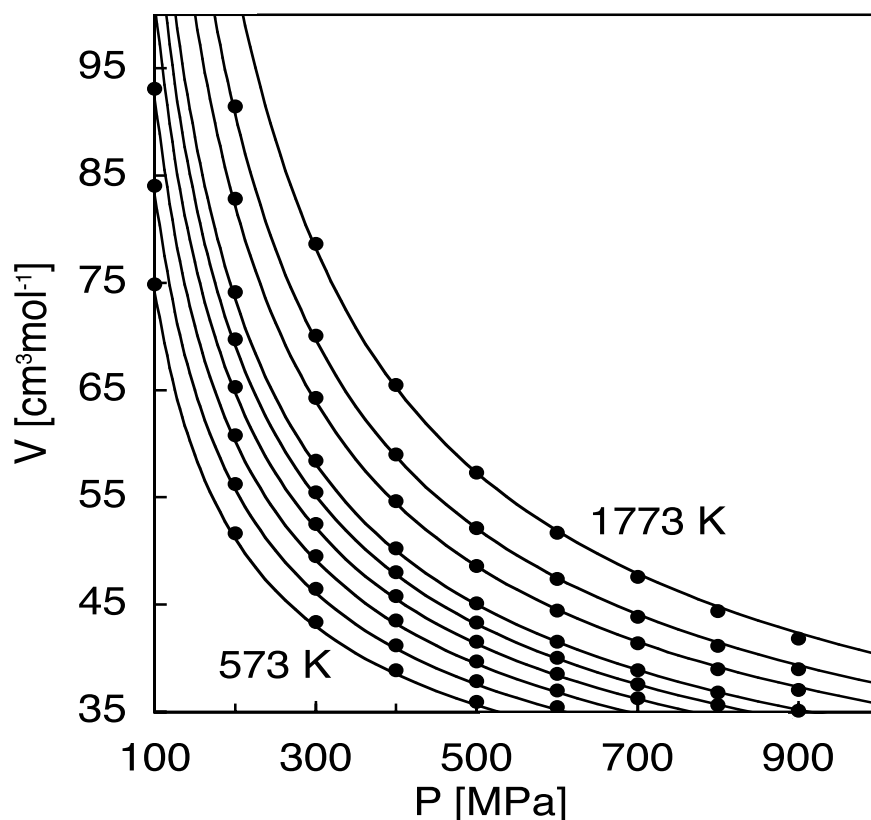


Fig. 5. The molar volumes of nitrogen as predicted by the presented EOS (curves) compared to the experimental values (points) reported by Jacobsen et al. (1986). Isotherms are for 573 to 1073 K in 100 K increments and for 1273, 1473 and 1773 K.

5.2.3. Noble gases,  $CH_4$ ,  $O_2$ ,  $H_2$ ,  $Cl_2$ ,  $F_2$ ,  $CS_2$ ,  $SiF_4$ ,  $C_2H_6$ ,  $C_3H_8$ ,  $C_2H_4$ ,  $S$ ,  $BF_3$ ,  $BCl_3$ ,  $Br_2$ ,  $I_2$ ,  $SiH_4$ ,  $SiCl_4$ ,  $C_4H_{10}$

Parameters of Lennard-Jones interaction for all these non-polar gases were determined from the critical temperatures and critical densities (Ambrose, 1993). The parameters are summarised in the Table 6.

Table 6. Parameters of Lennard-Jones interaction and molecular polarizabilities (Miller, 1993) for non-polar molecules derived from critical densities and temperatures (Ambrose, 1993) using the critical parameters of Lennard-Jones fluid reported by Potoff and Panagiotopoulos (1998).

	$T_c$ [K]	$\rho_c^* \times 10^2$ [mole cm <sup>-3</sup> ]	$\epsilon/k$ [K]	$\sigma$ [Å]	$\mu$ [D]	$\alpha$ [Å <sup>3</sup> ]
He	5.19	1.7544	3.96	3.104	0.0	0.204956
Ne	44.4	2.3810	33.84	2.804	0.0	0.3956
Ar	150.87	1.3333	114.99	3.402	0.0	1.6411
Kr	209.41	1.0989	159.61	3.628	0.0	2.4844
Xe	289.73	0.8475	220.83	3.957	0.0	4.044
F <sub>2</sub>	144.13	1.5152	109.86	3.260	0.0	1.38
Br <sub>2</sub>	588	0.7874	448.17	4.055	0.0	7.02
I <sub>2</sub>	819	0.6452	624.24	4.333	0.0	0.0**
Cl <sub>2</sub>	416.9	0.8130	317.76	4.012	0.0	4.61
O <sub>2</sub>	154.59	1.3699	117.83	3.371	0.0	1.5812
S	1314	0.6329	1001.52	4.361	0.0	2.9
N <sub>2</sub>	126.21	1.1111	96.20	3.615	0.0	1.7403
H <sub>2</sub>	32.97	1.5385	25.13	3.243	0.0	0.81
CS <sub>2</sub>	552	0.5780	420.73	4.495	0.0	8.74
CO <sub>2</sub>			*	*	0.0	2.65
CH <sub>4</sub>	190.53	1.0101	145.22	3.732	0.0	2.593
C <sub>2</sub> H <sub>6</sub> (ethane)	305.4	0.6757	232.77	4.267	0.0	4.47
C <sub>3</sub> H <sub>8</sub> (propane)	369.82	0.4926	281.88	4.741	0.0	6.29
C <sub>2</sub> H <sub>4</sub> (ethylene)	282.34	0.7634	215.20	4.097	0.0	4.252
C <sub>4</sub> H <sub>10</sub> (butane)	425.14	0.3922	324.04	5.115	0.0	8.2
BF <sub>3</sub>	260.8	0.8696	198.78	3.923	0.0	3.31
BCl <sub>3</sub>	455	0.4184	346.80	5.006	0.0	9.38
SiF <sub>4</sub>	259	0.5981	197.41	4.444	0.0	5.45
SiH <sub>4</sub>	269.7	20.6612	205.56	1.365	0.0	5.44
SiCl <sub>4</sub>	508.1	0.3067	387.27	5.552	0.0	0.0**

\* Parameters for CO<sub>2</sub> are temperature dependant (see text)

\*\* Polarizability is unknown. Zero value were used

## 6. CONCLUSIONS

It has been shown that even strong polar molecules like water can be quite accurately described by a four parameter equation of state based on the rigorous consideration of dipole-dipole and Lennard-Jones interactions particularly above the critical point. At such conditions the EOS shows an excellent extrapolation behaviour to high pressures and temperatures. However, at near critical conditions the description of the thermodynamic properties of highly polar fluids is relatively poor. It is obvious that in this region the proposed EOS is too simple and improvements are required. For molecules less polar than H<sub>2</sub>O having lower critical temperatures the EOS is in good agreement with experimental results.

Non-polar gases, with a relatively small quadrupole moment (e.g. N<sub>2</sub>) can be successfully described by a Lennard-Jones fluid, with potential parameters derived from its critical properties. Fluids of non-polar molecules with strong quadrupole moments are difficult to describe by a simple Lennard-Jones model. Significant improvements can be achieved, however, if the parameters used in the EOS depend on temperature.

Additionally, because the EOS describes a large number of species using the same formalism it can be extended to complex mixtures which will be presented in a second part of the communication (Churakov and Gottschalk, submitted to CGA).

**Acknowledgment.** The authors are grateful to A.G. Kalinichev for useful discussions and kindly providing the source code for the EOS of a Lennard-Jones fluid.

## REFERENCES

- Ambrose D. (1993) Critical constants, boiling points and melting points of selected compounds. In *CRC Handbook of chemistry and Physics*, (ed. D.R. Lide) CRC Press, Boca Raton pp. 6/54-6/65.
- Anderko, A., and Pitzer, K.S. (1993a) Equation-of-state representation of phase equilibria and volumetric properties of the system NaCl-H<sub>2</sub>O above 573 K. *Geochim. Cosmochim. Acta* **57**, 1657-1680.
- Anderko, A., and Pitzer, K.S. (1993b) Phase equilibria and volumetric properties of the systems KCl-H<sub>2</sub>O and NaCl-KCl-H<sub>2</sub>O above 573 K: equation of state representation. *Geochim. Cosmochim. Acta* **57**, 4885-4897.
- Andersen H. C., Chandler D. and Weeks J. D. (1972) Role of repulsive forces in liquids: The optimized random phase approximation. *J. Chem. Phys.* **56**, 3812-3823.
- Belonoshko A. and Saxena S.K. (1991a) A molecular dynamic study of pressure-volume-temperature properties of supercritical fluids: 1. H<sub>2</sub>O. *Geochim. Cosmochim. Acta* **55**, 381-387.
- Belonoshko A. and Saxena S.K. (1991b) A molecular dynamics study of the pressure-volume-temperature properties of supercritical fluids: 2. CO<sub>2</sub>, CH<sub>4</sub>, CO, O<sub>2</sub> and H<sub>2</sub>. *Geochim. Cosmochim. Acta* **55**, 3191-3208.
- Belonoshko A.B. and Saxena S.K. (1992) A unified equation of state for fluids of C-H-O-N-S-Ar composition and their mixtures up to very high temperatures and pressures. *Geochim. Cosmochim. Acta* **56**, 3611-3626.

- Brodholt J. and Wood B. (1990) Molecular dynamics of water at high temperatures and pressures. *Geochim. Cosmochim. Acta* **54**, 2611-2616.
- Brodholt J. and Wood B. (1993a) Simulation of the structure and thermodynamic properties of water at high pressures and temperatures. *J. Geophys. Res.* **98**, 519-536.
- Brodholt J. and Wood B. (1993b) Molecular dynamics simulations of the properties of CO<sub>2</sub> - H<sub>2</sub>O mixtures at high pressures and temperatures. *Amer. Miner.* **78**, 558-564.
- Carnahan N.F. and Starling K.E. (1969) Equation of state for non-attracting rigid spheres. *J. Chem. Phys.* **51**, 635-636.
- Churakov S.V. and Gottschalk M. (2001) Perturbation theory based equation of state for polar molecular fluids. II. Fluid mixtures. *Geochim. Cosmochim. Acta* ( submitted )
- Destigneville C.M., Brodholt J.P. and Wood B.J. (1996) Monte Carlo simulation of H<sub>2</sub>O-CO<sub>2</sub> mixtures to 1073.15 K and 30 kbar. *Chemical Geology* **133**, 53-65.
- Dohrn R., Prausnitz J. M. (1990) A simple perturbation term for the Carnhan-Starling equation of state. *Fluid Phase Equilib.* **61**, 53 - 69.
- Duan Z., Møller N. and Weare J. H. (1992a) An equation of state for the CH<sub>4</sub>-CO<sub>2</sub>-H<sub>2</sub>O system: I. Pure systems from 0 to 1000°C and 0 and to 8000 bar. *Geochim. Cosmochim. Acta* **56**, 2605 - 2617
- Duan Z., Møller N. and Weare J. H. (1992b) An equation of state for the CH<sub>4</sub>-CO<sub>2</sub>-H<sub>2</sub>O system: II, Mixtures from 50 to 1000°C and 0 to 1000 bar. *Geochim. Cosmochim. Acta* **56**, 2619-2631.
- Duan Z., Møller N. and Weare J. H. (1992c) Molecular dynamics simulation of PVT properties of geological fluids and a general equation of state of nonpolar and weakly polar gases up to 20000 bar. *Geochim. Cosmochim. Acta* **56**, 3839-3845.
- Duan Z., Møller N. and Weare J. H. (1995a) Molecular dynamics equation of state for nonpolar geochemical fluids. *Geochim. Cosmochim. Acta* **59**, 1533-1538.
- Duan, Z., Møller, N., and Weare, J.H. (1995b) Equation of state for the NaCl-H<sub>2</sub>O-CO<sub>2</sub> system: prediction of phase equilibria and volumetric properties. *Geochim. Cosmochim. Acta* **59**, 2869-2882.
- Duan Z., Møller N., Weare J. H. (1996) A general equation of state for supercritical fluid mixtures and molecular dynamics simulation of mixture PVTX properties. *Geochim. Cosmochim. Acta* **60**, 1209-1216.
- Duan Z. Møller N. and Weare J.H. (2000) Accurate prediction of the thermodynamic properties of fluids in the system. H<sub>2</sub>O-CO<sub>2</sub>-CH<sub>4</sub>-N<sub>2</sub> up to 2000K and 100 kbar from

- a corresponding states/one fluid equation of state. *Geochim. Cosmochim Acta* **64**, 1069-1075.
- Forresman J.B. and Frish A. (1996) Exploring chemistry with electronic structure methods. Gaussian Inc., Pittsburgh.
- Frank E.U. and Spalhoff W. (1957) Fluorwasserstoff I. Spezifische Wärme, Dampfdruck und Dichte bis zu 300°C und 300 atm. *Z. Electrochem* **61**, 348-357.
- Gray C.G. and Gubbins K. E. (1984) Theory of molecular fluids. I. Fundamentals. Clarendon Press, Oxford.
- Grevel K. D. and Chatterjee N. D. (1992) A modified Redlich-Kwong equation of state for H<sub>2</sub>-H<sub>2</sub>O fluid mixtures at high pressures and at temperatures above 400°C. *Eur. J. Mineral.* **4**, 1303-1310.
- Gubbins K.E. and Twu C.H. (1978) Thermodynamics of polyatomic fluid mixtures. I. Theory, *Chem. Eng. Sci.* **33**, 863-878.
- Halbach H. and Chatterjee N.D. (1982) An empirical Redlich-Kwong- type equation of state for water to 1,000°C and 200 kbar. *Contrib. to Mineral. Petrol.* **79**, 337-345.
- Hirschfelder, J.O., Curtiss, C.F. and Bird, R.B. (1964) Molecular theory of gases and liquids. John Wiley & Sons, New York.
- Holland T. and Powell R. (1991) A compensated-Redlich-Kwong (CORK) equation for volumes and fugacities of CO<sub>2</sub> and H<sub>2</sub>O in the range 1 bar to 50 kbar and 100-1600°C. *Contrib. Mineral. Petrol.* **109**, 265-273.
- Holloway, J.R. (1976) Fugacity and activity of molecular species in supercritical fluids. In D.G. Fraser, Ed. Thermodynamics in Geology, p. 161-181, Dordrecht-Holland/Boston
- Jacobs G.K. and Kerrick D.M. (1981) Methane: an equation of state with application to the ternary system H<sub>2</sub>O-CO<sub>2</sub>-CH<sub>4</sub>. *Geochim. Cosmochim. Acta* **45**, 607-614.
- Jacobsen R.T., Stewart R.B. and Jahangiri, M. (1986) Thermodynamic properties of nitrogen from the freezing line to 2000 K at pressures to 1000 MPa. *J. Phys. Chem. Ref. Data* **15**, 735-909.
- Jonson J.W. and Norton D. (1991) Critical phenomenon in the hydrothermal systems: state, thermodynamic, electrostatic and transport properties of H<sub>2</sub>O in the critical region. *Amer. J. Sci.* **291**, 541-648.
- Kalinichev A.G. and Heinzinger K. (1995) Molecular dynamic of supercritical water: computer simulation of vibration spectra with the flexible BJH potential. *Geochim. Cosmochim. Acta* **59**, 641-650.

- Kerrick D. M. and Jacobs G.K. (1981) A modified Redlich-Kwong equation for H<sub>2</sub>O, CO<sub>2</sub>, and H<sub>2</sub>O-CO<sub>2</sub> mixtures at elevated pressures and temperatures. *Amer. J. Sci.* **281**, 735-767.
- Leeuwen, van M.E. (1994) Derivation of Stockmayer potential parameters for polar fluids. *Fluid Phase Equilib.* **99**, 1-18.
- Lide D. R. (1993) Dipole moment of molecules in the gas phase. In *CRC Handbook of chemistry and Physics*, (ed. D.R. Lide) CRC Press, Boca Raton pp 9/42-9/50.
- Miller T. M. (1993) Atomic and molecular polarizabilities. In *CRC Handbook of chemistry and Physics*, (ed. D.R. Lide) CRC Press, Boca Raton, pp 10/192-10/204.
- Miyano Y. and Masuoka H. (1984) Equation of state based on Weeks-Chandler-Andersen perturbation theory. *Fluid Phase Equilib.* **18**, 131-146.
- Prausnitz, J. M., Lichtenthaler, R.N. and Azevedo, E.G. (1999) Molecular thermodynamics of fluid-phase equilibria. Third edition, Prentice Hall, New Jersey.
- Potoff J.J. and Panagiotopoulos A.Z. (1998). Critical Point and phase behaviour of the pure fluids and a Lennard-Jones mixture. *J. Chem. Phys.* **109**, 14-20.
- Ree F.H. (1984) A statistical mechanical theory of chemical reacting multiphase mixtures: Application to the detonation properties of PENT. *J. Chem. Phys.* **81**, 1251-1263.
- Saul A. and Wagner W. (1989) A fundamental equation for water covering the range from the melting line to 1273 K at pressures up to 2500MPa. *J. Chem. Phys. Ref. Data* **18**, 1537-1564.
- Saxena S.K. and Fei Y. (1987) Fluids at crustal pressures and temperatures. I. Pure species. *Contrib. Mineral. Petrol.* **95**, 370-375.
- Saxena S.K. and Fei Y. (1988) Fluid mixtures in the C-H-O system at high pressure and temperature. *Geochim. Cosmochim. Acta* **52**, 505-512.
- Shmonov V.M. and Shmulovich K.I. (1974) Molar volumes and equation of state of CO<sub>2</sub> at 100-1000°C and 2000-10000 bars. *Doclady Acad. Science USSR* **217**, 206-209.
- Simmorock K.H., Janowsky R. and Ohnesorge A. (1986) Critical data of pure substances. DECHEMA, Frankfurt a.M.
- Shmulovich K.I., Tereshchenko Ye.N. and Kalinichev A.G. (1982) An equation of state and isochors for nonpolar gases to 2000K and 10 GPa. *Geochem. Internat.* **19**, 49-64.
- Stell G., Rasaiah J.C. and Narang H. (1972) Thermodynamic perturbation theory for simple polar fluids. I. *Mol. Phys.* **23**, 393-406.

- Stell G., Rasaiah J.C. and Narang H. (1974) Thermodynamic perturbation theory for simple polar fluids. II. *Mol. Phys.* **27**, 1393-1414.
- Sterner S. M. and Pitzer K. S. (1994) An equation of state for carbon dioxide valid from zero to extreme pressures. *Contrib. Mineral. Petrol.* **117**, 362-374.
- Strunk W.G. and Wingate W.H. (1954) Density of liquid hydrogen bromide. *J. Am. Chem. Soc.* **76**, 1025-1027.
- Tereshchenko E.N., Kalinichev A.G., Shmulovich K.I. (1981) Application of the equation of state of the Lennard-Jones fluid to density calculations under high pressures. In: *Equations of State under Extreme Conditions*, Novosibirsk, ITPM SO AN SSSR, 12-19 (in Russian).
- Tillner-Roth R., Harms-Watzenberg F. and Baehr H.D., (1993) Eine neue Fundamentalgleichung für Ammoniak. *DKV-Tagungsbericht* **20**, 167-181.
- Verlet L. and Weis J.J. (1972a) Perturbation theory for the thermodynamic properties of simple liquids. *Mol. Phys.* **24**, 1013 - 1024.
- Verlet L. and Weis J.J. (1972b) Equilibrium theory of simple liquids. *Phys Rev.* **5**, 939-952.
- Weeks J. D., Chandler D. and Andersen H. C. (1971) Role of repulsive forces in determining the equilibrium structure of simple liquids. *J. Chem. Phys.* **54**, 5237-5247.
- Withers A.C., Kohn S.C., Brooker R.A. and Wood B.J. (2000) A new method for determining the P-V-T properties of high-density H<sub>2</sub>O using NMR: Results at 1.4-4.0 GPa and 700-1100°C. *Geochim. Cosmochim. Acta* **64**, 1051-1057.

## APPENDIX II.1

The residual Helmholtz free energy of a system ( $A^{res}$ ) can be calculated using a [0,1] Padé approximation as proposed by Stell et al. (1972):

$$A^{res} = A^{LJ} + A_2^{dip-dip} \left( 1 - \frac{A_3^{dip-dip}}{A_2^{dip-dip}} \right)^{-1} + A_1^{ind-dip} \quad (A1)$$

*Helmholtz free energy of the Lennard-Jones system*

To calculate  $A^{LJ}$  it is convenient to introduce the dimensionless parameters  $\rho^*$  and  $\beta$ :

$$\rho^* = \rho N_A \sigma^3 \quad (A2)$$

$$\beta = \frac{\varepsilon}{kT} \quad (A3)$$

$\varepsilon$  and  $\sigma$  are the parameters of the  $LJ$  potential of the fluid of interest.

According to the perturbation expansion of Weeks et al. (1971) and Andersen et al. (1972), the Helmholtz free energy of a Lennard-Jones fluid  $A^{LJ}$  is calculated as the sum of the following three terms:

$$A^{LJ} = A^{HS} + A^{HTA} + A^{RPA} \quad (A4)$$

The first step is to find the “effective hard sphere diameter” ( $d$ ). To determine  $d$  the following equation must be solved iteratively:

$$d = d_B \left[ 1 + \frac{\sigma_1}{2\sigma_0} \delta \right] \quad (A5)$$

where  $\sigma_1$  and  $\sigma_0$  are given by Verlet and Weis (1972b)

$$\sigma_0 = \frac{1 - 0.5\eta}{(1 - \eta)^3} \quad (A6)$$

$$\sigma_1 = \frac{2 - 7.5\eta + 0.5\eta^2 - 5.7865\eta^3 - 1.51\eta^4}{(1 - \eta)^4} \quad (A7)$$

with

$$\eta = \frac{\pi}{6} d^3 \rho^* \quad (\text{A8})$$

while  $d_B$  and  $\delta$  have been approximated by Tereshchenko et al.(1981), Shmulovich et al. (1982)

$$d_B = \frac{P_1 \beta^{1/12} + P_2 \beta^{7/12} + P_3 \beta + P_4 \beta^2 + P_5 \beta^3}{(1 + \beta)^3} \quad (\text{A9})$$

$$\delta = \frac{P_6 + P_7 \beta^{1/2}}{1 + P_8 \beta^{1/2} + P_9 \beta + P_{10} \beta^{3/2}} \quad (\text{A10})$$

using the following parameters:

$$\begin{aligned} P_1 &= 1.186892378996 \\ P_2 &= -0.4721963005527 \\ P_3 &= 3.259515855283 \\ P_4 &= 3.055229342609 \\ P_5 &= 1.095409321023 \\ P_6 &= 1.282306659774 \times 10^{-2} \\ P_7 &= 9.55712461425 \times 10^{-2} \\ P_8 &= 13.67807693107 \\ P_9 &= 35.75464856619 \\ P_{10} &= 16.04724381643 \end{aligned}$$

An expression for the term  $A^{HS}$  is given by Carnahan and Starling (1969):

$$\frac{A^{HS}}{RT} = \frac{4\eta - 3\eta^2}{(1 - \eta)^2} \quad (\text{A11})$$

The “random phase approximation”  $A^{RPA}$  is calculated as proposed by Miyano and Masuoka (1984)

$$\frac{A^{RPA}}{RT} = -\frac{12\beta^2}{\pi} f_1 + \frac{192\beta^3}{\pi} f_2 \quad (\text{A12})$$

with  $f_1$  and  $f_2$

$$f_1 = \sum_{i=1}^{10} C_{1,i} (\eta_w)^i \quad (\text{A13})$$

$$f_2 = \sum_{i=1}^{10} C_{2,i} (\eta_w)^{i+1} \quad \text{A(14)}$$

$$\eta_w = \eta - \frac{1}{16} \eta^2 \quad \text{A(15)}$$

and with the following parameters:

$i$	$C_{1i}$	$C_{2i}$
1	1.20110	0.588890
2	0.064890	-7.455360
3	-76.860	40.57590
4	562.686	-104.8970
5	-2280.090	60.25470
6	6266.840	390.6310
7	-11753.40	-1193.080
8	14053.8	1576.350
9	-9491.490	-1045.910
10	2731.030	283.7580

The approximation for  $A^{HTA}$  has been provided by Tereshchenko et al. (1981) and Shmulovich et al. (1982):

$$\frac{A^{HTA}}{RT} = 48\beta\eta_w \left[ \frac{I_1^{12}}{d_w^{12}} - \frac{I_1^6}{d_w^6} + I_2 \right] \quad \text{A(16)}$$

with

$$I_1^{12} = \frac{1}{9} \cdot \frac{1 + B_4\eta_w + B_5\eta_w^2 + B_6\eta_w^3}{1 + B_1\eta_w + B_2\eta_w^2 + B_3\eta_w^3} \quad \text{A(17)}$$

$$I_1^6 = \frac{1}{3} \cdot \frac{1 + A_4\eta_w + A_5\eta_w^2 + A_6\eta_w^3}{1 + A_1\eta_w + A_2\eta_w^2 + A_3\eta_w^3} \quad \text{A(18)}$$

$$\begin{aligned} I_2 = & d_w^{-6} \left( \frac{a_0}{4} + \frac{a_1}{12} + \frac{a_2}{24} + \frac{a_3}{24} \right) - d_w^{-12} \left( \frac{a_0}{10} + \frac{a_1}{90} + \frac{a_2}{720} + \frac{a_3}{5040} \right) + \\ & + \frac{1}{8} \left( a_0 - \frac{a_1}{3} + \frac{a_2}{12} - \frac{a_3}{60} \right) - \frac{9}{40} \xi^2 \left( a_0 - a_1 + \frac{a_2}{2} - \frac{a_3}{6} \right) - \\ & - \frac{2}{9} \xi^3 \left( a_1 - a_2 + \frac{a_3}{2} \right) - \frac{9}{64} \xi^4 (a_2 - a_3) - \frac{3}{35} \xi^5 a_3 \end{aligned} \quad \text{A(19)}$$

$$d_w = d \left( 1 - \frac{1}{16} \eta \right)^{1/3} \quad (\text{A20})$$

$$\xi = \frac{r_m}{d_w} \quad (\text{A21})$$

$$r_m = 2^{1/6} \quad (\text{A22})$$

$$a_0 = \frac{A_{00} + A_{01} \eta_w}{(1 - \eta_w)^2} \quad (\text{A23})$$

$$a_1 = \frac{A_{10} + A_{11} \eta_w + A_{12} \eta_w^2}{(1 - \eta_w)^3} \quad (\text{A24})$$

$$a_2 = \frac{A_{21} \eta_w + A_{22} \eta_w^2 + A_{23} \eta_w^3}{(1 - \eta_w)^4} \quad (\text{A25})$$

$$a_3 = \frac{A_{31} \eta_w + A_{32} \eta_w^2 + A_{33} \eta_w^3 + A_{34} \eta_w^4}{(1 - \eta_w)^5} \quad (\text{A26})$$

using the following the parameters:

$A_1$	=	-.120078459237	$A_{00}$	=	.9985937977069455
$A_2$	=	-.808712488307	$A_{01}$	=	.5079834224407451
$A_3$	=	.321543801337	$A_{10}$	=	1.021887697885469
$A_4$	=	1.16965477132	$A_{11}$	=	-5.136619463333883
$A_5$	=	-.410564939543	$A_{12}$	=	-5.196188074016755
$A_6$	=	-.516834310691	$A_{21}$	=	-6.049240839050804
			$A_{22}$	=	18.67848155616692
$B_1$	=	-2.18839961483	$A_{23}$	=	20.10652684217768
$B_2$	=	1.59897428009	$A_{31}$	=	9.896491419756988
$B_3$	=	-.392578806128	$A_{32}$	=	14.6738380473899
$B_4$	=	-.189396607904	$A_{33}$	=	-77.44825116542995
$B_5$	=	-.576898496254	$A_{34}$	=	-4.82871082941229
$B_6$	=	-.0185167641359			

Substitution of (A11), (A12) and (A16) into (A4) provides the Helmholtz free energy of the reference system.

*Perturbation contributions of the dipole-induced dipole and dipole-dipole interactions*

The perturbation contributions of the Helmholtz free energy is calculated as follows (Stell et al., 1972):

$$A_2^{dip-dip} = -\frac{2\pi N_A^2 \rho \mu^4}{3kT \sigma^3} J \quad (A27)$$

$$A_3^{dip-dip} = \frac{32\pi^3 N_A^3 \rho^2}{135(kT)^2} \left(\frac{14\pi}{5}\right)^{1/2} \frac{\mu^6}{\sigma^3} K \quad (A28)$$

$$A_1^{ind-dip} = -4\pi N_A^2 \rho \frac{\alpha \mu^2}{\sigma^3} J \quad (A29)$$

$$J = -\frac{1}{16\pi \rho^* \beta} \left[ 4 \frac{U^{LJ}}{RT} - Z^{LJ} + 1 \right] \quad (A30)$$

$$Z^{LJ} = 1 + \rho \frac{\partial(A^{LJ}/(RT))}{\partial \rho} \quad (A31)$$

$$U^{LJ} = -T^2 \frac{\partial(A^{LJ}/T)}{\partial T} \quad (A32)$$

Gubbins and Twu (1978) proposed the following expression for  $K$

$$\ln[K(\rho^*, \beta)] = -M_1 \rho^{*2} \ln(\beta) + M_2 \rho^{*2} - M_3 \rho^* \ln(\beta) + M_4 \rho^* - M_5 \ln(\beta) + M_6 \quad (A33)$$

with the following parameters:

$$\begin{aligned} M_1 &= -1.050534 \\ M_2 &= 1.747476 \\ M_3 &= 1.749366 \\ M_4 &= -1.999227 \\ M_5 &= -0.661046 \\ M_6 &= -3.028720 \end{aligned}$$

**Perturbation Theory Based Equation of State for Polar Molecular Fluids:**  
**II. Fluid Mixtures**

## **ABSTRACT**

The equation of state (EOS) for 98 pure organic and inorganic fluids formulated by Churakov and Gottschalk (submitted to GCA) has been extended to the complex fluid mixtures. For the calculation of the thermodynamic properties of mixtures theoretical combining rules from statistical mechanics are used. These mixing rules do not involve any empirical parameters. The properties of the fluid mixtures are derived directly from those of the pure constituents. It can be shown that the equation of state describes accurately the thermodynamic relations in the  $\text{H}_2\text{O}-\text{CO}_2$  and  $\text{H}_2\text{O}-\text{N}_2$  binaries at high pressures and temperatures. In particular the EOS correctly predicts high pressure phase separations in various mixtures of polar and nonpolar molecules.

## 1. INTRODUCTION

For many geological purposes, especially geothermobarometry, it seems to be sufficient to consider H<sub>2</sub>O as the only fluid constituent. If carbonates are involved, however, CO<sub>2</sub> and at lower O<sub>2</sub>-fugacities other species like CH<sub>4</sub>, CO and H<sub>2</sub> have to be considered additionally. Besides CO<sub>2</sub>, N<sub>2</sub>-rich fluids have been found in many fluid inclusions in granulite facies minerals (e.g. Touret and van den Kerkhof, 1986). Therefore fluids in lower crust rocks have to be described at least within the system C-O-H-N. At special geological conditions additional components like B, P, halogens, S, hydrocarbones and noble gases have to be taken into account. For the treatment of such complex systems the thermodynamic properties of the respective species in the mixture are essential. The equations of state (EOS), which generally provides the required thermodynamic properties, are calibrated using the following two approaches.

One is to use experimentally derived *PVT*-properties and/or activity relationships to calibrate the EOS directly. Experimental studies, however, are in most cases limited to binary systems (e.g. Seitz et al., 1994; Seitz et al., 1996a; Anovitz et al., 1998; Aranovich and Newton, 1999; Constantino and Rice, 1991; Seward and Frank, 1981; Sterner and Bodnar 1991; Wu et al., 1990; Shmulovich et al., 1980). Few investigations have been done in ternaries (e.g. Gehrig, 1980; Seitz et al., 1994; Seitz et al., 1996b). Because the number of necessary experiments increases dramatically with the number of components, experimentally determined *PVT*-properties of fluids with even more components are almost not available. Due to this sparse experimental database directly calibrated EOS for complex fluids are rare. Many experimentally calibrated EOS for mixtures involve ion pairs like NaCl and KCl which have a very strong dipole moment and which can not be treated otherwise without difficulty. Furthermore, because of dissociation even the simplest mixture like NaCl-H<sub>2</sub>O is essentially not a binary system. It is very difficult to describe such systems theoretically. Therefore these EOS use typically empirical parameters for the description of the mixing properties. The EOS for the systems NaCl-H<sub>2</sub>O-CO<sub>2</sub> (Bowers and Helgeson, 1983), NaCl-H<sub>2</sub>O (Anderko and Pitzer, 1993a), KCl-H<sub>2</sub>O and NaCl-KCl-H<sub>2</sub>O (Anderko and Pitzer, 1993b) and NaCl-H<sub>2</sub>O-CO<sub>2</sub> (Duan et al. 1995b), H<sub>2</sub>O-CO<sub>2</sub> (Sterner and Bodnar, 1991) do fall into this category.

Another approach is the use of an EOS for pure fluids and to interpolate the behaviour of fluid mixtures applying mixing rules. This requires that for all species involved in the mixture the EOS of the pure species are of the identical mathematical form, however.

Significant efforts have been made to describe the thermodynamic properties of complex fluid mixtures using such EOS (e.g. Holloway, 1976; Kerrick and Jacobs, 1981; Jacobs and Kerrick, 1981; Saxena and Fei, 1988; Sretenskaya et al., 1989; Belonoshko and Saxena, 1992; Grevel and Chatterjee, 1992; Duan et al., 1992, 1995a, 1995b, 1996, 2000; Bakker, 1999).

The choice of mixing rules is not unique. Many proposed mixing rules can be justified theoretically using the conformal fluid theory (e.g. Prausnitz et al. 1999) and these can be applied to many types of EOS (e.g. sophisticated forms of the van der Waals, virial equations and equations based on perturbation theory). This however does not guaranty the accuracy of the interpolation. A particular mixing model may work well for one fluid mixture but may fail for another. In particular if a parameter in the EOS is temperature dependent, which is often the case for semi-empirical EOS like modified van der Waals equations, mixing rules may become inapplicable at some conditions. For example the application of mixing rules is problematic if one of the coefficients describing the temperature dependency will be negative. Often the square root (geometric mean) of the product of such coefficients is required.

EOS based on perturbation theory have been successfully applied to vapour-liquid equilibria in various polar-non-polar gas systems using the generalised Stockmayer potential (e.g. Stell et al., 1972, 1974; Gubbins and Twu, 1978; Twu and Gubbins, 1978). Gubbins and Twu (1978) and Twu and Gubbins (1978) were able to mimic the different possible topologies of phase equilibria in fluid mixtures by choosing the appropriate parameters for the Lennard-Jones and multipolar interaction. The EOS just mentioned requires only mixing rules for the reference Lennard-Jones system, but no additional rules for the perturbation term. Furthermore the employed mixing rules for the reference system were verified by computer simulations.

Churakov and Gottschalk (submitted to GCA) proposed an EOS for 98 pure fluids which is also based on the Stockmayer interaction potential. In the following this EOS is extended to fluid mixtures. It will be shown that the EOS can be used to predict the thermodynamic properties of complex fluid mixtures up to high pressures and temperatures.

## **2. THERMODYNAMIC MODEL**

In the following the EOS proposed by Churakov and Gottschalk (submitted to GCA) is extended to fluid mixtures. Identical to the approach used for the pure fluids, the Helmholtz free energy  $A$  is expressed in form of a truncated power expansion,

$$A - A^{ideal} = A^{res} = A^{LJ} + A_2^{dip-dip} + A_3^{dip-dip} + A_1^{ind-dip} \quad (1)$$

where  $A^{LJ}$  is the residual Helmholtz free energy of a Lennard-Jones fluid which is used as the reference system,  $A_2^{dip-dip}$  and  $A_3^{dip-dip}$  are the second and third order perturbation contributions to the dipole-dipole interaction ( $A_1^{dip-dip}=0$ ) and  $A_1^{ind-dip}$  is the first order perturbation contribution to the induced dipole-dipole interaction.

According to Gubbins and Twu (1978) the explicit expressions for  $A_2^{dip-dip}$ ,  $A_3^{dip-dip}$  and  $A_1^{ind-dip}$  in the fluid mixture can be formulated as follows:

$$A_2^{dip-dip} = -\frac{2\pi N_A^2 \rho}{3kT} \sum_{ij} x_i x_j \frac{\mu_i^2 \mu_j^2}{\sigma_{ij}^3} J_{ij} \quad (2)$$

$$A_3^{dip-dip} = \frac{32\pi^3 N_A^3 \rho^2}{135(kT)^2} \left(\frac{14\pi}{5}\right)^{1/2} \sum_{ijk} x_i x_j x_k \frac{\mu_i^2 \mu_j^2 \mu_k^2}{\sigma_{ij} \sigma_{ik} \sigma_{jk}} K_{ijk} \quad (3)$$

$$A_1^{ind-dip} = -2\pi N_A^2 \rho \sum_{ij} x_i x_j \frac{1}{\sigma_{ij}^3} (\alpha_i \mu_j^2 + \alpha_j \mu_i^2) J_{ij} \quad (4)$$

where  $x_i$  is the mole fraction,  $\mu_i$  the dipole moment and  $\alpha_i$  the polarizability of the molecule  $i$ ,  $\rho$  the fluid density,  $N$  the number of molecules,  $k$  the Boltzman constant and  $T$  the temperature. The symbols  $J_{ij}$  and  $K_{ijk}$  are integrals over the pair and triple distribution functions due to the interaction of two ( $i$  and  $j$ ) and three molecules ( $i$ ,  $j$ , and  $k$ ) of the reference Lennard-Jones fluid, which depend on temperature and density. For  $J_{ij}$  and  $K_{ijk}$  the approximations of Stell et. al (1972) and Gubbins and Twu (1978) were used, respectively (see Appendix II.2).

For a pure fluid consisting of the molecules  $i$  the calculation of  $A^{LJ}$ ,  $A_2^{dip-dip}$ ,  $A_3^{dip-dip}$ ,  $A_1^{ind-dip}$ ,  $J$  and  $K$  requires the respective values for  $\sigma_i$  and  $\epsilon_i$  because the molecular interactions are all identical. In a mixture of molecules various interactions between different molecules ( $i$  and  $j$ ) have to be considered and therefore Lennard-Jones parameters  $\sigma_{ij}$  and  $\epsilon_{ij}$  are necessary for each  $i$ - $j$ -pair of molecular interaction. These parameters can be approximated using the standard Lohrentz-Bertholt combining rules:

$$\sigma_{ij} = \frac{\sigma_i + \sigma_j}{2} \quad (5)$$

$$\varepsilon_{ij} = (\varepsilon_i \varepsilon_j)^{1/2} \quad (6)$$

No further approximations are necessary to calculate the perturbation contributions for mixtures (eqs. 2-4).

The Lennard-Jones contributions to the mixture can be calculated using the van der Waals one-fluid theory. The respective mixing parameters are calculated from the following standard mixing rules, which are known to provide quite accurate results (Gray and Gubbins, 1984):

$$\sigma_{mix}^3 = \sum_{ij} x_i x_j \sigma_{ij}^3 \quad (7)$$

$$\varepsilon_{mix} = \frac{1}{\sigma_{mix}^3} \sum_{ij} x_i x_j \varepsilon_{ij} \sigma_{ij}^3 \quad (8)$$

The corresponding values of the  $\varepsilon$ ,  $\sigma$ ,  $\mu$  and  $\alpha$  parameters for the pure components were presented by Churakov and Gottschalk (submitted to GCA).

Finally, the fugacity coefficients  $\varphi_i$  of component  $i$  can be obtained by differentiation of the Helmholtz free energy  $A=A(T, \rho, n_1, n_2, \dots)$  with respect to  $n_i$ :

$$\ln(\varphi_i) = \left( \frac{\partial A / RT}{\partial n_i} \right)_{T, V, n_{j \neq i}} - \ln(Z) + Z - 1 \quad (9)$$

where  $n_i$  is the number of moles of molecule  $i$ . The compressibility is obtained in the same way as for the pure fluids:

$$Z = 1 + \rho \frac{\partial(A^{res} / (RT))}{\partial \rho}. \quad (10)$$

### 3. CALCULATED PROPERTIES IN THE SYSTEMS

#### H<sub>2</sub>O-CO<sub>2</sub>, H<sub>2</sub>O-N<sub>2</sub> AND H<sub>2</sub>O-CO<sub>2</sub>-CH<sub>4</sub>

Experimental determinations of *PVT*-properties of fluid mixtures at geological relevant conditions are scarce. The H<sub>2</sub>O-CO<sub>2</sub> binary is likely the best geologically relevant system investigated over a wide range of pressures and temperatures. For example in the range of intermediate pressures and temperatures the volumes of the H<sub>2</sub>O-CO<sub>2</sub> have been

directly measured by Greenwood (1969), Gehrig (1980) and Shmulovich et al. (1980) while Sterner and Bodnar (1991) determined densities of  $\text{H}_2\text{O}-\text{CO}_2$  mixtures in synthetic fluid inclusions. Fig. 1 shows the experimentally obtained molar volumes of  $\text{H}_2\text{O}-\text{CO}_2$  mixtures after Shmulovich et al. (1980), Sterner and Bodnar (1991) and the calculated volumes using the EOS in the range of 673-973K and 200-600MPa. The calculated volumes agree with most experimental results within the experimental uncertainties

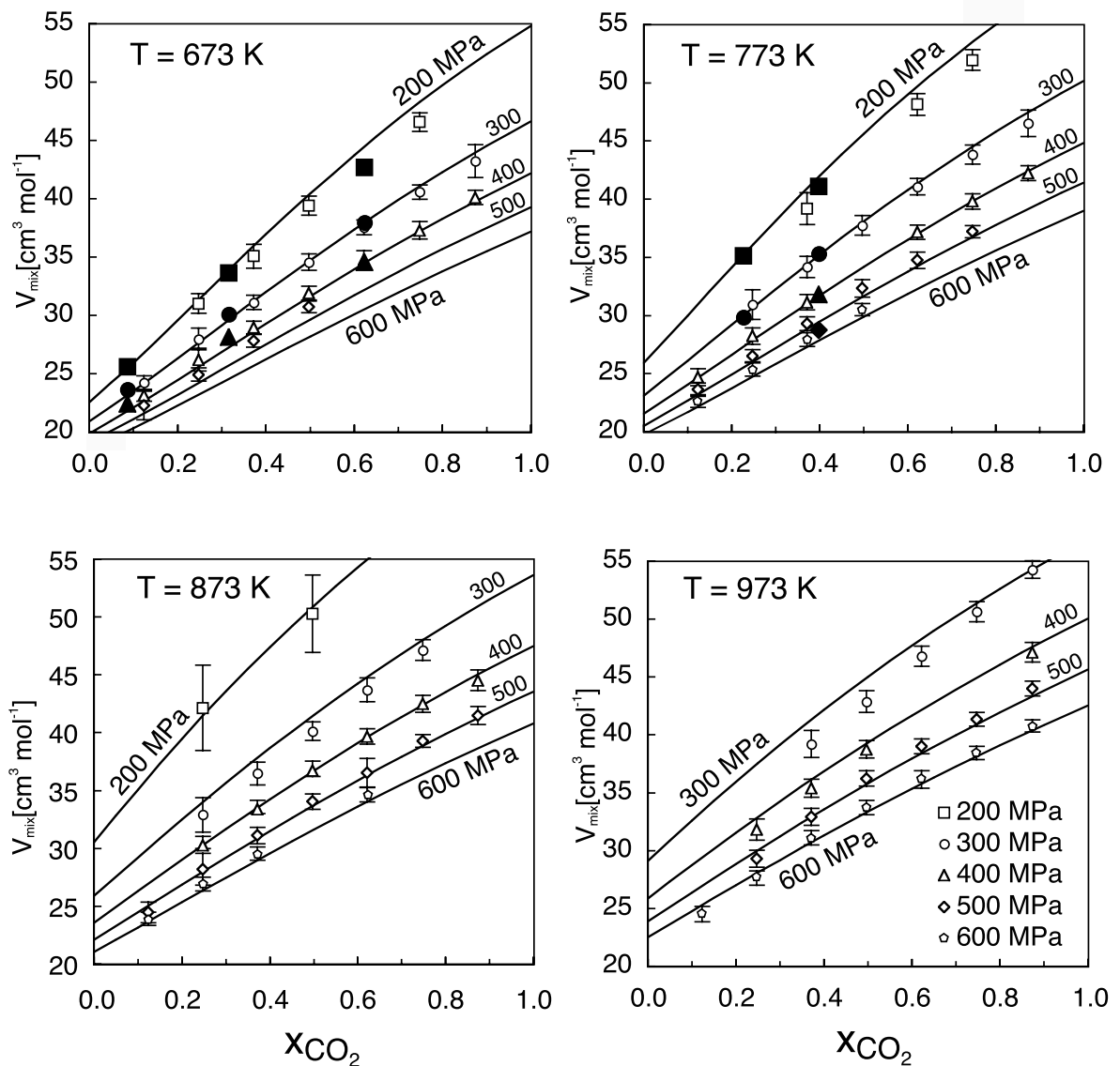


Fig. 1. Experimentally determined (Sterner and Bodnar, 1991, open symbols with error bars, Shmulovich et al., 1980, large filled symbols) and calculated (EOS, lines) molar volumes of  $\text{H}_2\text{O}-\text{CO}_2$  mixtures.

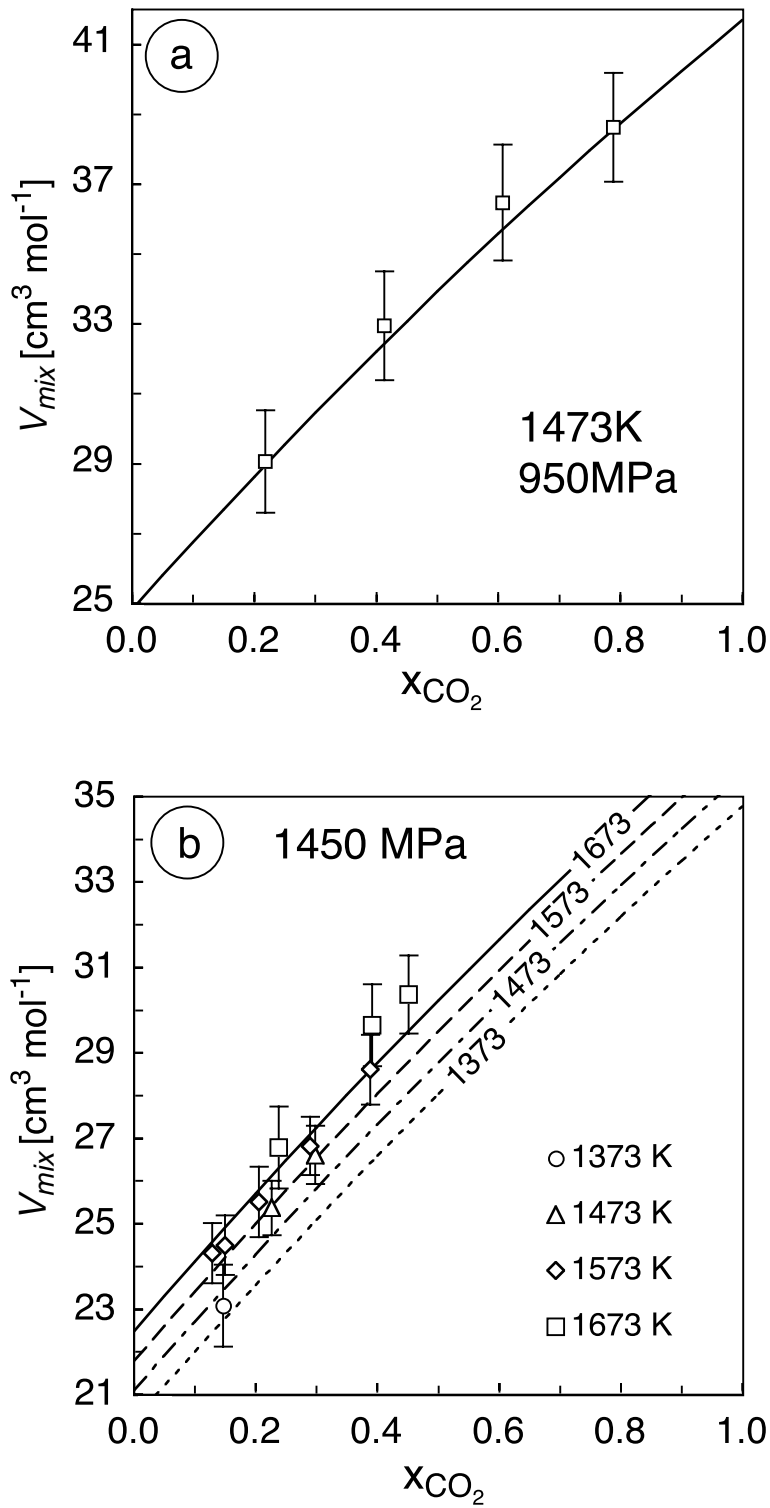


Fig. 2. Experimentally determined (Frost and Wood, 1997, symbols) and calculated (EOS, lines) molar volumes of  $\text{H}_2\text{O}-\text{CO}_2$  mixtures at high pressures and temperatures.

At more extreme conditions in the range of 1473-1673K and 950-1450 MPa the properties of  $\text{H}_2\text{O}-\text{CO}_2$  mixtures have been studied by Frost and Wood (1997) using synthetic fluid inclusions in corundum. The density of fluid inclusions at  $P$  and  $T$  conditions of trapping were performed in two steps. First, the density was measured by microthermometry and then corrected to the non-isochoric behaviour of the inclusion due to the thermal expansion and compression of the host mineral. In Fig. 2 the experimental results of Frost and Wood (1997) and the predictions of the EOS are shown. The experimentally determined volumes are always slightly higher than those predicted by the EOS, but considering the respective errors ( $2\sigma$ ), all experimental results are consistent with the EOS.

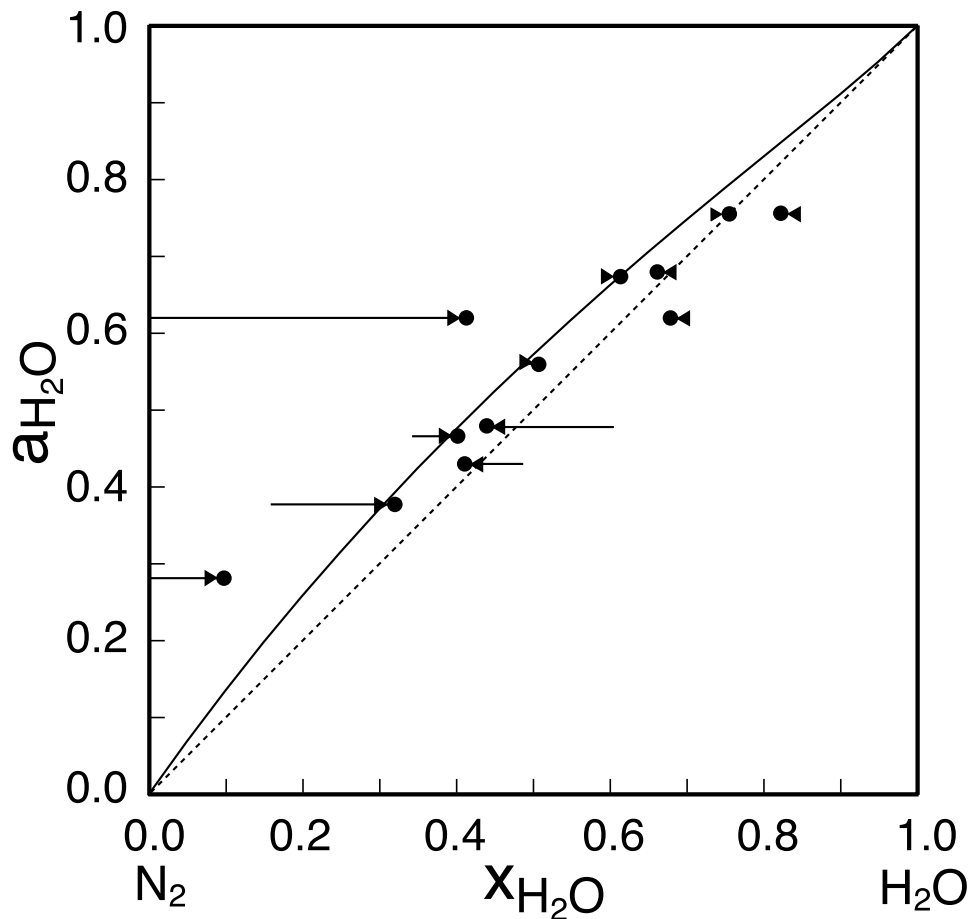


Fig. 3. Experimental brackets (Anovitz et al., 1998) narrowing the activity of  $\text{H}_2\text{O}$  in  $\text{H}_2\text{O}-\text{N}_2$  mixtures and calculated activities (EOS, lines) at 773K and 50MPa.

Activity-composition relations in the system  $\text{H}_2\text{O}-\text{N}_2$  have been studied experimentally at 773K and 50MPa by Anovitz et al. (1998). In the Fig. 3 the brackets narrowing the activity coefficients of  $\text{H}_2\text{O}$  are compared with the activities predicted by the EOS. The calculated activities of  $\text{H}_2\text{O}$  are slightly higher than experimentally determined.

Table 1. Calculated and experimentally determined molar volumes in the system  $\text{CO}_2-\text{CH}_4-\text{N}_2$  at 773.15 K and 99.93 MPa.

$x_{\text{CO}_2}$	$x_{\text{CH}_4}$	$x_{\text{N}_2}$	$V_{\text{exp}}^\dagger$ [cm <sup>3</sup> /mol]	EOS <sup>*</sup> [cm <sup>3</sup> /mol]	Duan <sup>††</sup> [cm <sup>3</sup> /mol]	Duan <sup>‡</sup> [cm <sup>3</sup> /mol]
0.2	0.4	0.4	72.46	72.50	70.20	71.99
0.4	0.3	0.3	70.93	71.33	68.61	70.49
0.6	0.2	0.2	69.11	70.05	66.77	68.60
0.6	0.3	0.1	68.85	69.79	67.33	68.44
0.6	0.1	0.3	69.30	70.30	67.13	68.71
0.8	0.1	0.1	67.04	68.67	64.82	66.30
0.1	0.8	0.1	71.74	72.40	69.86	71.48
0.2	0.6	0.2	71.78	72.11	69.57	71.45
0.1	0.6	0.3	72.52	72.79	70.52	72.20
0.3	0.6	0.1	70.88	71.39	68.54	70.63
0.3	0.4	0.3	71.54	71.83	69.28	71.18
0.4	0.2	0.4	71.10	71.55	69.08	70.66
0.1	0.1	0.8	74.00	73.54	72.00	73.16
0.2	0.2	0.6	73.01	72.85	70.95	72.35
0.1	0.3	0.6	73.53	73.28	71.39	72.91
0.3	0.1	0.6	72.41	72.40	70.30	71.67
0.3	0.3	0.4	71.81	72.03	69.63	71.39
0.4	0.4	0.2	70.61	71.11	68.32	70.29

<sup>†</sup> Experimental measurements of Seitz et al. (1996)

<sup>\*</sup> EOS this work

<sup>††</sup> EOS by Duan et al. (2000) with mixing rules given by their equations 6 and 7 assuming van der Waals model of mixing.

<sup>‡</sup> EOS by Duan et al. (1996) using additional empirical parameters

Molar volumes in the ternary  $\text{H}_2\text{O}-\text{N}_2-\text{CH}_4$  have been measured by Seitz et al. (1996). In the Table 1 the experimental results are compared with the volumes predicted by our EOS. The calculated volumes using the EOS by Duan et al. (1996, 2000) are given for comparison. The two EOS of Duan et al. (1996, 2000) use either van der Waals mixing rules or a empirical mixing model derived by fitting to the original experimental results. The latter EOS shows the best agreement. However, our EOS does not use these experimental results but nevertheless reproduces the experimental results well. In addition, if compared to the EOS of Duan et al. (2000) which uses van der Waals mixing rules, our calculations are more consistent with the

experimental results. There is no doubt that by introducing empirical mixing parameters a better agreement with experimental results can be established. Our approach shows, however, that a reasonable description of fluid mixtures can be achieved without using any empirical parameters. Showing that for this particular system, we are further confident, that the proposed EOS works for other complex fluid mixtures as well.

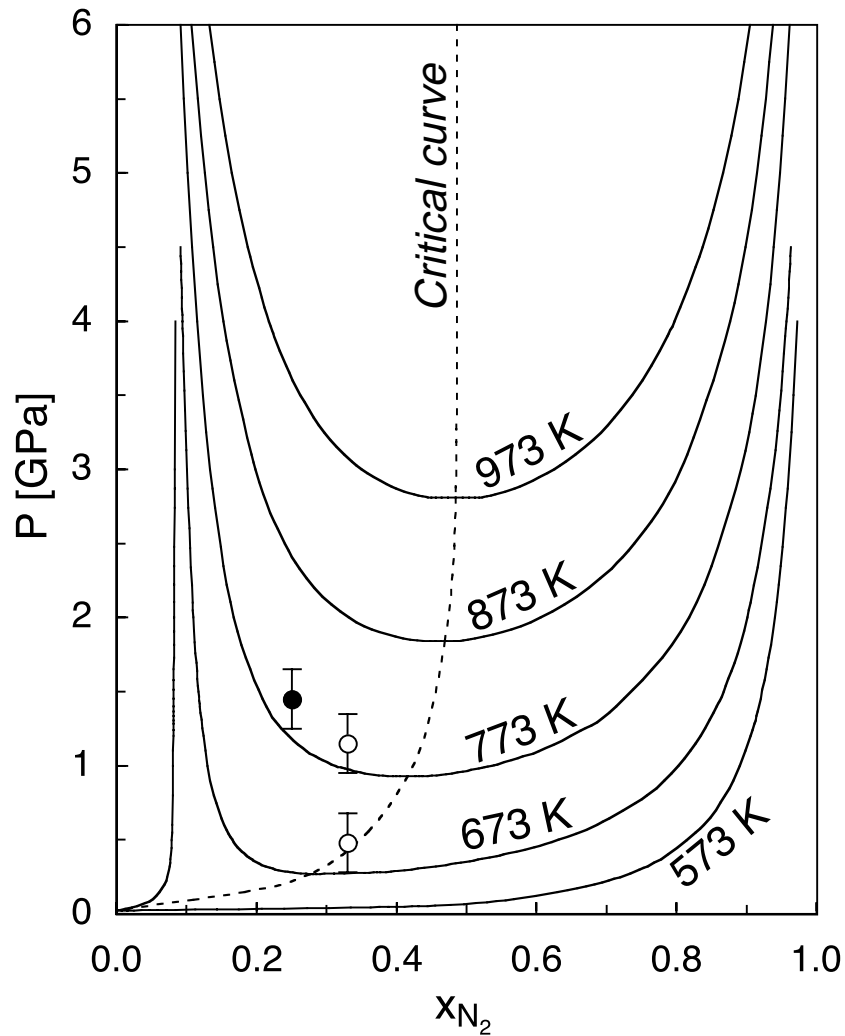


Fig. 4. Calculated phase equilibria in the H<sub>2</sub>O-N<sub>2</sub> binary (lines) from 575 K to 973 K in 100 K intervals and experimentally determined phase equilibria for 673K and 773K (empty circle: Constantino and Rice, 1991; filled circle: van Hinsburg et al., 1993).

#### 4. PHASE SEPARATIONS AT HIGH PRESSURES

Phase relation in various  $\text{H}_2\text{O}$ -non-polar gas systems have been studied systematically near the critical temperature of water ( $647 \text{ K} \pm 100$ ) below 250 MPa. Wu et al. (1990) for example, determined phase equilibria in the  $\text{H}_2\text{O}$ -Ar binary in the temperature range of 573-650 K and pressures up to 250 MPa. The topology of the system  $\text{H}_2\text{O}$ - $\text{N}_2$  was investigated by Japas and Frank (1985) up to 673 K and 250 MPa. All these systems are characterized by immiscibilities at high pressures (Heilig and Frank, 1990). In these systems, the projection of the critical curve on the P-T plane starts at the critical point of water and then passes through a minimum between 100-200 MPa and after that proceeds with a positive slope ( $dP/dT > 0$ ) to higher temperatures. For some systems like  $\text{H}_2$ - $\text{H}_2\text{O}$ , the minimum might not exist (Seward and Frank, 1981), but the positive slope of the critical curve is persistent.

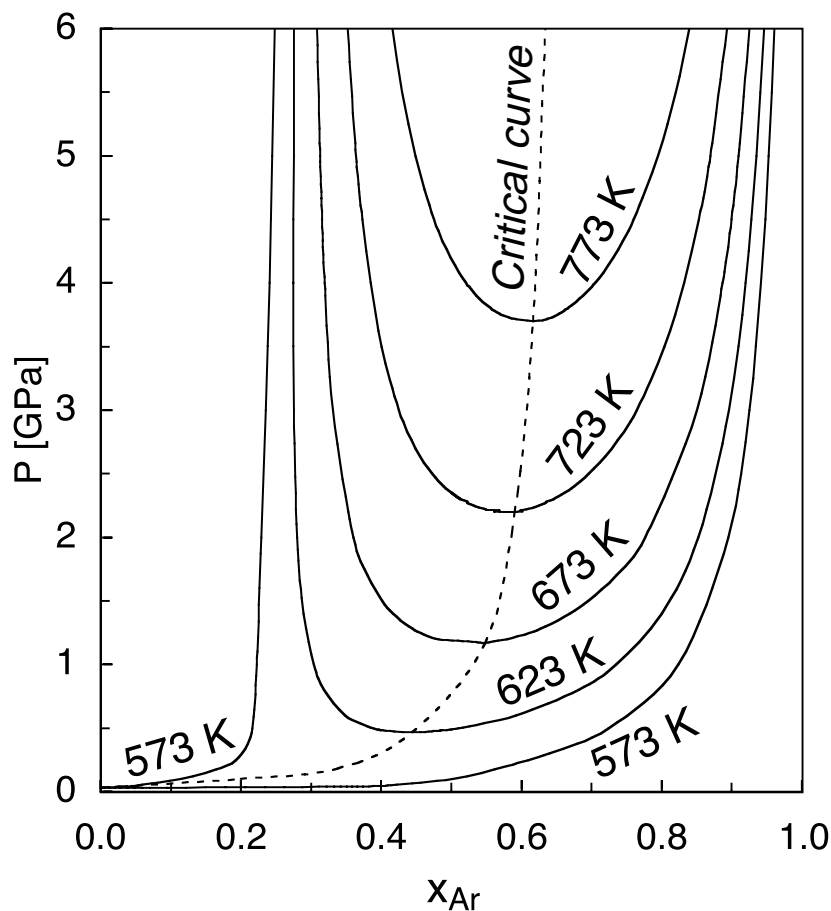


Fig. 5. Predicted high pressure equilibria in the system  $\text{H}_2\text{O}$ -Ar.

With exception of the system  $\text{H}_2\text{O}-\text{N}_2$ , the phase relations at higher pressures are not well known. Constantino and Rice (1991) and van Hinsburg (1993) used the diamond anvil cell to study fluid immiscibilities in the system  $\text{H}_2\text{O}-\text{N}_2$  at pressures up to 2 GPa. In Fig. 4 the calculated phase relations are compared with some experimental results. In comparison to the experimental results the calculated equilibrium temperatures of two phase boundary are slightly overestimated by approximately 20 K. Considering the simplicity of the proposed EOS this is a rather good agreement, as far as the EOS neglects the small quadrupole moment of the nitrogen molecule.

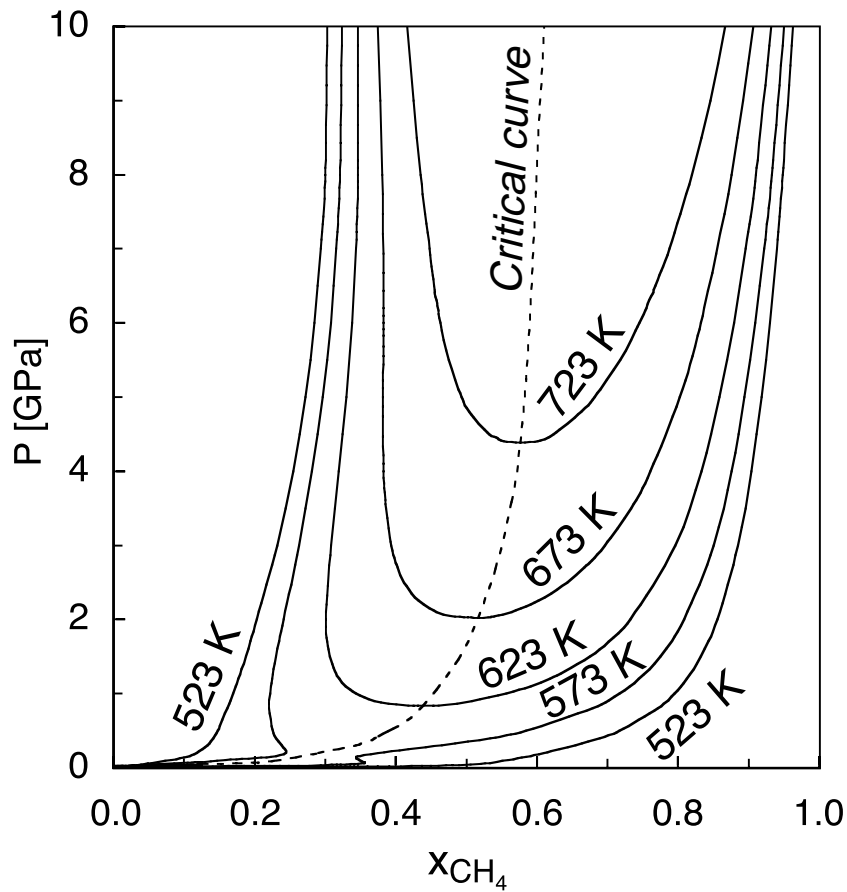


Fig. 6. Predicted high pressure equilibria in the system  $\text{H}_2\text{O}-\text{CH}_4$ .

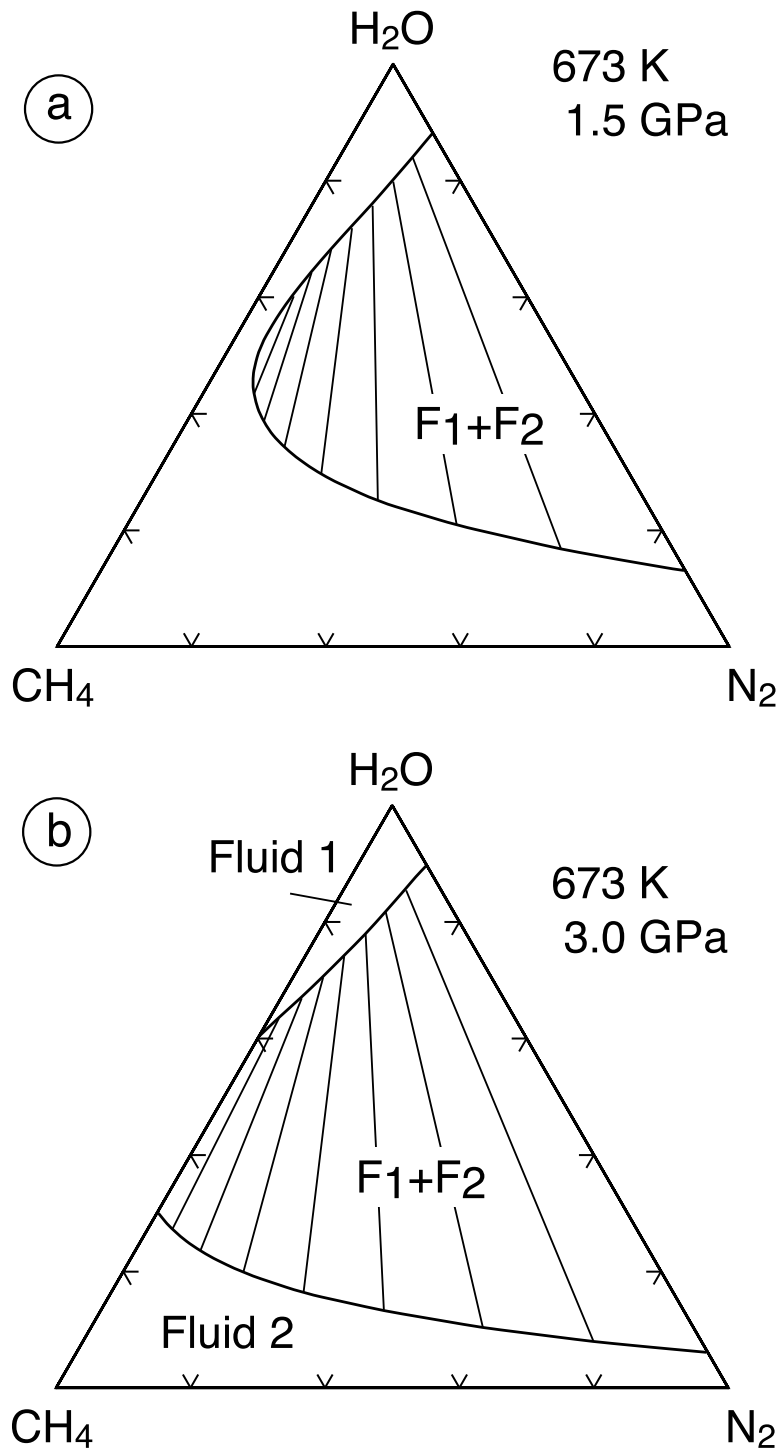


Fig. 7. Calculated gas-liquid phase relations in the ternary  $\text{H}_2\text{O}-\text{N}_2-\text{CH}_4$  at  $673\text{ K}$  and (a)  $1.5\text{ GPa}$  and (b)  $3\text{ GPa}$ .

In Fig. 5 and Fig. 6 the calculated phase relations in the system  $\text{H}_2\text{O}$ -Ar and  $\text{H}_2\text{O}$ - $\text{CH}_4$  are shown, respectively. These systems are characterized by a more ideal behaviour in comparison to the  $\text{H}_2\text{O}$ - $\text{N}_2$  binary. Thus at 673K the predicted phase separation in the systems  $\text{H}_2\text{O}$ -Ar and  $\text{H}_2\text{O}$ - $\text{CH}_4$  would occur at pressures above 1 and 2 GPa, respectively. In the case of systems with the three and more components the fluid equilibria inherit the phase relations observed in the binary subsystems. The calculated phase equilibria in the  $\text{H}_2\text{O}$ - $\text{N}_2$ - $\text{CH}_4$  ternary are shown in the Fig. 7 for a temperature of 673 K and for pressures of 1.5 and 3 GPa, respectively. According to the calculations,  $\text{CH}_4$  is more soluble in  $\text{H}_2\text{O}$  than  $\text{N}_2$ . At 1.5 GPa a phase separation is predicted in the system  $\text{H}_2\text{O}$ - $\text{N}_2$  but not in the  $\text{H}_2\text{O}$ - $\text{CH}_4$  binary. In the ternary a large two phase field separating a  $\text{H}_2\text{O}$ -rich liquid and a  $\text{N}_2$ - $\text{CH}_4$ -rich gas is predicted. At 3 GPa the two phase field will extend over the whole ternary. It is interesting to note, that independent on pressure the  $\text{N}_2/\text{CH}_4$  ratio in both coexisting phases is approximately identical and only the concentrations of the polar molecule in the two fluids is substantially different.

## 5. CONCLUSIONS

The EOS based on the thermodynamic perturbation theory using a generalized Stockmayer interaction potential has been applied to mixtures of strongly polar and non-polar molecular fluids over a wide range of pressures and temperatures. The EOS reproduces the experimental determined activity-composition relations accurately and high pressure phase separations in the various fluid mixtures are predicted correctly without any empirical parameters. The accuracy of the predicted thermodynamic properties for fluid mixtures depends on the nature of the fluid, however. In comparison to fluids containing spherically symmetric molecules like noble gases or slightly polar ones like CO, the accuracy is definitely lower for fluids involving highly polar molecules like  $\text{H}_2\text{O}$  or non-polar molecules with a strong quadruple moment like  $\text{CO}_2$ . An improvement could be obviously achieved if quadruple and higher order multipolar interactions as well as anisotropic inductions and dispersion forces would be explicitly included. It would be also desirable to apply a non-spherical reference system to account for anisotropic molecules.

**Acknowledgment.** The authors are grateful to A.G. Kalinichev for useful discussions and kindly providing the source code for the EOS of a Lennard-Jones fluid.

**REFERENCES**

- Anderko, A., and Pitzer, K.S. (1993a) Equation-of-state representation of phase equilibria and volumetric properties of the system NaCl-H<sub>2</sub>O above 573 K. *Geochim. Cosmochim. Acta* **57**, 1657-1680.
- Anderko A. and Pitzer K. S. (1993b) Phase equilibria and volumetric properties of the systems KCl-H<sub>2</sub>O and NaCl-KCl-H<sub>2</sub>O above 573 K; equation of state representation. *Geochim. Cosmochim. Acta* **57**, 4885-4897.
- Anovitz M.A., Blencoe J.G. Joyce D.B. and Horita J. (1998) Precise measurement of activity/compositions of H<sub>2</sub>O-N<sub>2</sub> and H<sub>2</sub>O-CO<sub>2</sub> fluids at 500°C, 500 bars. *Geochim. Cosmochim. Acta* **62**, 815-829.
- Aranovich L.Y. and Newton R.C. (1999) Experimental determination of CO<sub>2</sub>-H<sub>2</sub>O activity-composition relations at 600-1000°C and 6-14 kbar by reversed decarbonation dehydration reactions. *Amer. Mineral.* **84**, 1319-1332.
- Bakker R. J. (1999) Adaptation of the Bowers and Helgeson (1983) equation of state to the H<sub>2</sub>O-CO<sub>2</sub>-CH<sub>4</sub>-N<sub>2</sub>-NaCl system. *Chem. Geol.* **154**, 225-236.
- Belonoshko A.B. and Saxena S.K. (1992) A unified equation of state for fluids of C-H-O-N-S-Ar composition and their mixtures up to very high temperatures and pressures. *Geochim. Cosmochim. Acta* **56**, 3611-3626.
- Bowers T. S. and Helgeson H. C. (1983) Calculation of the thermodynamic and geochemical consequences of nonideal mixing in the system H<sub>2</sub>O-CO<sub>2</sub>-NaCl on phase relations in geologic systems: Equation of state for H<sub>2</sub>O-CO<sub>2</sub>-NaCl fluids at high pressures temperatures. *Geochimica et Cosmochimica Acta* **47**, 1247-1275.
- Churakov S.V. and Gottschalk M. (2001) Perturbation theory based equation of state for polar molecular fluids. I. Pure fluids. *Geochim. Cosmochim. Acta* (submitted).
- Constantino M. and Rice S.F. (1991) Supercritical phase separation in the H<sub>2</sub>O-N<sub>2</sub> mixtures. *J. Chem. Phys.* **95**, 9034-9036.
- Duan Z., Møller N. and Weare J. H. (1992) An equation of state for the CH<sub>4</sub>-CO<sub>2</sub>-H<sub>2</sub>O system: II. mixtures from 50 to 1000°C and 0 to 1000 bar. *Geochim. Cosmochim. Acta* **56**, 2619-2631.
- Duan Z., Møller N. and Weare J. H. (1995a) Molecular dynamics equation of state for nonpolar geochemical fluids. *Geochim. Cosmochim. Acta* **59**, 1533-1538.

- Duan, Z., Møller, N., and Weare, J.H. (1995b) Equation of state for the NaCl-H<sub>2</sub>O-CO<sub>2</sub> system: prediction of phase equilibria and volumetric properties. *Geochim. Cosmochim. Acta* **59**, 2869-2882.
- Duan Z., Møller N. and Weare J. H. (1996) A general equation of state for supercritical fluid mixtures and molecular dynamics simulation of mixture PVTX properties. *Geochim. Cosmochim. Acta* **60**, 1209-1216.
- Duan Z. Møller N. and Weare J.H. (2000) Accurate prediction of the thermodynamic properties of fluids in the system. H<sub>2</sub>O-CO<sub>2</sub>-CH<sub>4</sub>-N<sub>2</sub> up to 2000K and 100 kbar from a corresponding states/one fluid equation of state. *Geochim. Cosmochim Acta* **64**, 1069-1075.
- Frost D.J. and Wood B.J (1997) Experimental measurements of the properties of H<sub>2</sub>O-CO<sub>2</sub> mixtures at high pressures and temperatures. *Geochim. Cosmochim Acta* **61**, 3301-3309
- Gehrig M. (1980) Phasengleichgewichte und PVT-Daten ternärer Mischungen aus Wasser, Kohlendioxid und Natriumchlorid. Dissertation, University Karlsruhe.
- Gray C.G. and Gubbins K. E. (1984) Theory of molecular fluids. I. Fundamentals. Clarendon Press, Oxford.
- Greenwood H. J. (1969) The compressibility of gaseous mixtures of carbon dioxide and water between 0 and 500 bars. *Amer. Jour. Sci.* **267A**, 191-208.
- Grevel K. D. and Chatterjee N. D. (1992) A modified Redlich-Kwong equation of state for H<sub>2</sub>-H<sub>2</sub>O fluid mixtures at high pressures and at temperatures above 400°C. *Eur. J. Mineral.* **4**, 1303-1310.
- Gubbins K.E. and Twu C.H. (1978) Thermodynamics of polyatomic fluid mixtures. I. Theory, *Chem. Eng. Sci.* **33**, 863-878.
- Heilig M. and Frank E.U. (1990) Phase equilibria in the multicomponent fluid systems to high pressure and temperature. *Ber. Bunsenges Phys Chem.* **94**, 27-35.
- Hinsburg van M.G.E. Verbrugge R. and Schouten J.A. (1993) High temperature high-pressure experiments on H<sub>2</sub>O-N<sub>2</sub>. *Fluid Phase Equilib.* **88**, 115-121
- Holloway, J.R. (1976) Fugacity and activity of molecular species in supercritical fluids. In D.G. Fraser, Ed. Thermodynamics in Geology, p. 161-181, Dordrecht-Holland/Boston
- Jacobs G.K. and Kerrick D.M. (1981) Methane: an equation of state with application to the ternary system H<sub>2</sub>O-CO<sub>2</sub>-CH<sub>4</sub>. *Geochim. Cosmochim. Acta* **45**, 607-614.

- Japas M.L. and Franck E.U. (1985) High pressure phase equilibria and PVT-data of the water-nitrogen system to 673 K and 250 MPa. *Ber. Bunsenges. Phys. Chem.* **89**, 793-800.
- Kerrick D. M. and Jacobs G.K. (1981) A modified Redlich-Kwong equation for H<sub>2</sub>O, CO<sub>2</sub>, and H<sub>2</sub>O-CO<sub>2</sub> mixtures at elevated pressures and temperatures. *Amer. J. Sci.* **281**, 735-767.
- Prausnitz, J. M., Lichtenthaler, R.N. and Azevedo, E.G. (1999) Molecular thermodynamics of fluid-phase equilibria. Third edition, Prentice Hall, New Jersey.
- Saxena S.K. and Fei Y. (1988) Fluid mixtures in the C-H-O system at high pressure and temperature. *Geochim. Cosmochim. Acta* **52**, 505-512.
- Seitz J.C., Blencoe J.G., Joyce D.B. and Bodnar J. R. (1994) Volumetric properties of CO<sub>2</sub>-CH<sub>4</sub>-N<sub>2</sub> fluids at 200°C and 1000 bars: A comparison of equations of state and experimental data. *Geochim. Cosmochim. Acta* **58**, 1065-1071.
- Seitz J.C., Blencoe J.G. and Bodnar J. R. (1996a) Volumetric properties for  $\{(1 - x)\text{CO}_2 + x\text{CH}_4\}$ ,  $\{(1 - x)\text{CO}_2 + x\text{N}_2\}$ , and  $\{(1 - x)\text{CH}_4 + x\text{N}_2\}$  at the pressures (9.94, 19.94, 29.94, 39.94, 59.93, 79.93, and 99.93) MPa and temperatures (323.15, 373.15, 473.15, and 573.15) K. *J. Chem. Thermodyn.* **28**, 521-538.
- Seitz J.C., Blencoe J.G. and Bodnar J. R. (1996b) Volumetric properties for  $\{(x_1\text{CO}_2 + x_2\text{CH}_4 + (1 - x_1 - x_2)\text{N}_2\}$  at the pressures (19.94, 39.94, 59.93, 79.93, and 99.93) MPa and temperatures (323.15, 373.15, 473.15, and 573.15) K. *J. Chem. Thermodyn.* **28**, 539-550.
- Seward T.M. and Frank E.U. (1981) The system hydrogen-water up to 440°C and 2500 bar pressure. *Ber. Bunsengen. Phys. Chem.* **85**, 2-7
- Shmulovich K.I., Shmonov V.M., Mazur V.A. and Kalinichev A.G. (1980) P-V-T and activity concentration relations in the H<sub>2</sub>O-CO<sub>2</sub> system (homogeneous solutions). *Geochem. Int.* **17**, 123-139.
- Sretenskaya N.G., Razina M.V. and Belonozhko A.B. (1989) Calculation of thermodynamic properties for the KCl-H<sub>2</sub>O system under high parameters using the modified Redlich-Kwong equation. *Geochem. Int.* **26**, 70-80.
- Stell G., Rasaiah J.C. and Narang H. (1972) Thermodynamic perturbation theory for simple polar fluids, I. *Mol. Phys.* **23**, 393-406.
- Stell G., Rasaiah J.C. and Narang H. (1974) Thermodynamic perturbation theory for simple polar fluids, II. *Mol. Phys.* **27**, 1393-1414.

- Sterner S.M. and Bodnar R.J. (1991) Synthetic fluid inclusions. X: Experimental determination of P-V-T-X properties in the CO<sub>2</sub>-H<sub>2</sub>O system to 6kb and 700°C. *Amer J. Sci.* **291**, 1-54.
- Touret J. and Kerkhof, van den A.M. (1986) High density fluids in the lower crust and upper mantle. *Physica* **139 & 140B**, 834-840.
- Twu C.H. and Gubbins K.E. (1978) Thermodynamics of polyatomic fluid mixtures. II Polar, quadrupolar, octopolar. *Chem. Eng. Sci.* **33**, 879-887.
- Wu G., Heileg M. Lentz H. and Frank E.U. (1990) High pressure phase equilibria in the water-argon system. *Ber. Bunsenges Phys Chem.* **94**, 27-35.

## APPENDIX II.2

The residual Helmholtz free energy of a system ( $A^{res}$ ) can be calculated using a [0,1] Padé approximation as proposed by Stell et al. (1972):

$$A^{res} = A^{LJ} + A_2^{dip-dip} \left( 1 - \frac{A_3^{dip-dip}}{A_2^{dip-dip}} \right)^{-1} + A_1^{ind-dip} \quad (A1)$$

The appendix of Churakov and Gottschalk(submitted to GCA) treats the calculation of the Helmholtz free energy of pure fluids. In the following the required additions needed to treat fluid mixtures are presented.

### *Helmholtz free energy for mixtures of Lennard-Jones fluids*

To calculate the Helmholtz free energy for mixtures of Lennard-Jones fluids the van der Waals one-fluid theory is used. The parameters  $\epsilon_{mix}$  and  $\sigma_{mix}$  for a fluid mixture can be approximated as follows:

$$\sigma_{mix}^3 = \sum_{ij} x_i x_j \sigma_{ij}^3 \quad (A2)$$

$$\epsilon_{mix} = \frac{1}{\sigma_{mix}^3} \sum_{ij} x_i x_j \epsilon_{ij} \sigma_{ij}^3 \quad (A3)$$

$$\sigma_{ij} = \frac{1}{2} (\sigma_i + \sigma_j) \quad (A4)$$

$$\epsilon_{ij} = (\epsilon_i \epsilon_j)^{1/2} \quad (A5)$$

where  $x_i$ ,  $\epsilon_i$  and  $\sigma_i$  are the mole fraction and Lennard-Jones parameters of the pure component  $i$ . Using  $\epsilon_{mix}$  and  $\sigma_{mix}$  the reduced parameters for mixtures are defined as:

$$\rho^* = \rho N_A \sigma_{mix}^3 \quad (A6)$$

$$\beta = \frac{\varepsilon_{mix}}{kT} \quad (A7)$$

Using eqs. A1-A7 in addition to the expressions given in the appendix of Churakov and Gottschalk (submitted to GCA)  $A^{LJ}$  can be calculated.

*Perturbation contribution of the dipole-induced dipole and dipole-dipole interaction*

The perturbation contributions to the Helmholtz free energy can be calculated as follows:

$$A_1^{ind-dip} = -2\pi N_A^2 \rho \sum_{ij} x_i x_j \frac{1}{\sigma_{ij}^3} (\alpha_i \mu_j^2 + \alpha_j \mu_i^2) J_{ij} \quad (A8)$$

$$A_2^{dip-dip} = -\frac{2\pi N_A^2 \rho}{3kT} \sum_{ij} x_i x_j \frac{\mu_i^2 \mu_j^2}{\sigma_{ij}^3} J_{ij} \quad (A9)$$

$$A_3^{dip-dip} = \frac{32\pi^3 N_A^3 \rho^2}{135(kT)^2} \left(\frac{14\pi}{5}\right)^{1/2} \sum_{ijk} x_i x_j x_k \frac{\mu_i^2 \mu_j^2 \mu_k^2}{\sigma_{ij} \sigma_{ik} \sigma_{jk}} K_{ijk} \quad (A10)$$

with (Stell et al. 1972):

$$\rho_{ij}^* = \rho N_A \sigma_{ij}^3 \quad (A11)$$

$$\beta_{ij} = \frac{\varepsilon_{ij}}{kT}$$

$$J_{ij} = -\frac{1}{16\pi \rho_{ij}^* \beta_{ij}} \left[ 4 \frac{U_{ij}^{LJ}}{RT} - Z_{ij}^{LJ} + 1 \right] \quad (A12)$$

$$Z_{ij}^{LJ} = 1 + \rho \frac{\partial(A^{LJ}(\rho_{ij}^*, \beta_{ij})/(RT))}{\partial \rho} \quad (A13)$$

$$U_{ij}^{LJ} = -T^2 \frac{\partial(A^{LJ}(\rho_{ij}^*, \beta_{ij})/T)}{\partial T} \quad (A14)$$

$$K_{ijk} = \left[ K(\rho_{ij}^*, \beta_{ij}) K(\rho_{ik}^*, \beta_{ik}) K(\rho_{jk}^*, \beta_{jk}) \right]^{1/3} \quad (\text{A15})$$

$$\ln \left[ K(\rho_{ij}^*, \beta_{ij}) \right] = -M_1 \rho_{ij}^{*2} \text{Ln}(\beta_{ij}) + M_2 \rho_{ij}^{*2} - M_3 \rho_{ij}^* \text{Ln}(\beta_{ij}) + M_4 \rho_{ij}^* - M_5 \text{Ln}(\beta_{ij}) + M_6 \quad (\text{A16})$$

The coefficients  $M_1$  to  $M_6$  are identical to those for pure fluids (Churakov and Gottschalk submitted to GCA).

**Size and Topology of Molecular Clusters in Supercritical Water:  
a Molecular Dynamics Simulation**

**Abstract**

A hybrid criterion of hydrogen bonding is applied to the analysis of molecular dynamics trajectories simulated for several near- and supercritical thermodynamic conditions. Even at vapor-like densities supercritical water is shown to contain large molecular clusters, consisting of up to 10 molecules. Relative abundances of topologically different trimers, tetramers, and pentamers are examined, and chain-like clusters are found predominant under supercritical conditions. In contrast to the results of quantum-chemical calculations for isolated water clusters, ring-like clusters are only rarely formed in supercritical water.

## 1. Introduction

In the near-critical region the properties of any fluid change dramatically over a relatively narrow range of temperatures and pressures [1]. These changes also affect the fluid structure. The structure of liquid water is known to be dominated by the formation of hydrogen bonds connecting all water molecules. However, the very persistence of hydrogen bonding up to the critical point of water ( $T_c = 647 \text{ K} = 374^\circ\text{C}$ ;  $P_c = 22.1 \text{ MPa}$ ;  $\rho_c = 0.32 \text{ g/cm}^3$ ) has been a matter of significant controversy until recently [2–17].

It is now well established both experimentally [10,13–15] and by molecular computer simulations [3–9,11,12,16,17] that H-bonds in water do persist even above the critical temperature. Although the infinite percolating network of H-bonds breaks apart with the increase of temperature, individual molecules in supercritical water for significant amount of time remain bonded in smaller molecular aggregates, or clusters [16]. Quantitative understanding of the size and structure of such clusters is important for many fundamental and practical reasons. For example, recent estimations suggest that large pressure effects on the isotope fractionation between high-temperature aqueous solutions and minerals can be explained by taking into account the degree of clusterization in water vapor [18].

A hybrid criterion of H-bonding based on molecular distance–energy distribution functions has already been applied to the analysis of molecular configurations generated by Monte Carlo computer simulations over wide ranges of temperature and pressure [5,16] and has shown to give quantitative results consistent with all available experimental data [10,13–15]. In this Letter we apply the same criterion to the analysis of molecular dynamics trajectories simulated for several near- and supercritical thermodynamic conditions. Based on this analysis we calculate size and shape distributions of molecular clusters in supercritical water, and examine topological and structural characteristics of the most common clusters, such as trimers, tetramers, and pentamers.

## 2. Molecular dynamics simulations

The MD simulations were performed using a conventional molecular dynamics algorithm for the canonical ( $NVE$ ) ensemble [19]. The systems studied consisted of 200 water molecules in a cubic box with periodic boundary conditions. The side length of the simulation box was adjusted from run to run to give the required density in the range between 0.17 and 1.28  $\text{g/cm}^3$  which corresponded to the pressure range of  $25 \text{ MPa} < P < 3000 \text{ MPa}$ . Five

simulation runs were performed for these pressure/density conditions at temperatures from 623 to 773 K (Fig. 1). The flexible BJH water model [20] was employed to calculate the energy of intermolecular interactions during the simulations. Ewald summation in tabulated form was used for the long-range Coulombic part of the interactions, and the ‘shifted-force’ method [19] was used for the non-Coulombic parts of the BJH potential.

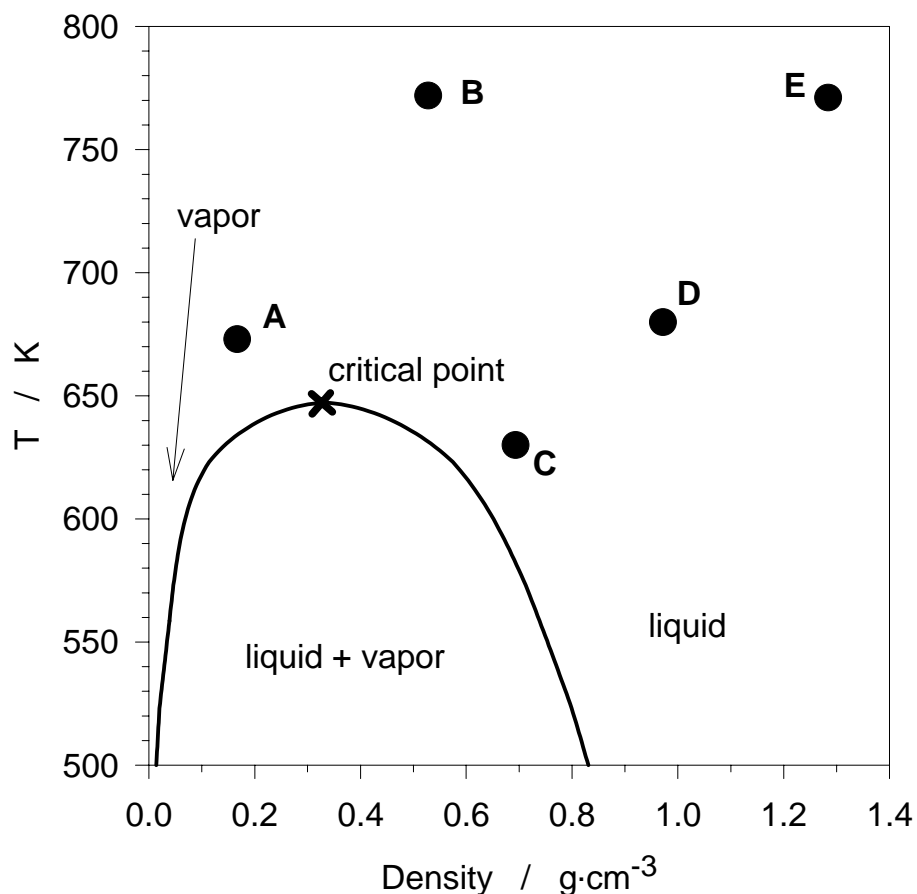


Fig. 1. A fragment of the phase diagram for near-critical water with indicated thermodynamic conditions of the present MD simulations.

Equilibrium properties of supercritical water at every thermodynamic state point were calculated as time averages over a trajectory of  $> 15\,000$  time steps after a pre-equilibration stage of approximately the same length. A detailed comparison of thermodynamic, structural, kinetic and spectroscopic results of these MD-simulations with available experimental data is presented elsewhere, together with the analysis of translational, librational and vibrational dynamics of individual water molecules under supercritical conditions [8,21]. A few hundred configurations uniformly distributed along each of the simulated MD-trajectories were selected for the present analysis of the topology and connectivity of H-bonded clusters in supercritical water. Points A, B, D, and E are located above the critical point of water, while point C is positioned in the vicinity of the vapor–liquid equilibrium curve. It is worth noting,

that the phase diagram for the computer-simulated water corresponding to the BJH potential model is not known in detail over this region of temperatures and densities. However, recent analysis of the CF water model [22], which constitutes the inter-molecular part of the flexible BJH potential function [20], led to a liquid–vapor coexistence curve in reasonable agreement with that of real water ( $T_c^{CF} = 609.5$  K;  $P_c^{CF} = 27.5$  MPa;  $\rho_c^{CF} = 0.378$  g/cm<sup>3</sup> [23]).

While analyzing simulated molecular configurations of supercritical water, two molecules  $i$  and  $j$  were considered H-bonded if they satisfied the hybrid geometric–energetic criterion of H-bonding [5,16] which can be formulated as follows: (1) the distance between the O-atom of the molecule  $i$  and the H-atom of the molecule  $j$  is equal to  $R_{O \dots H} \leq R_{HB}$ ; and (2) the total energy of interaction between these two molecules is equal to  $E_{ij} \leq E_{HB}$ . Here  $R = 2.4$  Å is the maximum allowable length of an H-bond, and  $E_{HB} = -10$  kJ/mol is the minimum (by absolute value) allowable H-bonding energy. This criterion of H-bonding reflects two most natural parameters of a bond – its length and strength. Its implementation in computer simulations for water is based on the distance–energy pair distribution functions, and it has already proved its reliability in the quantitative comparison of computer-simulated data with the estimates of the degree of H-bonding in supercritical water from all available experimental sources [5,16]. This criterion of H-bonding was applied to every pair of molecules in a computer-generated configuration. From the resulting molecular connectivity matrix we constructed cluster size distributions and analyzed the topology of the clusters formed. A molecule was considered belonging to a cluster if it had at least one H-bond with some other molecule in the cluster. Only the analysis of instantaneous configurations so-called I-structures [24] is reported below. Taking the H-bonding lifetimes into consideration can, certainly, affect the quantitative results discussed in the next section and will be the subject of our future studies [25].

### 3. Results and discussion

Some characteristics of H-bonds found in super-critical BJH water, such as the average number of H-bonds per one water molecule,  $\langle n_{HB} \rangle$ , the average energy of H-bonds,  $\langle U_{HB} \rangle$ , the average length of H-bonds,  $\langle R_{HB} \rangle$ , and the average H-bonding angle,  $\langle \theta_{HB} \rangle = \langle \angle O-H \dots O \rangle$ , are presented in Table 1 for all thermodynamic points studied.  $\langle f_i \rangle$  in this table denotes the average fractions of molecules participating in exactly  $i$  H-bonds under given thermodynamic conditions. The numerical values of H-bonding parameters in Table 1 for the flexible BJH water model are very close to the values reported previously for the rigid

TIP4P water model at comparable temperatures and densities [5,16]. Similar structural and H-bonding results have also been obtained in computer simulations of supercritical water using a number of other intermolecular models: rigid, flexible, polarizable, *ab-initio* (see Refs. [16,26] for detailed discussion). Thus, we can hope that our present results can be considered as not being specific to any particular potential model used in the simulations, but indeed reflect real H-bonding phenomena in supercritical water. As long as the temperature difference of  $\sim 100$ - $150$  K between the supercritical thermodynamic states in Table 1 can be neglected in the first approximation [8,12,21], only the effect of density on the redistribution of molecules between various cluster types will be discussed further.

Table 1. Average parameters of hydrogen bonds in supercritical BJH water

	Thermodynamic state points				
	A	B	C	D	E
T (K)	673	772	630	680	771
$\rho$ (g/cm <sup>3</sup> )	0.167	0.528	0.693	0.972	1.284
$\langle n_{\text{HB}} \rangle$	0.42	0.83	1.41	1.65	1.75
$\langle U_{\text{HB}} \rangle$ (kJ/mol)	-17.34	-17.34	-17.47	-17.38	-17.19
$\langle R_{\text{HB}} \rangle$ (Å)	2.038	2.027	2.014	2.006	1.991
$\langle \theta_{\text{HB}} \rangle$ (°)	150.9	150.8	151.9	150.9	148.4
$\langle f_0 \rangle$ (%)	64.6	39.4	16.8	11.6	10.5
$\langle f_1 \rangle$ (%)	29.7	41.1	39.6	33.7	31.4
$\langle f_2 \rangle$ (%)	5.5	16.8	31.7	35.5	35.4
$\langle f_3 \rangle$ (%)	0.3	2.6	10.6	16.2	18.3
$\langle f_4 \rangle$ (%)	0.0	0.1	1.3	2.8	4.2

It is important to emphasize that the relatively small number of molecules in the basic simulation cell used in computer simulations,  $N$ , poses natural limits on the size of unique interconnected H-bonded structures available for the analysis. Thus, the presence of clusters consisting of  $\geq 180$  molecules in our simulations ( $N = 200$ ) can already indicate the existence a macroscopic infinite network of H-bonds, if we take into account that periodic boundary conditions are imposed on the simulation cell. The precise calculation of the

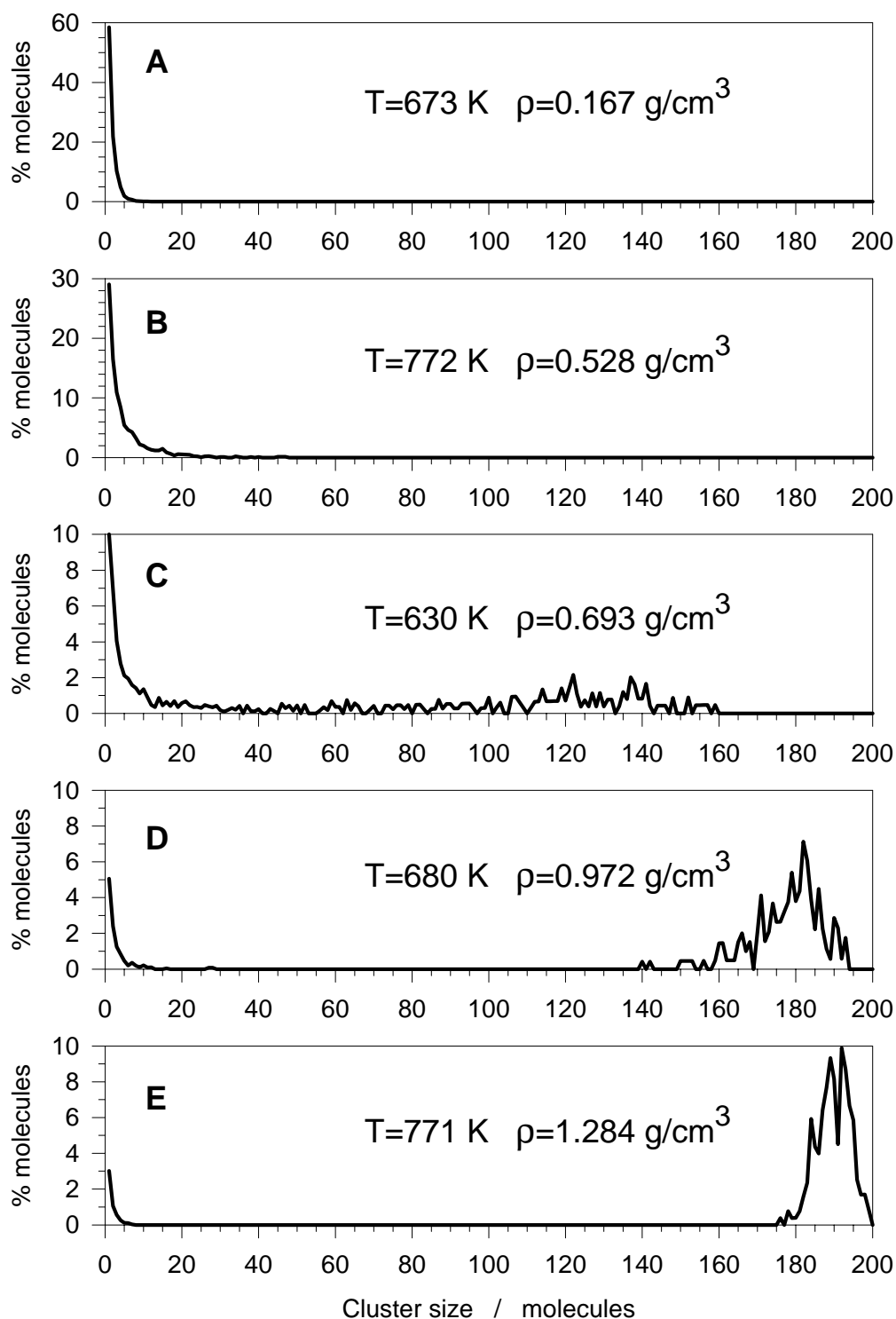


Fig. 2. Participation of water molecules in clusters of different size under supercritical conditions.

minimum size of the cluster which would allow for the percolating network of H-bonded molecules to be formed was not the aim of our study. However, the number of 100–150 molecules seems to be a reasonable lower estimate for such a limiting cluster size. For an

arbitrary number of molecules in the simulation cell we can roughly estimate the minimum size of the limiting cluster as  $N_c^{\min} = N/2$ .

A more accurate quantitative criterion for existence in the system of the infinite percolating molecular cluster can be obtained by comparing the calculated  $\langle n_{\text{HB}} \rangle$  for a specific thermodynamic state with the *percolation threshold*, which is known to be  $n_p \approx 1.56$  for a 3-dimensional random tetrahedrally ordered network of bonds typical for water [27]. In our supercritical simulations, the low-density points A and B (Fig. 1; Table 1) are definitely below the percolation threshold ( $\langle n_{\text{HB}} \rangle_{\text{A}} = 0.42$  and  $\langle n_{\text{HB}} \rangle_{\text{B}} = 0.83$ ), while the high-density point E is above it ( $\langle n_{\text{HB}} \rangle_{\text{E}} = 1.75$ ). On the other hand, points C and D are both quite close to the percolation threshold ( $\langle n_{\text{HB}} \rangle_{\text{C}} = 1.41$  and  $\langle n_{\text{HB}} \rangle_{\text{D}} = 1.65$ ). It is important to remember that for normal liquid water under ambient conditions  $\langle n_{\text{HB}} \rangle_{\text{w}} = 3.2$  (see Ref. [16] for details).

The estimation of  $\langle n_{\text{HB}} \rangle$  from computer simulations or experimental data [10,13,14], although being a very useful average topological parameter of a H-bonded system, does not tell us much about the size and topology of specific H-bonded clusters. Fig. 2 shows cluster size distributions (normalized to the total number of molecules) calculated from our MD-simulations. As might have been expected, the increase of density results in the formation of larger clusters. There is a notable difference between the distributions for lower-density states (A, B) and higher-density states (D, E). Only relatively small clusters are found at lower densities. However, even at the vapor-like density of point A, clusters of up to 10 water molecules can be present, and at the intermediate density (point B) clusters of  $> 20$  molecules are observable.

In contrast to this picture, the distributions at high densities (D, E) show two distinct maxima corresponding to relatively small clusters ( $< 15$  molecules), as well as to very large clusters ( $> 150$  molecules). Remarkably, no clusters of intermediate size are found under these conditions. It is reasonable to assume that the right-hand peak of the high-density distributions at 150–200 molecules indicates the existence of a dynamic infinite percolating network in the system. The statistical characteristics of such H-bonded networks in supercritical water has already been discussed in some detail [16]. The left-hand peak on the diagrams (Fig. 2D and E) is due to small molecular groups temporarily detached from this network.

The cluster size distribution for the point C differs dramatically from the both cases discussed above. Here we can observe clusters of virtually any size with a continuous transition between small-size and large-size branches of the distribution. Such a continuous shape of the distribution reflects the large-scale structural fluctuations accompanying the

transition of the water structure from its liquid-like state, characterized by the percolating network of H-bonds, to the vapor-like state where this network is broken down into several smaller low-molecular fragments. Point C is, indeed, located the most closely to the vapor-liquid coexistence curve.

We analyzed the topology of relatively simple clusters observable under both vapor-like as well as liquid-like conditions: trimers, tetramers, and pentamers. No distinction was made between donor and acceptor types of H-bonds originating at a particular water molecule. Thus, every molecule is depicted as a structureless dot in Fig. 3 where all observable topological types of 3-, 4-, and 5-mers are shown along with their relative abundances (normalized as a fraction of molecules participating in clusters of certain type) under various thermodynamic conditions.

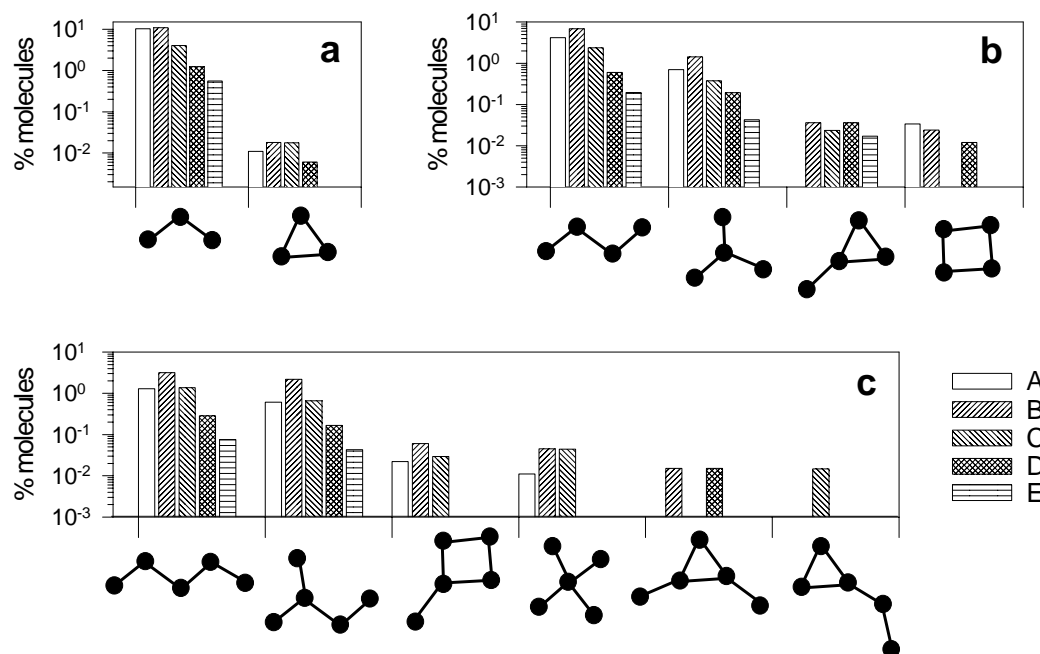


Fig. 3. Topological types of trimers, tetramers, and pentamers, and their relative abundance in supercritical water under thermodynamic conditions indicated in Fig. 1.

Fig. 3 demonstrates that, despite the obvious domination of the most simple linear chain-like clusters, more complex structures are also present. Since only instantaneous configurations were analyzed in this work, some of the observed clusters might in reality have a rather short lifetime, and thus represent only transient structures. Nevertheless, all bonds in the observed clusters satisfied both geometric and energetic criteria for H-bonding, and none of the observed structures can be considered energetically unfavorable within the given definitions.

Only two topological types are possible for trimers: a chain and a 3-member ring. As seen in Fig. 3a, > 99% of all trimers are present in the form of linear chains under supercritical conditions. This is, of course, not surprising, since the formation of a 3-member ring can only be possible by significant bending of all three H-bonds, thus making this structure energetically less favorable.

Four water molecules can theoretically form 6 topologically different types of tetramers, 4 of which were observed in our simulations. Fig. 3b shows that the most abundant tetramers have chain-like structure (1) under all thermodynamic conditions studied. Such linear structures constitute >80% of all tetramers, while another 17% are represented by an open structure (2), which can be described as a branched chain. Configurations containing 3- or 4- member rings constitute in total < 3% of all tetramers.

Five water molecules can form 14 topologically different types of pentamers. Some of them are, obviously, energetically unfavorable and never materialize. In supercritical water we have found only 6 topological types of pentamers shown in Fig. 3c. Once again, the simplest linear chain-like cluster (1) is the most abundant type and constitutes ~ 63% of all pentamers. Almost twice less abundant (35% of pentamers) are slightly branched linear clusters (2). The remaining four types observed in the simulations constitute together ~2%, and poor statistics prevents us to analyze the density dependence of their relative abundances.

It is interesting to note that present results on the topology of H-bonded molecular clusters in supercritical water significantly differ from the results of quantum-chemical calculations which consistently identify ring-like cluster structures as the most stable ones (see e.g. Ref. 28). Five-member rings were not found in our simulations even as less abundant species, while the presence of 3- and 4-member rings is very small. This contradiction can be explained by the fundamental difference in the thermodynamic conditions of these two types of calculations. Under high supercritical temperatures of our simulations, ring-like structures are becoming unstable because of the high kinetic energy of the constituting water molecules. This can also be confirmed by the molecular dynamics simulations of isolated pentamers [29,30], where 5-member rings have been found at the limit of their stability even at near-ambient temperatures.

Almost total absence of pentamers organized in complete tetrahedral clusters (4 in Fig. 3c) is also remarkable, since tetrahedral local ordering is the most distinct feature of H-bonded networks in water. Furthermore, the experimental data on X-ray diffraction in supercritical water [10,31] show a peak of molecular distribution function corresponding to tetrahedrally-ordered second-nearest neighbors exactly under the thermodynamic conditions

of point B of the present study. This apparent contradiction is easily resolved if we note that tetrahedrally-coordinated second-neighboring molecules can be found in any of the observed clusters starting from trimers. Therefore, all these clusters, and not just full tetrahedra, can represent the fragments of a larger tetrahedrally-coordinated H-bonded network. Similar to the ring-like structures, such pentamers are, obviously, less stable at supercritical temperatures.

#### 4. Conclusions

Our analysis of MD simulation results for supercritical water using the hybrid geometric and energetic criterion of hydrogen bonding [5,16] demonstrates that even low-density water vapor ( $\rho < 0.2 \text{ g/cm}^3$ ) under supercritical conditions can contain quite large molecular clusters, consisting of up to 10 molecules. No significant density dependence of relative abundances for topologically different water clusters of small size is observed, and chain-like clusters are found predominant under supercritical conditions. In contrast to the results of quantum-chemical calculations for isolated water clusters which identify ring-like structures as the most stable energetically, such structures are only rarely formed under supercritical conditions. Somewhat counterintuitively, the fraction of pentamers topologically organized as complete tetrahedra is also insignificant under these conditions.

#### Acknowledgements

The work has been supported by INTAS (Grants UA-95-0096 and 96-1989), CRDF (Grant RC1-170), and the Russian Foundation for Basic Research (Grant 95-03-32587). The authors are grateful to Yu.E. Gorbaty for permanent interest in this work and useful discussions, and to A.A. Chialvo and P.T. Cummings for kindly providing the manuscript of their review paper prior to publication.

#### References

1. R.W. Shaw, T.B. Brill, A.A. Clifford, C.A. Eckert, E.U. Franck, Chem. Eng. News 69(51) (1990) 26.
2. P. Postorino, R.H. Tromp, M.A. Ricci, A.K. Soper, G.W. Neilson, Nature (London) 366 (1993) 668

3. A. Chialvo, P.T. Cummings, *J. Chem. Phys.* 101 (1994) 4466.
4. E.S. Fois, M. Sprik, M. Parrinello, *Chem. Phys. Lett.* 223 (1994) 411.
5. A.G. Kalinichev, J.D. Bass, *Chem. Phys. Lett.* 231 (1994) 301.
6. T.I. Mizan, P.E. Savage, R.M. Ziff, *J. Phys. Chem.* 98 (1994) 13067.
7. G. Loffler, H. Schreiber, O. Steinhauser, *Ber. Bunsenges. Phys. Chem.* 98 (1994) 1575.
8. A.G. Kalinichev, K. Heinzinger, *Geochim. Cosmochim. Acta* 59 (1995) 641.
9. R.D. Mountain, *J. Chem. Phys.* 103 (1995) 3084.
10. Yu.E. Gorbaty, A.G. Kalinichev, *J. Phys. Chem.* 99 (1995) 5336.
11. A. Chialvo, P.T. Cummings, *J. Phys. Chem.* 100 (1996) 1309.
12. T.I. Mizan, P.E. Savage, R.M. Ziff, *J. Phys. Chem.* 100 (1996) 403.
13. M.M. Hoffmann, M.S. Conradi, *J. Am. Chem. Soc.* 119 (1997) 3811.
14. A.K. Soper, F. Bruni, M.A. Ricci, *J. Chem. Phys.* 106 (1997) 247.
15. N. Matubayasi, C. Wakai, M. Nakahara, *J. Chem. Phys.* 107 (1997) 9133.
16. A.G. Kalinichev, J.D. Bass, *J. Phys. Chem. A* 101 (1997) 9720.
17. P. Jedlovsky, J.P. Brodholt, F. Bruni, M.A. Ricci, A.K. Soper, R. Vallauri, *J. Chem. Phys.* 108 (1998) 8528.
18. T. Driesner, *Science* 277 (1997) 791.
19. M.P. Allen, D.J. Tildesley, *Computer Simulation of Liquids*, Oxford University Press, New York, 1987.
20. P. Bopp, G. Jancso, K. Heinzinger, *Chem. Phys. Lett.* 98 (1983) 129.
21. A.G. Kalinichev, *Ber. Bunsenges. Phys. Chem.* 97 (1993) 872.
22. F.H. Stillinger, A. Rahman, *J. Chem. Phys.* 68 (1978) 666.
23. B. Guillot, Y. Guissani, *J. Chem. Phys.* 108 (1998) 10162.
24. D. Eisenberg, W. Kauzmann, *The Structure and Properties of Water*, Oxford University Press, Oxford, 1969.
25. A.G. Kalinichev, S.V. Churakov in preparation
26. A.A. Chialvo, P.T. Cummings, *Adv. Chem. Phys.* (1999), in. print.
27. H.E. Stanley, J. Teixeira, *J. Chem. Phys.* 73 (1980) 3404.
28. J.K. Gregory, D.C. Clary, *J. Phys. Chem.* 100 (1996) 18014.
29. P.L.M. Plummer, T.S. Chen, *J. Chem. Phys.* 86 (1987) 7149.
30. W.B. Bosma, L.E. Fried, S. Mukamel, *J. Chem. Phys.* 98 (1993) 4413.
31. Yu.E. Gorbaty, Yu.N. Demianets, *Chem. Phys. Lett.* 100 (1983) 450.

**Size, Structure and Abundance of Molecular Clusters  
in Supercritical Water Over Wide Range of Densities:  
Monte Carlo Simulations**

**ABSTRACT**

The extent of hydrogen-bonded cluster formation in near- and supercritical water has been explored by application of a hybrid hydrogen-bonding criterion to the analysis of Monte Carlo computer simulation results. Up to 10% of water molecules were found to constitute clusters even in dilute supercritical water vapor ( $T^*=1.04$ ,  $\rho^*=0.06$ ), while the maximum size of H-bonded complexes formed under these conditions may be as large as 7 molecules per cluster. Relative abundance of topologically different trimers, tetramers, and pentamers were also examined. Open chain- and tree-like clusters are preferentially formed in supercritical water, while cyclic ring-like structures occur only rarely. Partitioning of molecules between clusters of the same size, but topologically different structure is found to be virtually independent of temperature and density. Geometric characteristics of small hydrogen-bonded clusters in supercritical water only slightly vary with temperature and density.

## INTRODUCTION

Over the last several years, significant efforts have been made to examine the structure of supercritical water using both experimental methods and computer simulations [1-19]. More recently, the formation of small molecular clusters in high temperature water vapor, as well as in supercritical fluid has attracted particular attention [18,20,21]. The nucleation of clusters results in local structural and density heterogeneity in the fluid. In different clusters water molecules possess slightly different properties such as the dipole moment and lengths of interatomic bonds [9]. So, topologically different water complexes may be even considered as distinct chemical compounds. Quantitative understanding of the size and structure of such clusters is important for many fundamental and practical reasons. For example, recent calculations suggest that the large effects of pressure on the isotope fractionation between high temperature aqueous solutions and minerals can be explained by taking into account the degree of clusterization in water vapor [21].

We applied Monte Carlo computer simulations to investigate the statistics of size and topology distributions of hydrogen-bonded water clusters over wide ranges of near- and supercritical temperatures and densities. Particular emphasis has been made on the geometry of the most abundant trimers, tetramers, and pentamers of water molecules.

## METHOD OF MODELING

The simulations were performed using a conventional Monte Carlo algorithm for the isothermal-isobaric (*NPT*) ensemble [22]. The investigated systems consisted of 216 water molecules interacting via the TIP4P [23] rigid four site effective pair potential in the cubic box with periodic boundary conditions. About 50 million MC steps were performed for each of the ~40 thermodynamic points studied, and about 5000 equilibrium statistically independent molecular configurations (separated by 10000 MC steps) were accumulated at every thermodynamic point for further analysis of the structure of hydrogen-bonded network. Other specific details of the simulation technique are reported elsewhere [13,19,20].

While analyzing the simulated molecular configurations of supercritical water, two molecules *i* and *j* were considered hydrogen-bonded if they satisfied the hybrid geometric-energetic

criterion of H-bonding [13,19] which can be formulated as follows: (1) the distance between the O-atom of the molecule  $i$  and the H-atom of the molecule  $j$  is equal to  $R_{O\dots H} \leq R_{HB}$ , and (2) the total energy of interaction between these two molecules is equal to  $E_{ij} \leq E_{HB}$ . Here  $R_{HB} = 2.4 \text{ \AA}$  is the maximum allowable length of a hydrogen bond, and  $E_{HB} = -10 \text{ kJ/mol}$  is the minimum (by absolute value) allowable H-bonding energy. This criterion of H-bonding is directly related to the two most natural parameters of a bond — its length and strength. The implementation of this criterion in computer simulations for water is based on the distance-energy pair distribution functions, and it has already proved its reliability in the quantitative comparison of computer-simulated data with the estimates of the degree of hydrogen bonding in supercritical water from all available experimental sources [13, 19]. This criterion of H-bonding was applied to every pair of molecules in a computer-generated configuration. From the resulting connectivity matrix, the groups of molecules interconnected by a network of H-bonds were collected to obtain cluster size distributions. By indexing the interconnected molecules, geometric and energetic characteristics of each isolated cluster were obtained. A molecule was considered belonging to a cluster if it had at least one H-bond with some other molecule in the cluster. Following this method, the maximum cluster size is limited by the total number of molecules in the simulation box (216 in the current study). Molecules were considered to form an infinite percolating H-bonded network, if a periodic image of at least one of them belonged to the same cluster as its origin. Due to the time-independent nature of the Monte Carlo simulations, only the analysis of instantaneous configurations (so called I-structures [24]) is reported here. Taking the H-bonding lifetimes into consideration can, certainly, affect the quantitative results discussed below (e.g., [18]) and will be the subject of our future molecular dynamics simulations.

## RESULTS AND DISCUSSION

While accurately predicting the structure and volumetric properties of liquid water [23], the TIP4P potential has critical parameters slightly shifted with respect to the experimental data [25]. However, our goal was not the most accurate prediction of the volumetric properties, but rather the detailed quantitative analysis of the structure of fluid water at varying pressures, temperatures, and densities. The discrepancies between simulated and experimental properties of water can be accounted for by an appropriate choice of the critical parameters. Following the method of Guissani and Guillot [26], the equation of state[27]:

$$Z=P/(\rho RT)=1+B_1x+B_2x^2+B_3x^3+B_4x^4+B_{10}x^{10} - (1/T^*)^{0.5} (C_1x+2C_2x^2+3C_3x^3+4C_4x^4+5C_5x^5), \quad (1)$$

was fitted to results of simulations, where  $x=\rho^*/T^{*0.25}$ ,  $T^*=T/T_c$ , and  $\rho^*=\rho/\rho_c$ . Using this equation, the critical parameters of the TIP4P water are predicted to be  $T_c=600.7$  K,  $P_c=18.1$  MPa, and  $\rho_c=0.328$  g/cm<sup>3</sup> in good agreement with preliminary estimates [25]. While expressed in reduced units, simulated thermodynamic properties of TIP4P water agree very well with the data for real water [28]. Thus, the following discussion is developed in terms of the reduced units:  $T^*$ ,  $P^*$ , and  $\rho^*$ . Some results of our simulations are listed in Table 1.

It has been recently shown [18,20], that the size of the H-bonded network is mainly controlled by water density. Simulations over a wide range of densities  $0.03 < \rho^* < 3.02$  allowed us to trace gradual changes in the structure of supercritical water, from dilute vapor to dense liquid-like fluid. In Fig. 1 cluster size distributions (normalized probabilities for a randomly selected molecule to participate in a cluster of given size) are shown at a supercritical temperature of  $T^*=1.04$ . Dilute vapor consists mostly of individual monomers. However, even at  $\rho^*=0.06$ , up to 10 % of molecules form dimers, and noticeable amounts of trimers and tetramers are present. The largest water cluster observed under these conditions consisted of seven molecules, contributing  $5.4 \cdot 10^{-3}$  % to the cluster size distribution. It is quite remarkable, that even at very low densities such large clusters may occur. As density increases, water molecules form even larger clusters. At a certain density, when the concentration of H-bonds achieves the percolation threshold, an infinite cluster of H-bonded molecules is formed. At a density above the percolation threshold molecules have higher probability to join the percolating cluster. That decreases the fraction of molecules forming smaller isolated complexes, and, considering finite system size  $N$ , one can observe bimodal cluster size distributions.

The theoretical value for the bond-percolation threshold of infinite diamond-like lattices is  $p_{cb}=0.3886$  [29]. This network topology was successfully applied to describe the anomalous properties of liquid and supercooled water [30], and is assumed here to be valid under supercritical conditions. If the small amount of water molecules forming more than 4 bonds is neglected,  $4p_{cb} = 1.5544$  gives the percolation threshold for the average number of hydrogen bonds per water molecule,  $\langle n_{HB} \rangle_p$ . This result is valid for an infinite lattice, while in a finite system  $p_c$  is depends on the system size like  $[p_c - p_c(L)] \sim L^{-1/\nu}$ , where  $L$  is the simulation box

length and  $\nu_p$  is a universal critical exponent [31]. Thus,  $p_c(L)$  is an effective system size dependant percolation threshold. The systems considered in our study are obviously too small to explore the average size and structure of clusters in the vicinity of the percolation threshold,  $S_p$ . However, clusters satisfying  $S \ll S_p$  or  $S \gg S_p$  should not be affected by the system size [32]. We calculated the probability for the largest observed cluster to percolate

**Table 1.** Parameters of the hydrogen bonding networks formed by TIP4P water molecules under various thermodynamic conditions.  $\langle n_{\text{HB}} \rangle$  – average number of hydrogen bonds per molecule;  $\langle S \rangle$  – average cluster size;  $\langle S_{\text{max}} \rangle$  – average size of the biggest cluster;  $\langle f_p \rangle$  – average fraction of molecules belonging to the infinite percolating cluster.

$P$ / MPa	$\rho$ / g·cm <sup>-3</sup>	$P^*$	$\rho^*$	$\langle n_{\text{HB}} \rangle$	$\langle S \rangle$	$\langle S_{\text{max}} \rangle$	$\langle f_p \rangle$ / %
$T=573$ K ( $T^*=0.96$ )							
10	0.06	0.55	0.18	0.49	1.82	5.79	0.00
30	0.62	1.66	1.89	1.61	49.30	88.73	33.74
50	0.67	2.76	2.05	1.70	71.65	113.86	49.57
100	0.76	5.52	2.31	1.82	107.14	146.99	67.68
200	0.84	11.04	2.57	1.95	142.12	173.57	80.44
$T=623$ K ( $T^*=1.04$ )							
5	0.02	0.28	0.06	0.13	1.15	2.39	0.00
10	0.05	0.55	0.15	0.29	1.39	3.78	0.00
20	0.15	1.10	0.46	0.72	2.59	8.76	0.00
30	0.37	1.66	1.13	1.15	6.77	21.19	0.26
50	0.55	2.76	1.68	1.40	17.45	43.69	7.12
100	0.68	5.52	2.07	1.58	43.35	82.22	31.19
200	0.79	11.04	2.41	1.76	89.83	131.91	60.26
300	0.86	16.56	2.61	1.86	121.17	158.36	73.38
$T=673$ K ( $T^*=1.12$ )							
10	0.04	0.55	0.12	0.20	1.23	2.88	0.00
20	0.10	1.10	0.30	0.44	1.66	4.99	0.00
30	0.19	1.66	0.58	0.69	2.45	8.06	0.00
50	0.40	2.76	1.22	1.06	5.22	17.01	0.02
100	0.59	5.52	1.80	1.35	13.72	36.97	4.53
200	0.74	11.04	2.24	1.57	42.17	80.89	31.39
300	0.81	16.56	2.47	1.69	73.48	116.28	52.41
500	0.91	27.59	2.77	1.85	118.80	156.76	72.74
$T=773$ K ( $T^*=1.29$ )							
10	0.03	0.55	0.09	0.11	1.12	2.19	0.00
20	0.07	1.10	0.21	0.23	1.28	3.13	0.00
30	0.11	1.66	0.34	0.35	1.48	4.08	0.00
50	0.22	2.76	0.67	0.58	2.03	6.38	0.00
100	0.43	5.52	1.31	0.95	3.87	12.76	0.00
300	0.72	16.56	2.21	1.39	17.52	44.55	9.11
500	0.84	27.59	2.56	1.58	45.99	86.01	35.99
1000	1.00	55.19	3.04	1.84	117.58	156.15	72.58
$T=298$ K ( $T^*=0.50$ ) (Liquid water under ambient conditions)							
0.1	0.99	0.01	3.02	3.19	215.14	215.58	99.80

$P(S_{max})$  depending on the hydrogen bond concentration  $\langle n_{HB} \rangle$  at different temperatures. From these data, the size of a percolation cluster at  $T^* = 1.04$  is estimated to be  $\sim 65$  molecules. This value divides cluster size distributions into two parts. One of them represents infinite percolating clusters, while another part represents smaller isolated clusters (Fig.1).

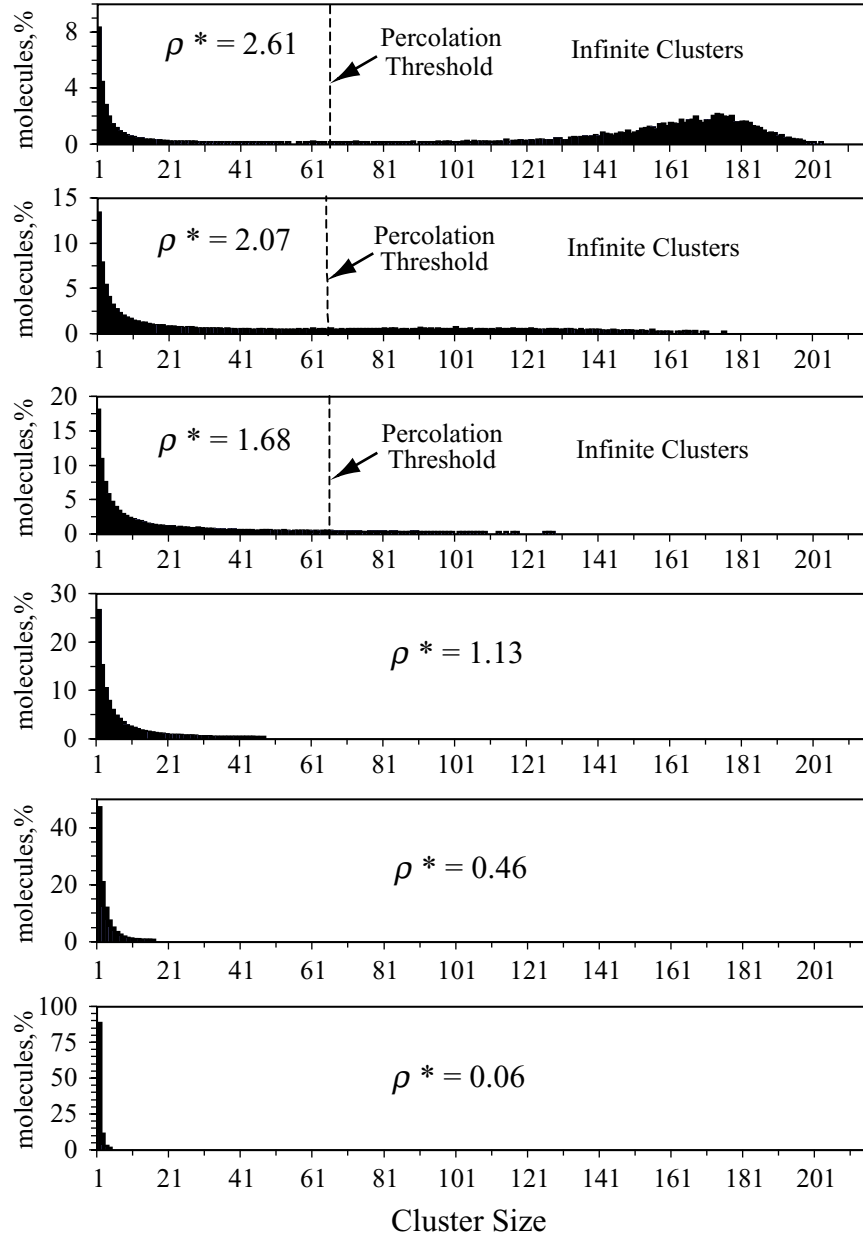


Fig 1. Participation of water molecules between clusters of different size under supercritical conditions at  $T^*=1.04$

Temperature and density dependencies of the average number of H-bonds per molecule,  $\langle n_{HB} \rangle$ , average cluster size,  $\langle S \rangle$ , average size of the largest cluster in the system,  $\langle S_{max} \rangle$ , and

average fraction of molecules belonging to the infinite percolating cluster,  $\langle f_p \rangle$ , are summarized in Table 1. In the low-density limit,  $\langle n_{HB} \rangle \rightarrow 0$  and  $\langle S_{max} \rangle \rightarrow \langle S \rangle \rightarrow 1$ . On the other hand, at high density (and low temperature) cluster size parameters  $\langle S \rangle$  and  $\langle S_{max} \rangle$  converge to the number of molecules in the simulation box,  $N$ .

**Table 2.** Geometric and energetic parameters of the most abundant clusters in supercritical water.

												
$\rho^*$	Relative abundance of topologically different water clusters at $T^*=1.04$											
0.06	95.6	4.39	78.3	15.5	5.13	1.07	55.5	32.2	3.42	3.42	0.00	3.42
0.15	97.2	2.94	77.5	16.9	3.63	2.00	54.1	34.6	3.58	2.72	1.00	1.14
0.46	98.3	1.69	78.8	17.3	2.60	1.35	56.3	36.1	2.27	1.70	1.44	0.48
0.79	98.6	1.55	79.2	17.4	2.23	1.16	55.9	37.3	2.17	1.67	1.25	0.38
1.13	98.6	1.37	78.9	17.8	2.11	1.19	56.7	37.2	1.92	1.12	1.17	0.46
1.68	98.9	1.15	79.4	17.7	1.94	0.93	56.3	37.3	2.21	1.40	1.19	0.40
2.07	98.9	1.09	80.2	16.9	2.05	0.91	55.4	38.4	1.51	1.38	1.40	0.49
Geometry and energy of small supercritical water clusters at $T^*=1.04$ , $\rho^*=1.13$												
$\langle \angle \text{O}\cdots\text{O}\cdots\text{O} \rangle_1 / ^\circ$	109	60	110	107	114	87	110	108	112	107	105	
$\langle \angle \text{O}\cdots\text{O}\cdots\text{O} \rangle_2 / ^\circ$					60				86	60		
$\langle \angle \text{O}\cdots\text{O}\cdots\text{O} \rangle_3 / ^\circ$										119		
$\langle R_{\text{O-H}} \rangle / \text{\AA}$	2.04	2.07	2.04	2.04	2.06	2.03	2.04	2.04	2.05	2.06	2.05	
$\langle R_{\text{O-O}} \rangle / \text{\AA}$	2.90	2.89	2.91	2.91	2.90	2.90	2.91	2.91	2.91	2.90	2.92	
$\langle \angle \text{O}\cdots\text{H}\cdots\text{O} \rangle / ^\circ$	149	143	150	150	146	150	150	150	149	146	150	
$\langle U_{\text{HB}} \rangle / \text{kJ/mol}$	-16.9	-16.4	-16.9	-16.7	-16.3	-17.0	-16.9	-16.8	-16.7	-16.3	-16.8	

Since the properties of small clusters are definitely not affected by the system size, we are focusing our discussion on the structure and topology of trimers, tetramers, and pentamers, which are most abundant under typical supercritical conditions. Relative abundance of topologically different cluster types depending on density has already been briefly discussed recently [20]. In our analysis we make no distinction between donor and acceptor types of hydrogen bonds originating at a particular water molecule. Thus, every molecule is depicted as a structureless dot in Table 2 where all observable topological types of 3-, 4-, and 5-mers are schematically shown along with some parameters of such clusters under near-critical thermodynamic conditions of  $T^* = 1.04$  and  $\rho^* = 1.13$ .

Only two topologically different types of clusters can be formed by three water molecules: 3-member rings 3(2) constitute less than 2% of all trimers, while 98% of them are represented by simple chain-like clusters 3(1). Four water molecules also mainly form chains 4(1) (~80% of all tetramers) or pyramid-like clusters 4(2) (~17%). More complex clusters containing 3- or 4-member rings, 4(3) and 4(4), constitute together less than 3% of all tetramers. Similarly, the pentamer distribution mostly consists of linear chains 5(1) (~56%) and branched chains 5(2) (about 38%). All five other pentamer cluster types (4 of them are shown in Table 2) contribute together less than 10%. Interestingly, the most branched non-cyclic 5-member cluster, the tetrahedron-like structure 5(5), represents only ~1% of all pentamers. A noticeable increase of the fraction of 5-member rings 5(6) is observed with isothermally decreasing density. Thus, 5-member rings may play an appreciable role in very dilute supercritical water vapor. However, it is important to keep in mind that at  $\rho^*=0.06$ ,  $T^*=1.04$  all possible pentamers contribute just 0.07% to the cluster size distribution, while at  $\rho^*=0.03$ ,  $T^*=1.29$  their fraction is only 0.004%. In the latter case, hexamers and larger clusters were not observed at all.

To summarize, H-bonded molecular clusters containing open chain-like or tree-like structures are found to predominate over clusters containing cyclic ring-like elements. It is observed that the relative distribution of water molecules between topologically different clusters of same size is not significantly affected by changes of the thermodynamic conditions – temperature, pressure, or density. These observations may appear to disagree with the results of *ab initio* calculations, which predict ring-like configurations to be the most stable structures [7,8,10]. One might argue that an empirical potential simply fails to describe molecular interaction adequately enough. However, recent molecular mechanics studies utilizing the TIP4P water model [33] have successfully predicted global energetic minima for the geometry of water clusters similar to the results of *ab initio* simulations [7,8,10,33,34]. Thus, the interaction potential is not to be blamed. Moreover, our previous analysis of the structure of supercritical water clusters based on completely different water potential gave almost identical results [20]. The real reason for these discrepancies seems to be in the different settings of two types of calculations. *Ab initio* calculations, as well as molecular mechanics modeling, predict static molecular configurations (minimum energy structures) which are stable in vacuum at 0 K. On the other hand, molecular clusters obtained by Monte-Carlo and molecular dynamics [20] simulations are equilibrium “dynamic” structures, which represent a compromise between intermolecular (intercluster) interactions, effects of cluster interactions with surrounding molecules, and thermal kinetic motion. Thus, it is not surprising to observe higher abundance

of 5-member molecular rings at low density in our study. They are predicted to be stable in vacuum. This observation seems to support our point. There is another possible confusion to be commented on. Various 4,5,6-member ring-like structures are reported to exist in low temperature water [35]. However, in the case of liquid water such structures represent only specific details of an infinite percolating molecular cluster. These structural elements are not the subject of our study, although it seems safe to believe that they exist in dense supercritical water, as well. Here we discuss only the structure and topology of isolated water complexes.

We have analyzed several geometric and energetic parameters of hydrogen bonds forming the most abundant molecular trimers, tetramers and pentamers in supercritical water. The results for some less abundant pentamers are not reported because of their very rare occurrence and poor statistics. Average hydrogen-bonding angles  $\langle \angle \text{O}\cdots\text{O}\cdots\text{O} \rangle$  and  $\langle \angle \text{O}\cdots\text{H}-\text{O} \rangle$ , distances  $\langle R_{\text{O}\cdots\text{O}} \rangle$  and  $\langle R_{\text{O}\cdots\text{H}} \rangle$ , and energies  $\langle U_{\text{HB}} \rangle$  are reported in Table 2 for the supercritical thermodynamic point  $T^*=1.04$  and  $\rho^*=1.13$ . It is noteworthy, that the most abundant clusters, with topologies 3(1), 4(1), 4(2), 5(1) and 5(2) have almost identical geometric and energetic characteristics. So, H-bond lengths were found for all clusters to be 2.04 Å, while H-bonding angles  $\langle \angle \text{O}\cdots\text{O}\cdots\text{O} \rangle$  have values  $\sim 109^\circ$ , which corresponds to the geometry of an ideal tetrahedrally ordered lattice. Cluster geometry was also studied at other thermodynamic conditions. With increasing temperature and/or decreasing density H-bond distances  $\langle R_{\text{O}\cdots\text{O}} \rangle$  and  $\langle R_{\text{O}\cdots\text{H}} \rangle$  increase, in agreement with other observations [13,14,19]. However, it is quite remarkable, that average angles  $\langle \angle \text{O}\cdots\text{O}\cdots\text{O} \rangle$  for the most abundant clusters remain almost constant at  $\sim 109^\circ$  over the whole range of supercritical conditions studied. This result is in excellent agreement with available X-ray diffraction data for supercritical water [2,36] which show a noticeable peak of molecular distribution function at  $\sim 4.5$  Å corresponding to tetrahedrally ordered second nearest neighbors.

There are two ways to compare energy of clusters – energy per hydrogen bond or energy per water molecule. Obviously, these quantities are different since clusters of the same size may have different number of internal bonds. Because cluster definition is based on strength of its bonds,  $\langle U_{\text{HB}} \rangle$  is employed. Generally, one may expect that cluster abundance is proportional to  $\exp(-\beta U)$ , where  $\beta = (k^*T)^{-1}$ ,  $k$  – Boltzmann constant,  $T$  – temperature and  $U$  – potential energy of intermolecular interactions. At a constant temperature, the most abundant clusters generally should have lower energy. This assumption, however, is not always supported by the data in Table 2. So,  $\langle U_{\text{HB}}^{3(1)} \rangle < \langle U_{\text{HB}}^{3(2)} \rangle$ ,  $\langle U_{\text{HB}}^{4(1)} \rangle < \langle U_{\text{HB}}^{4(2)} \rangle < \langle U_{\text{HB}}^{4(3)} \rangle$ . On the other

hand,  $\langle U_{\text{HB}}^{4(4)} \rangle < \langle U_{\text{HB}}^{4(1)} \rangle$ , in contrast with the low abundance of 4-member rings. Similarly,  $\langle U_{\text{HB}}^{5(5)} \rangle \approx \langle U_{\text{HB}}^{5(2)} \rangle$ , while the latter topology is much more abundant. Apparently, not only energetic, but also entropic effects play significant role in determining the abundance of particular cluster types. For instance, despite the low potential energy of the configuration 5(5), such pentamers can evidently form only when very specific conditions for mutual distances and angles are satisfied for all 5 molecules forming such a structure.

This work was partly supported by INTAS (grants UA-95-0096 and 96-1989).

### REFERENCES

- [1] M.M. Hoffmann and M.S. Conradi, *J. Am. Chem. Soc.*, **119**, 3811 (1997).
- [2] Yu.E. Gorbaty and A.G. Kalinichev, *J. Phys. Chem.*, **99**, 5336 (1995).
- [3] A.K. Soper, F. Bruni and M.A. Ricci, *J. Chem. Phys.*, **106**, 247 (1997).
- [4] N. Matubayasi, C. Wakai and M. Nakahara, *J. Chem. Phys.*, **107**, 9133 (1997).
- [5] J.B. Paul, C.P. Collier, R.J. Saykally, J.J. Sherer, A. O'Keefe, *J. Phys. Chem. A*, **101**, 5211 (1997).
- [6] A. Chialvo and P.T. Cummings, *J. Chem. Phys.*, **101**, 4466 (1994).
- [7] K. Liu, M.G. Brown, J.D. Cruzan, R.J. Saykally, *Science*, **271**, 62 (1996).
- [8] K. Liu, J.D. Cruzan, R. J. Saykally, *Science*, **271**, 929 (1996).
- [9] J.K. Gregory, D.C. Clary, K. Liu, M.G. Brown, R. J. Saykally, *Science*, **275**, 814 (1997).
- [10] K. Liu, M.G. Brown, C. Carter, R.J. Saykally, J.K. Gregory, D.C. Clary, *Nature*, **381**, 501 (1996).
- [11] E.S. Fois, M. Sprik and M. Parrinello, *Chem. Phys. Lett.*, **223**, 411 (1994).
- [12] A. Luzar and D. Chandler *Nature*, **379**, 55 (1996).
- [13] A.G. Kalinichev and J.D. Bass, *Chem. Phys. Lett.*, **231**, 301 (1994).
- [14] T.I. Mizan, P.E. Savage and R.M. Ziff, *J. Phys. Chem.*, **98**, 13067 (1994).
- [15] G. Löffler, H. Schreiber and O. Steinhauser, *Ber. Bunsenges. Phys. Chem.*, **98**, 1575 (1994).
- [16] A.G. Kalinichev and K. Heinzinger, *Geochim. Cosmochim. Acta.*, **59**, 641 (1995).
- [17] R.D. Mountain, *J. Chem. Phys.*, **103**, 3084 (1995).
- [18] R.D. Mountain, *J. Chem. Phys.*, **110**, 2109 (1999).
- [19] A.G. Kalinichev and J.D. Bass, *J. Phys. Chem. A*, **101**, 9720 (1997).

- 
- [20] A.G. Kalinichev and S.V. Churakov, *Chem. Phys. Lett.*, **302**, 411 (1999).
- [21] T. Driesner, *Science*, **277**, 791 (1997).
- [22] M.P. Allen and D.J. Tildesley, *Computer Simulation of Liquids*, Oxford University Press, New York, 1987.
- [23] W.L. Jorgensen, J. Chandrasekhar, J.D. Madura, R.W. Impey and M.L. Klein, *J Chem. Phys.*, **79**, 926 (1983).
- [24] D. Eisenberg and W. Kauzmann, *The Structure and Properties of Water*, Oxford University Press, Oxford, 1969.
- [25] A.G. Kalinichev, *Z.Naturforschung*, **46a**, 433 (1991).
- [26] Y. Guissani and B. Guillot, *J Chem. Phys.*, **99**, 8221 (1993).
- [27] J.P. Hansen *Phys. Rev. A*, **2**, 221 (1970).
- [28] Pruss, A. and W. Wagner, *J. Phys. Chem. Ref. Data* (in press);  
(available at <http://webbook.nist.gov>).
- [29] M. Sahimi, *Applications of Percolation Theory*, Taylor & Francis Ltd, 1994.
- [30] H.E. Stanley and J. Teixeira, *J. Chem. Phys.*, **73**, 3404 (1980).
- [31] M. Levinstein, M.S. Shur and E.L. Efros, *Soviet Phys.-JETP*, **42**, 1120 (1976).
- [32] D. Stauffer, and A. Aharony, *Introduction to percolation theory*, Taylor & Francis, London, 1992.
- [33] S.S. Xantheas and T.H. Dunning, Jr. *J. Chem. Phys.*, **99**, 8774 (1993).
- [34] S.S. Xantheas, *J. Chem. Phys.*, **100**, 7523 (1994).
- [35] R.J. Speedy, J.D. Madura and W.L. Jorgensen, *J. Phys. Chem.*, **91**, 909 (1987).
- [36] Yu.E. Gorbaty and Yu.N. Demianets, *Chem. Phys. Lett.*, **100**, 450 (1983).

## LIST OF PUBLICATIONS

1. Shmulovich K.I. & **Churakov S.V.** (1998) Natural fluid phases at high temperatures and low pressures. *Journal of Geochemical Exploration*, 62, 183-191.
2. Kalinichev A.G. & **Churakov S.V.** (1999) Size and topology of molecular clusters in supercritical water: A molecular dynamics simulation. *Chem. Phys. Letters* (302) 5-6, 411-417.
3. **Churakov S.V.** & Kalinichev A.G. (1999) Size and structure of molecular clusters in supercritical water. *Journal of Structural Chemistry*, 40(4), 548-553.
4. **Churakov S.V.**, Tkachenko S.I., Korzhinskii M.A., Bocharnikov R.E. & Shmulovich K.I. (2000) Evolution of Composition of High-Temperature Fumarolic Gases from Kudryavy Volcano, Iturup, Kuril Islands: the Thermodynamic Modeling. *Geochemistry International*, 38(5), 436-451.
5. **Churakov S.V.** & Kalinichev A.G. (2000) Size structure and abundance of molecular clusters in supercritical water over a wide range of densities: Monte-Carlo simulations. In: Tremaine, P.R, Hill, P.G., Irish, D.E., and Balakrishnan, P.V. (*Editors*). 2000. *Steam, Water, and Hydrothermal systems: Physics and Chemistry Meeting the Needs of Industry*. NRC Research Press, Ottawa, Canada. 418-425.
6. Kalinichev A.G. & **Churakov S.V.** (2001) Thermodynamics and structure of molecular clusters in supercritical water. *Fluid Phase Equilibria* 183–184, 271–278.
7. Frolova T.I., Plechov P.Yu., Tikhomirov P.L., and **Churakov S.V.** (2001) Melt Inclusions in Minerals of Allivalites of the Kuril-Kamchatka Island Arc. *Geochemistry International*, 39(4), 336-346.
8. **Churakov S.V.** & Gottschalk M. (2001) Perturbation theory based equation of state for polar molecular fluids. I Pure fluids. *Geochimica et Cosmochimica Acta* (in press).
9. **Churakov S.V.** & Gottschalk M. (2001) Perturbation theory based equation of state for polar molecular fluids. II Fluid mixtures. *Geochimica et Cosmochimica Acta* (in press).

## ACKNOWLEDGMENTS

First, I would like to express my deep gratitude to Prof. Dr. Kiril Shumulovich who has had and still has an enormous influence on the development of my scientific interests since I first met him as a student. I would also like to acknowledge Dr Sergey I. Tkachenko, Dr Mikhail A. Korzinskii and all other staff members of the “laboratory of hydrothermal fluids” of Institute of Experimental Mineralogy (Chernogolovka, Russia) for a very fruitful collaboration with my computer modeling of the thermodynamic equilibria in volcanic gases. I am grateful to Prof. Dr. Andrey G. Kalinichev for introducing me to and instructing me in the field of computer simulations of fluids, as well as constructive criticism of my work and useful discussions.

Prof. Dr. Wilhelm Heinrich gave me the opportunity to work on my PhD thesis at the GeoForschungsZentrum, Potsdam and showed an insistent interest in my work. I am highly indebted to my supervisor PD Dr. Matthias Gottschalk for bringing my thoughts in order and losing his nerve cells when correcting my terrible English.

I am also very thankful to all staff members in PB 4.1 of the GeoForschungsZentrum, namely Ulf Andersson, Ingeborg Bauer, Anne Feenstra, Daniel Harlov, Beate Hein, Stefan Melzer, Ralf Milke, Hans-Josef Reichmann, Frank Schilling, Christian Schmidt, Reiner Schulz, Anne-Magali Seydoux, Richard Wirth, and Bernd Wunder for everyday help and comradeship. Special thanks to PhD students Jens Najorka, Michael Höfer and Birgit Pöter for explaining to me the tangled and impenetrable rules for living in Germany.

## CURRICULUM VITAE

Surname: Churakov  
Given Name: Sergey  
Date of birth: 28 December, 1974  
Place of birth: Moscow, Russia  
Citizenship: Russia Federation  
Official address: GeoForschungsZentrum, Potsdam  
Telegrafenberg,  
D-14473 Potsdam, Germany  
E-mail: sergey@gfz-potsdam.de  
Telephone: +49 0331 288 1853  
Fax: +49 0331 288 1402  
  
Private address: Neuendorfer Str. 10, D-14480 Potsdam, Germany

### Scientific carrier:

1991:  
High School certificate

1991-1997:  
Student in the Moscow State University

1994-1995:  
Laboratory in the Institute of Experimental Mineralogy Russia Academy of Science  
(Chernogolovka Moscow distract, Russia).

1995-1996:  
Software administrator in Computer Center of Russian Academy of Science.

1996:  
Graduated from “geological department” of Moscow State University. Diploma in  
Geochemistry (Equivalent to the Master Degree of Science).

1997:  
Graduated from “mathematics and computer science department” of Moscow State  
University. Diploma in Mathematics (Equivalent to the Master Degree of Science).

1998-2001:  
PhD student in GeoForschungsZentrum, Potsdam, Germany.

## Erklärung

Hiermit erkläre ich an Eides statt, dass ich die vorliegende Arbeit selbständig und nur mit den angegebenen Mitteln angefertigt habe.

Sergey Churakov